Universidad Nacional Autónoma de México

Programa de Maestría y Doctorado en Ingeniería

Instituto de Ciencias Aplicadas y Tecnología

Acoustic travelling wave separation in the time-domain using electronic delay circuits

T E S I S

Que para optar por el grado de:

Doctor en Ingeniería Eléctrica

Presenta:

José María Gómez Pérez

Tutor:

Dr. Felipe Orduña Bustamante. ICAT

Comité Tutor:

Dr. Pablo R. Pérez Alcázar. Facultad de Ingeniería

Dr. Saúl De la Rosa Nieves. Facultad de Ingeniería

Dr. Roberto Velasco Segura. ICAT

Ciudad Universitaria, CD. MX., Diciembre, 2022

Jurado asignado:

Presidente:	Dr. Pablo Roberto Pérez Alcázar
Secretario:	Dr. Caleb A. Rascón Estebané
1er vocal:	Dr. Felipe Orduña Bustamante
2^{o} vocal:	Dr. Saúl De La Rosa Nieves
3er vocal:	Dr. Roberto Velasco Segura

Lugar: Instituto de Ciencias Aplicadas y Tecnología, Ciudad Universitaria, Cd. de México, México.

Tutor de tesis:

Dr. Felipe Orduña Bustamante

Firma

"Bonum certamen certavi, cursum consummavi, fidem servavi."
2 Tm 4:7.

A mis padres...

Acknowledgements

- To my parents for all their love and attention, and to my brother, for his unconditional support.

- Dr. Felipe Orduña Bustamante: for his help and patience during the years of work together. For helping me realize my goals and for everything he taught me.

- Dr. Roberto Velasco Segura, Dr. Saúl de la Rosa Nieves, Dr. Pablo Roberto Pérez Alcázar, Dr. Jesús Santiago Pérez Ruíz, y Dr. Caleb Antonio Rascón Estebané: for their contribution to this project.

- Dr. José Ismael Martínez López: for his friendship and advice, for helping me during my years of academic formation.

- Dr. Francisco Javier Martínez López: for his friendship and all the long conversations.

- Dr. Jorge Rodríguez Cuevas: for his friendship and all the opportunities provided to me.

- M.I. Antonio Martínez López: for his friendship and his teachings.

- M.A. Alfonso Eduardo Salinas Palacio: for being an old friend and for helping me proofread this work.

- M.I. Gloria Correa Palacios: for her kindness and administrative support.

- Ing. Ricardo Dorantes Escamilla: for the good conversations.

- Ms. Lilia Granados Ramírez: for always being kind to me.

- Consejo Nacional de Ciencia y Tecnología (CONACYT): for the scholarship granted, CVU: 706364.

- Laboratorio de Acústica y Vibraciones del Instituto de Ciencias Aplicadas y Tecnología (ICAT): For the technical and financial support for this project.

- Universidad Nacional Autónoma de México (UNAM).

- Finally, *ad Deum, Rex mirabilis maiestatis, et Mariam, mater dulcissima mea.*

Contents

List of Figures

Introduction

The need to separate a sound wave inside a duct into its forward and backward travelling components arises frequently in the industry and in academia (e.g., [2, 3, 4, 5]). Having the ability to distinguish the two components that make up the sound field inside a duct also opens up the possibility to many applications, for instance: to investigate the damping and radiation of tubes [6], to measure several duct properties [2] even in the presence of mean flow [7]; something really useful in the development of mufflers in the automotive industry [4]. Measurements of duct properties can also be conducted in industrial applications [8] or in the presence of measurement noise [9]. The medical field also benefits from travelling wave separation, for example, it can be used as part of a non-invasive technique to measure properties of the human airway [10]. Characterization of wind musical instruments is also possible [11, 12] even under playing conditions [13]. The acoustic properties of materials inside a duct can also be determined [14, 15], and the ability to manipulate the sound field components separately gives rise to active control of sound [16], like active sound absorption [17] and real-time wave suppression [18]. A system capable of splitting a sound wave into its forward and backward components can be referred to as a Travelling Wave Separation System (TWSS).

A very important consideration to be made when selecting a particular TWSS is whether it is meant to be used in a real-time application or not; a plethora of options then arise which can be tailored towards solving a specific problem. In some cases, the most important aspects of a TWSS are processing speed and low latency (e.g. in active control of sound); in other cases (e.g. when measuring acoustic materials) it might not be a relevant feature, since data can be recorded and processed at a later time. Many performance factors can be used for the characterization of a TWSS, for example [1]: processing speed, level of separation (i.e., the ability of the TWSS to discriminate between the forward and backward traveling waves), latency, complexity of the apparatus and of the calibration procedure; quantity of transducers, ease of use, reconfigurability for different acoustic ducts and microphone separations, bandwidth, flatness of frequency response, adaptability towards changing enviromental conditions, and cost.

The most simple and rudimentary way to separate a sound field inside a duct into its forward and backward travelling wave components consists on mounting a single microphone along the wall of the test tube in order to sense the sound field and perform time windowing. This way it is possible to separate the incident (forward component) from the reflected (backward component) wave. However, this method is only viable if the tube is

long enough and the travelling wave duration is short, otherwise, when multiple reflections are present or if the tube is not long enough to isolate the forward and backward travelling wave components with time windowing, using a single microphone will not produce satisfactory results, also, this method most commonly implies that the separation process will not be performed in real-time. For these reasons, methods which overcome these issues by using two or more microphones to separate the sound field into its forward and backward travelling wave components have been published since the second half of the last century.

Some methods published in the literature are capable of achieving a very high level of travelling wave separation. Yet many of them carry out all the required processing in the frequency domain, which inherently produces long delay times and might negate the possibility for real-time operation in applications such as active control of sound, which require very short processing delays. In this case a time domain solution represents the most suitable choice. Only a handful of travelling wave separation methods operating in the time domain have been published so far, but the majority of them require a complex calibration procedure and a somehow sophisticated computational system.

The theory and methods presented in this work propose different ways to realize a Travelling Wave Separation System in the continuous time domain with analog electronic circuitry, which are capable of producing systems that require a simple calibration procedure and provide real-time operation with low latency. The circuits obtained by the methods proposed in this work are also capable of attaining good levels of separation between the forward and backward travelling wave components, and possess the ability to overcome the effect of unknown initial conditions or other sources of error that might arise during operation; making them most suitable for active control of sound applications. Some of the experimental results obtained with these techniques were published in [1].

Objectives

- To design and implement Travelling Wave Separation Systems in the continuous time domain capable of achieving levels of separation comparable to those obtained with similar techniques in the frequency domain or in the discrete time domain.

- To obtain an analog TWSS that rivals or surpasses other analog TWSSs currently available in the literature, while at the same time being capable of using less of microphones and a simple calibration procedure.

Contributions of This Work

- A formulation based on approximation theory that suits the implementation of a TWSS in continuous time domain, and the extension of previous work, whilst establishing a relationship between certain circuit components and a leaky recursive factor used for stabilization purposes.

- The development of two design methods to attain analog circuits of varying complexities to perform travelling wave separation in the time domain.
- The establishment of a theoretical foundation for circuits capable of adapting to different tube dimensions and microphone separations, varying atmospheric conditions, as well as offering dynamic control of certain circuit parameters.
- A technique based on transfer function optimization capable of matching the responses of two microphones. The resulting transfer functions can then be synthesized and implemented with analog circuits.
- Experimental measurements of two circuits used to validate each of the two design methods.

In Chapter 1 some of the most relevant techniques to perform travelling wave separation available in the published literature are reviewed, and the theory to implement the wave separation process in the continuous time domain using two and three microphones is introduced. Chapter 2 discusses different approximation methods to implement time delays in continuous time, something fundamental to successfully perform travelling wave separation by means of the theory laid out in Chapter 1. In Chapter 3 the building blocks and circuitry required to realize travelling wave separation circuits in the time domain is presented. Chapter 4 exhibits experimental results obtained with some of these circuits. Finally, the conclusions and recommendations for future work are discussed in Chapter 5.

Chapter 1

Acoustic Travelling Wave Separation Theory

1.1 Introduction and Previous Work

This chapter introduces the theory that will be used throughout this entire thesis to perform travelling wave separation in the time domain. But first, it is important to review some of the most relevant techniques that have been published over the years to perform travelling wave separation using two or more microphones. Much of this information can also be found in [1].

One of the first travelling wave separation methods using a two microphone technique in the frequency domain was proposed by Seybert and Ross [14], it consists of two spaced microphones mounted on the wall of a tube, which are used to sample the sound wave at two different but known positions. By using the auto- and cross-spectra of the signals sensed by the two microphones, it is possible to obtain the forward and backward traveling wave components and the phase angle between them. A pre-requisite is that the spacing between the microphones should be much larger than the diameter of the microphone capsules. This method allows for the presence of mean flow inside the tube.

Louis *et al.* [19] presented another two-microphone technique, which was later emended by Poort and Fredberg [20], and that was originally intended for biomedical applications. It also makes use of two spaced microphones mounted on the wall of a tube. For the formulation of the wave equations some assumptions were made, namely, that the forward traveling wave being sensed by the second microphone is an exact replica of the wave being sensed by the first microphone, with the only difference being that the one being sensed by the second microphone exhibits a time delay; the same thing could be said about the backward traveling wave but in reverse, therefore, this technique neglects the effect of any losses inside the tube. Time domain convolution is used to relate the forward and backward traveling waves at both microphone positions. In order to do this, the calculation of two impulse responses is required, which take into account the effect of any elements outside the

domain between the two microphones. These impulse responses can be computed from the sound pressures being sensed at each microphone.

Kemp *et al.* [21] presented a technique which uses time-domain convolution and multiple microphones to perform travelling wave separation inside ducts. The use of multiple microphones and the resulting algebraically over-determined system reduces the effect of singularities that occur between two microphones when the distance between each pair matches an integer multiple of half the sound wavelength [1, 21]. This separation method relies on the absence of any forward or backward traveling waves between the microphones at the start time of the analysis. An initial calibration procedure to extract the transfer functions between each pair of microphones is required, this is achieved by executing two calibration runs. In the first one, the forward traveling wave transfer functions are obtained by reproducing a logarithmic sine sweep through a speaker positioned at one end of the apparatus and an anechoic termination at the other end. The second run involves reversing the position of the speaker and the anechoic termination to the opposite sides of the apparatus, this time for the backwards propagating wave. As a result, this method accounts for the effect of losses and gain ratios in inter-microphone transfer functions. Any previous knowledge of the sound speed, propagation constants, distance between microphones or the location of their acoustic center is not required, as long as the conditions do not change over time. In case, however, that the frequency response of the microphones is vastly different, the tube must be longer to accurately extract the transfer functions.

The most obvious difficulty about this method has to do with the calibration process, which requires placing different elements at both ends of the tube for each calibration run, this is unpractical, especially in many industrial applications in which tubes can be exceptionally long or repositioning of the elements may not be possible at all. To overcome this complication, Groves and Lennox [8] proposed a simpler calibration method, which applies discrete time domain filters to the first run in order to emulate the attenuation response of the second one, this way the second calibration run is omitted and estimated form the first, so there is no need for the relocation of elements. The authors also expand the method of Louis *et al.* [19] to be used with multiple microphones.

A method which considers propagation losses and time varying conditions inside the tube, such as the presence of varying mean flow, was proposed by Van Walstijn *et al.* [7]. The travelling wave separation is realized in the frequency domain with a calibration process that relies on minimization of estimates for the forward- and backward-travelling wave components from two microphone pairs in a three microphone arrangement. This method attains high levels of travelling wave separation whilst taking into account changes in the conditions inside the tube.

Groves *et al.* [18] further developed these techniques in the time-domain with a method capable of obtaining excellent levels of separation; with applications concerning real-time active suppression of the forward travelling wave. Still, it requires that the separation between the speaker and the microphones to be long enough in order for the TWSS to have enough time to compute the necessary output to perform active absorption of the reflected wave. This condition might not always be met when shorter tubes are used or higher system

requirements might be necessary.

One of the few reported methods that operates in continuous time by making use of analog electronics was developed by Guerard and Boutillon [22]. It uses a total of five microphones, the central microphone senses the sound pressure signal, whilst the remaining microphones are used to estimate the sound pressure gradient, which is integrated electronically to obtain the acoustic particle velocity. With these two quantities the travelling wave components are estimated in an approach quite similar to the theory developed in this chapter. However, the accuracy of the travelling wave components becomes less reliable as the frequency increases since the pressure gradient estimation deteriorates.

The use of leaky recursion when performing travelling wave separation reduces the system's over-dependence on initial conditions and other sources of error that might arise during operation. The basic formulation and error analysis of leaky recursion was laid down initially in [23, 24]. Discrete time domain implementations relying on digital filters were presented in [25, 26], whilst preliminary continuous time domain implementations using analog electronics, which predate the work of this thesis, were introduced in [27, 28]. A frequency domain application that hints at the same techniques discussed in this chapter was published in [11].

From the previous review of some of the most relevant works published in the literature we can conclude the following: several travelling wave separation techniques have been developed over the years, many of them provide very excellent levels of performance. The majority of them work in the frequency domain, while a few operate in the time domain. The latter are the most suitable techniques for real-time implementation applications, which require very small processing times, however, even the most recent of these techniques have some downsides, namely, that they require a very complex calibration procedure and a somehow sophisticated computational system, whilst still working in discrete time. Current methods that operate in the continuous time domain either require a lot of microphones or are not capable of obtaining results that are truly comparable to the any of the other techniques. Likewise, there is not a robust method for the realization of analog circuits for such task. The purpose of this work is to fill in this gap to allow the designer several options with different degrees of precision to attain an analog TWSS.

The following sections introduce the theory proposed in this work to implement travelling wave separation in the time domain using two or three microphones. First, ideal equations are obtained, afterwards, their stabilization by means of leaky recursion is presented. Finally, some figures of merit are introduced, which will serve as a means to evaluate the performance of the circuits developed in this thesis.

1.2 Two-Microphone Travelling Wave Separation

Consider the apparatus shown in Figure 1.1. It consists of a cylindrical tube, a pressure driver located at the "upstream" side of the tube, and two microphones at positions $x_1 = x_0 - \delta$ and $x_2 = x_0 + \delta$ mounted along the wall of the tube. The distance between the microphones

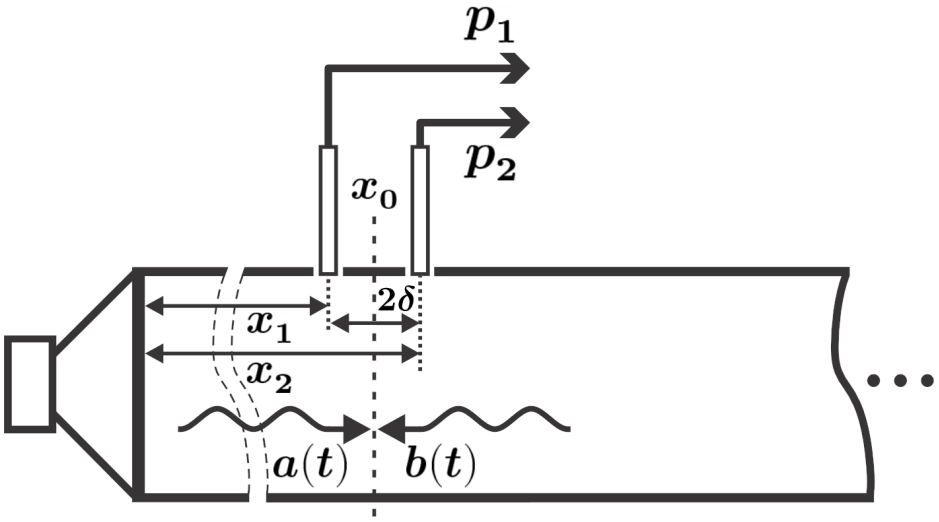

Figure 1.1: Cylindrical tube with two microphones mounted along its wall and a pressure driver located at the "upstream" (left) side.

is defined as $2\delta = x_2 - x_1$. The forward- and backward-travelling wave components are represented by $a\,(t)$ and $b\,(t)$, respectively, measured at the reference point x_0, which is located midway between the two microphones.

If the wavelength of the sound wave traveling along the tube is larger than roughly twice the diameter of the tube, plane wave propagation can be assumed [29]. Hence, the sound pressures $P_1\,(\omega)$ and $P_2\,(\omega)$ present at the first and second microphones, respectively, can be written in terms of forward and backward traveling wave components using the standard solution of the linear acoustic wave equation in one dimension:

$$P_1\,(\omega) = A\,(\omega)\,e^{+j\omega\tau} + B\,(\omega)\,e^{-j\omega\tau} \tag{1.1a}$$

$$P_2\,(\omega) = A\,(\omega)\,e^{-j\omega\tau} + B\,(\omega)\,e^{+j\omega\tau} \tag{1.1b}$$

Where $\tau = \delta/c$, c is the speed of sound, k is the wave number and the substitution $k = \omega/c$ was used to express the equations in terms of the angular frequency ω. $A\,(\omega)$ and $B\,(\omega)$ represent the forward- and backward-travelling wave components, respectively, in the frequency domain.

Equations (1.1a) and (1.1b) define a 2×2 algebraic system, which can be solved for $A\,(\omega)$ and $B\,(\omega)$ as [1]

$$A\,(\omega) = \frac{P_1\,(\omega) - P_2\,(\omega)\,e^{-2j\omega\tau}}{1 - e^{-4j\omega\tau}} e^{-j\omega\tau} \tag{1.2a}$$

$$B\,(\omega) = \frac{P_2\,(\omega) - P_1\,(\omega)\,e^{-2j\omega\tau}}{1 - e^{-4j\omega\tau}} e^{-j\omega\tau} \tag{1.2b}$$

Equations (1.2a) and (1.2b) show that it is possible to obtain the forward and backward

travelling waves at the reference point x_0 in the frequency domain, from the sound pressures being sensed by the two microphones.

The sound pressure $P(\omega)$ and particle velocity $U(\omega)$ at x_0 are related to the the forward- and backward-travelling waves by the following equations [1]:

$$P(\omega) = A(\omega) + B(\omega) \tag{1.3a}$$
$$\rho_0 c_0 U(\omega) = A(\omega) - B(\omega) \tag{1.3b}$$
$$A(\omega) = (1/2)\left[P(\omega) + \rho_0 c_0 U(\omega)\right] \tag{1.3c}$$
$$B(\omega) = (1/2)\left[P(\omega) - \rho_0 c_0 U(\omega)\right] \tag{1.3d}$$

where ρ_0 is the mass density of air, and c_0 is the speed of sound.

Equations relating the complex amplitudes $P(\omega)$ and $U(\omega)$ to the sound pressure amplitudes at the two microphones can be obtained as [1]

$$P(\omega) = \frac{P_1(\omega) + P_2(\omega)}{1 + e^{-2j\omega\tau}} e^{-j\omega\tau} \tag{1.4a}$$
$$\rho_0 c_0 U(\omega) = \frac{P_1(\omega) - P_2(\omega)}{1 - e^{-2j\omega\tau}} e^{-j\omega\tau} \tag{1.4b}$$

Equations (1.4) are simpler than (1.2), because they exhibit less $e^{-j\omega\tau}$ delay operators and shorter delay times. Thus, it is generally convenient to first calculate $P(\omega)$ and $\rho_0 c_0 U(\omega)$, and then compute $A(\omega)$ and $B(\omega)$ from (1.3c) and (1.3d). Also, Equations (1.4) are easier to synthesize as transfer functions, an approach that will be developed in Section 3.3.

All the expressions obtained hitherto are expressed in the frequency-domain, but they can be transformed into the time-domain by means of the inverse Fourier transform, which results in a set of recursive expressions [1]:

$$p(t) = p_1(t - \tau) + p_2(t - \tau) - p(t - 2\tau) \tag{1.5a}$$
$$\rho_0 c_0 u(t) = p_1(t - \tau) - p_2(t - \tau) + \rho_0 c_0 u(t - 2\tau) \tag{1.5b}$$

Equations (1.5) require knowledge of past values in a time frame of up to 2τ in order to allow for an exact calculation that could be carried out for future values of time t. To overcome the effect of the unknown initial conditions (and similar sources of error during operation) these expressions have to be modified since, at its present form, they are potentially unstable. Stabilization will be discussed in Section 1.4.

1.3 Three-Microphone Travelling Wave Separation

A third microphone can be added between the two microphones of the arrangement discussed in the previous section, as shown in Figure 1.2, the three equidistant microphones are now placed at positions $x_1 = x_0 - \delta$, x_0 and $x_2 = x_0 + \delta$. The reference point is again

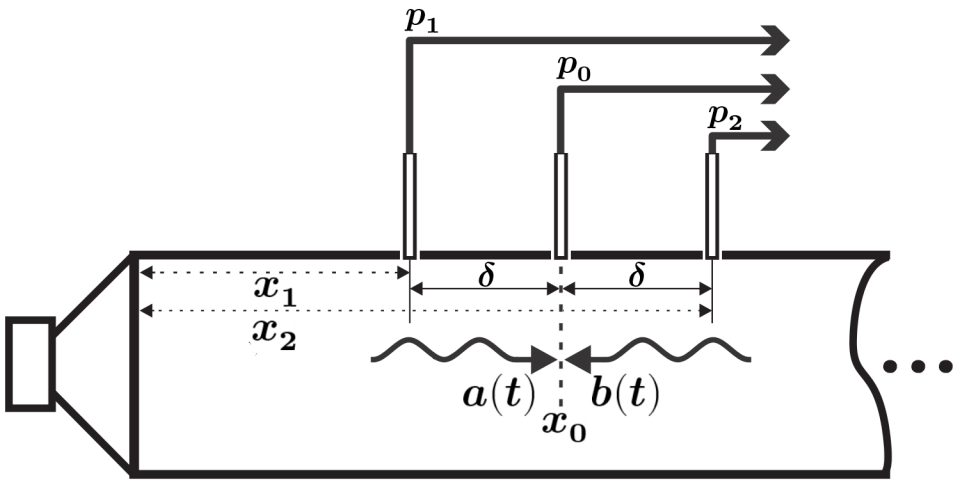

Figure 1.2: Cylindrical tube with three microphones mounted along its wall and a pressure driver located at the "upstream" (left) side.

chosen to be at x_0, which corresponds to the second microphone location; the two neighboring microphones will be at a distance δ from this reference point. Sound pressures $P_1(\omega)$, $P_0(\omega)$ and $P_2(\omega)$ can be expressed as:

$$P_1(\omega) = A(\omega)\, e^{+j\omega\tau} + B(\omega)\, e^{-j\omega\tau} \tag{1.6a}$$

$$P_0(\omega) = A(\omega) + B(\omega) \tag{1.6b}$$

$$P_2(\omega) = A(\omega)\, e^{-j\omega\tau} + B(\omega)\, e^{+j\omega\tau} \tag{1.6c}$$

The expressions in (1.6) define an over-determined algebraic system of equations, but some important properties can be readily seen: Eq. (1.6b) is identical to (1.3a), thus, the sound pressure at x_0 is simply $P(\omega) = P_0(\omega)$, which means that it can be obtained directly from the center microphone alone. Also, Eqs. (1.6a) and (1.6c) are the same as (1.1a) and (1.1b) which implies that the expression for $\rho_0 c_o U(\omega)$ for the three-microphone case is the same as (1.4b), which corresponds to the two-microphone case. After $P(\omega)$ and $\rho_0 c_o U(\omega)$ are obtained, $A(\omega)$ can be computed from (1.3c), and $B(\omega)$ can be obtained either from (1.3d) or from (1.6b) as $B(\omega) = P_0(\omega) - A(\omega)$.

To sum up, the required expressions for the three-microphone case are

$$P(\omega) = P_0(\omega) \tag{1.7a}$$

$$\rho_0 c_0 U(\omega) = \frac{P_1(\omega) - P_2(\omega)}{1 - e^{-2j\omega\tau}} e^{-j\omega\tau} \tag{1.7b}$$

These results greatly simplify the computational process at the expense of a more complex apparatus, also, adding an extra microphone requires higher manufacturing precision to insure that the distance between each pair is as exact as possible, since the equations assume that the microphone positioned at x_0 is exactly equidistant between the other two. This technique can be further expanded to consider an M number of microphones, which

will produce an $M \times 2$ system of M algebraic equations with two unknowns, to be solved for $A(\omega)$ and $B(\omega)$ in terms of the M number of sound pressure amplitudes; a result for this algebraic system can be obtained by employing a least-squares solution.

1.4 Stabilization by Means of Leaky Recursion

Most of the content in this section was extracted and paraphrased from [1].

The recursive time-domain expressions obtained in the previous sections for $p(t)$ and $\rho_0 c_0 u(t)$ are exact, however, the recursive terms make the system overly-sensitive to initial conditions or any other error sources which might arise during operation. One possible way to alleviate this is to introduce leaky recursion factors to obtain approximate equations [1]:

$$p'(t) = \alpha [p_1(t-\tau) + p_2(t-\tau)] - \beta p(t-2\tau) \tag{1.8a}$$
$$\rho_0 c_0 u'(t) = \alpha [p_1(t-\tau) - p_2(t-\tau)] + \beta \rho_0 c_0 u(t-2\tau) \tag{1.8b}$$

or equivalently:

$$P'(\omega) = \frac{\alpha [P_1(\omega) + P_2(\omega)]}{1 + \beta e^{-2j\omega\tau}} e^{-j\omega\tau} \tag{1.9a}$$
$$\rho_0 c_0 U'(\omega) = \frac{\alpha [P_1(\omega) - P_2(\omega)]}{1 - \beta e^{-2j\omega\tau}} e^{-j\omega\tau} \tag{1.9b}$$

where $\{\alpha, \beta \in \mathbb{R}^+ \mid 0 < \alpha < 1, 0 < \beta < 1\}$ are leaky recursion factors and they are chosen to be as close to 1 according to the criteria that will now be explained.

The travelling wave components can be estimated in the time domain as [1]:

$$a'(t) = (1/2)[p'(t) + \rho_0 c_0 u'(t)] \tag{1.10a}$$
$$b'(t) = (1/2)[p'(t) - \rho_0 c_0 u'(t)] \tag{1.10b}$$

It is possible then to define error tracking signals $e_p = p'(t) - p(t)$ and $e_u(t) = u'(t) - u(t)$, that satisfy the following equations [1]:

$$e_p(t) = (\alpha - 1) p(t-\tau) - (\beta - \alpha) p(t-2\tau) - \beta e_p(t-2\tau) \tag{1.11a}$$
$$e_u(t) = (\alpha - 1) u(t-\tau) + (\beta - \alpha) u(t-2\tau) + \beta e_u(t-2\tau) \tag{1.11b}$$

where frequency response functions can be expressed as [1]:

$$G_p(\omega) = E_p(\omega)/P(\omega) = \frac{(\alpha - 1) e^{-j\omega\tau} - (\beta - \alpha) e^{-2j\omega\tau}}{1 + \beta e^{-2j\omega\tau}} \tag{1.12a}$$
$$G_u(\omega) = E_u(\omega)/U(\omega) = \frac{(\alpha - 1) e^{-j\omega\tau} + (\beta - \alpha) e^{-2j\omega\tau}}{1 - \beta e^{-2j\omega\tau}} \tag{1.12b}$$

Eqs. (1.12) can be expanded using infinite series containing delay terms of the form $\pm\beta^k e^{-2kj\omega\tau}$, with absolute values proportional to β^k and delay times $t = 2k\tau$, such that $k \in \mathbb{Z}$. Hence, the effect due to unknown initial conditions and the amplitude envelope of eqs. (1.11) are weighted by the time factor $\beta^{t/2\tau}$, or in quadratic units: $\beta^{t/\tau}$ [1]. If a relative quadratic decay $\beta^{T/\tau} = 1/e$ in give relaxation time T is prescribed, we obtain [1]:

$$\beta = e^{-\tau/T} \approx 1 - \tau/T \tag{1.13a}$$

$$T = -\tau/\log\beta \approx \tau/(1-\beta) \tag{1.13b}$$

Therefore, β is related to the relaxation time T, which must be $T \gg \tau$ in order to bring β close to 1. After a fixed value of β is obtained, an optimum value for α can also be obtained, such that it minimizes the frequency average of the quadratic error calculated from the squared magnitude of the transfer functions: $|G_p(\omega)|^2$, $|G_u(\omega)|^2$, averaged in the frequency interval within $|\omega| \leq \pi/\tau$, or $|f| \leq 1/2\tau$, corresponding to the full spectral average for an equivalent digital formulation with sampling period τ [1]. In both cases, for G_p and G_u, the following optimum values are obtained [1]:

$$\alpha_{opt} = (1+\beta)/2 \tag{1.14a}$$

$$E^2_{min} = |G_p|^2_{min} = |G_u|^2_{min} = (1-\beta)/2 \approx \tau/T \tag{1.14b}$$

where $|G_p|^2_{min}$ and $|G_u|^2_{min}$ are the optimum values of the error transfer functions. It can be seen that the relative error diminishes as the value of β gets closer to 1, however, this also means that the tracking speed will be slower.

1.5 Figures of Merit

As far as this author's knowledge there is no standardized metric to characterize the accuracy of a TWSS, although most recently, two figures of merit have been proposed: the separation index Ψ [7], and the normalized travelling wave separation error E_{TWS} [1].

The use of a separation index Ψ expressed in dB which takes into account the sum of the normalized errors between the forward and backward travelling wave components $\Phi[k]$ with respect to the discrete frequency k within a specified bandwidth was initially proposed in [7] and further utilized in [8] and [18] as a reference.

The separation index is given as follows [7]:

$$\Psi = 10\log_{10}\left(\sum_{k=k_1}^{k_2}\Phi[k]\right) \tag{1.15}$$

where

$$\Phi[k] = \frac{|P_0[k] - A'[k]|^2}{N\eta^+} + \frac{|B[k]|^2}{N\eta^-} \tag{1.16a}$$

$$\eta^+ = \sum_{n=n_f}^{n_f+N-1} p_0^2[n] \tag{1.16b}$$

$$\eta^- = \sum_{n=n_b}^{n_b+N-1} p_0^2[n] \tag{1.16c}$$

N is the total number of samples and the terms $P_0[k]$, $A'[k]$ and $B[k]$ are the DFTs of the center microphone and the estimated forward and backward travelling waves, respectively.

The separation index is heavily reliant on time windowing to isolate the first reflection from the forward travelling wave, consequently, this requires a long enough tube to perform such isolation in the time-domain; a requirement that cannot always be met. The terms η^+ and η^- are the normalizing energies measured in the sample intervals for the time windows of the forward: $n_f \leq n < n_f + N$, and backward: $n_b \leq n < n_b + N$ travelling waves.

The separation index is not the best metric to validate the results in this work because it is really only applicable when a center microphone is present (i.e., when three microphones are being used), since the estimated waves and the sound pressure measured by the center microphone are both located in the same plane of reference. When only two microphones are used to perform travelling wave separation the estimated waves are located at a plane of reference midway between the two microphones, so the sound pressure being sensed by either of the two microphones does not correspond to the same reference plane of the estimated wave components. Also, as mentioned earlier, the separation index requires that the tube is long enough in order to isolate the forward and backward waves using time windowing and, in the case of the present work, the tube used for the experimental validation is not long enough to satisfy this requirement.

A different metric which accommodates more to the two- and three-microphone travelling wave separation arrangements is the normalized travelling wave separation error E_{TWS}, which was recently proposed in [1], and it is defined as follows:

$$E_{TWS}(\omega) = \frac{|A'(\omega) - A(\omega)|^2}{|A(\omega)|^2} + \frac{|B'(\omega) - B(\omega)|^2}{|A(\omega)|^2} \tag{1.17}$$

where $A'(\omega)$ and $B'(\omega)$ are the complex amplitudes of the estimated forward and backward travelling waves, whilst $A(\omega)$ and $B(\omega)$ are the reference travelling wave amplitudes obtained from the exact equations (non-stabilized equations).

Another useful figure of merit is the impulse response, which can be obtained with

respect to the forward reference waveform or to the tube excitation signal $X(\omega)$ as follows

$$h_{a'}(t) = \mathcal{F}^{-1}\left\{\frac{A'(\omega)}{A(\omega)}\right\} \tag{1.18a}$$

$$h_{b'}(t) = \mathcal{F}^{-1}\left\{\frac{B'(\omega)}{A(\omega)}\right\} \tag{1.18b}$$

or

$$h_{a'_x}(t) = \mathcal{F}^{-1}\left\{\frac{A'(\omega)}{X(\omega)}\right\} \tag{1.19a}$$

$$h_{b'_x}(t) = \mathcal{F}^{-1}\left\{\frac{B'(\omega)}{X(\omega)}\right\} \tag{1.19b}$$

$$h_{a_x}(t) = \mathcal{F}^{-1}\left\{\frac{A(\omega)}{X(\omega)}\right\} \tag{1.19c}$$

$$h_{b_x}(t) = \mathcal{F}^{-1}\left\{\frac{B(\omega)}{X(\omega)}\right\} \tag{1.19d}$$

Chapter 2

The Time Delay Operator Approximation (TDOA)

2.1 Introduction

Approximation theory is a well established field of classical mathematics, which seeks to obtain approximate solutions for many problems that cannot be solved analytically [30]. It is believed that the first published text in this area might date back to 1905 [31]. In the specific context of the present work, approximation theory is used to obtain approximate functions which, otherwise, could not be easily synthesized using electronic circuits.

A pure time delay equates to a $e^{-s\tau}$ operator in the frequency domain, where s is the complex frequency and τ is the delay time in seconds. Achieving the equivalent to this ideal time delay operator in discrete time is relatively simple, however, in the continuous time domain one has to resort to an approximation in order for the time delay to be physically realizable. One way this can be achieved is by means of a transfer function

$$H(s) = \prod_{k=1}^{M} \frac{C_k - D_k s\tau + E_k (s\tau)^2}{F_k + G_k s\tau + J_k (s\tau)^2} \approx e^{-s\tau} \tag{2.1}$$

henceforth referred to as a Time Delay Operator Approximation (TDOA). By proper selection of the C_k to J_k coefficients and the M number of stages, the complexity, accuracy and characteristics of a TDOA can be modified and tailored to suit a specific application.

Equation (2.1) may be separated into its even and odd parts as [32]

$$H(s) = H_{even}(s) + H_{odd}(s) \tag{2.2}$$

where

$$H_{even}(s) = \frac{1}{2}\left[H(s) + H(-s)\right] \tag{2.3a}$$

$$H_{odd}(s) = \frac{1}{2}\left[H(s) - H(-s)\right] \tag{2.3b}$$

are the even and odd parts, respectively.

To obtain the magnitude and phase response, the substitution $s = j\omega$ is performed in (2.2) and rewritten as [32]

$$H(\omega) = R(\omega) + jX(\omega) \tag{2.4}$$

where

$$R(\omega) = H_{even}(\omega) \tag{2.5a}$$

$$X(\omega) = \frac{1}{j}H_{odd}(\omega) \tag{2.5b}$$

represent the real and imaginary parts, respectively.

The magnitude response is then given by

$$|H(\omega)| = \sqrt{R^2(\omega) + X^2(\omega)} \tag{2.6}$$

while the phase response is obtained as

$$\phi(\omega) = \arctan\left[\frac{X(\omega)}{R(\omega)}\right] \tag{2.7}$$

A very important parameter, which will serve to quantify the delay characteristics of any given TDOA in the frequency domain, is the *group delay* $\tau_{gd}(\omega)$, defined as

$$\tau_{gd}(\omega) = -\frac{d}{d\omega}\phi(\omega) \tag{2.8}$$

which, by means of (2.5a), (2.5b) and (2.7), can be rewritten in terms of the real and imaginary parts of (2.4) as [32]

$$\tau_{gd}(\omega) = \frac{-R(\omega)\left[dX(\omega)/d(\omega)\right] + X(\omega)\left[dR(\omega)/d(\omega)\right]}{R^2(\omega) + X^2(\omega)} \tag{2.9}$$

The group delay of (2.1) as a function of the group delay of each individual k^{th} stage satisfies the following expression:

$$\tau_{gd}(\omega) = \sum_{k=1}^{M} \tau_{gd_k}(\omega) \tag{2.10}$$

In the following sections, different approximations and their implementation in a TDOA with electronic circuitry are presented; their main characteristics, advantages and disadvantages are discussed. The primary focus will be placed on the frequency response characteristics, whilst the transient or time-domain performance will be briefly mentioned. The use of approximation theory in the field of network functions is extremely vast, thus, only the most relevant aspects for the present work will be covered in this chapter.

2.1.1 Maclaurin Approximation

One of the most basic and popular methods to approximate analytic functions consists on using a Taylor series expansion, for the special case when the series is centered at zero it is called a Maclaurin series expansion. The expansion of the exponential time delay operator with a Maclaurin series can be performed as follows:

$$e^{-s\tau} = \frac{1}{e^{s\tau}} = \frac{1}{\sum_{n=0}^{\infty} \frac{(s\tau)^n}{n!}} \tag{2.11}$$

If the higher order terms are truncated for $n > 1$, the following transfer function is obtained

$$H(s) = \frac{1}{1 + s\tau} \tag{2.12}$$

Equation (2.12) represents a first-order TDOA; commonly used in control systems [33]. In the specific case of (2.12) it exhibits the same transfer function of a low-pass filter, which, entails some disadvantages: first, the resulting delay produced by the approximation drifts away from the value of the ideal time delay τ as the frequency increases. This can be best observed from (2.12) by making $s = j\omega$ and obtaining its group delay as in (2.8):

$$\tau_{gd}(\omega) = \frac{\tau}{1 + (\omega\tau)^2} \tag{2.13}$$

It can be seen from (2.13) that $\omega \to 0 \Rightarrow \tau_{gd} \to \tau$; but as soon as the frequency increases, the group delay of the filter starts to deviate more and more from the value of the ideal time delay τ. This effect can be lessened if the order of the approximation is increased, which would necessarily involve a low-pass filter of a higher order. A second inconvenience has to do with the magnitude response of the transfer function, since it involves a low-pass filter, the response will drop as the frequency increases. One alternative to solve this problem is to use a two-polynomial Maclaurin rational expansion:

$$e^{-s\tau} = \frac{e^{-s\tau/2}}{e^{s\tau/2}} = \frac{\sum_{n=0}^{\infty} \frac{(-s\tau/2)^n}{n!}}{\sum_{n=0}^{\infty} \frac{(s\tau/2)^n}{n!}} \tag{2.14}$$

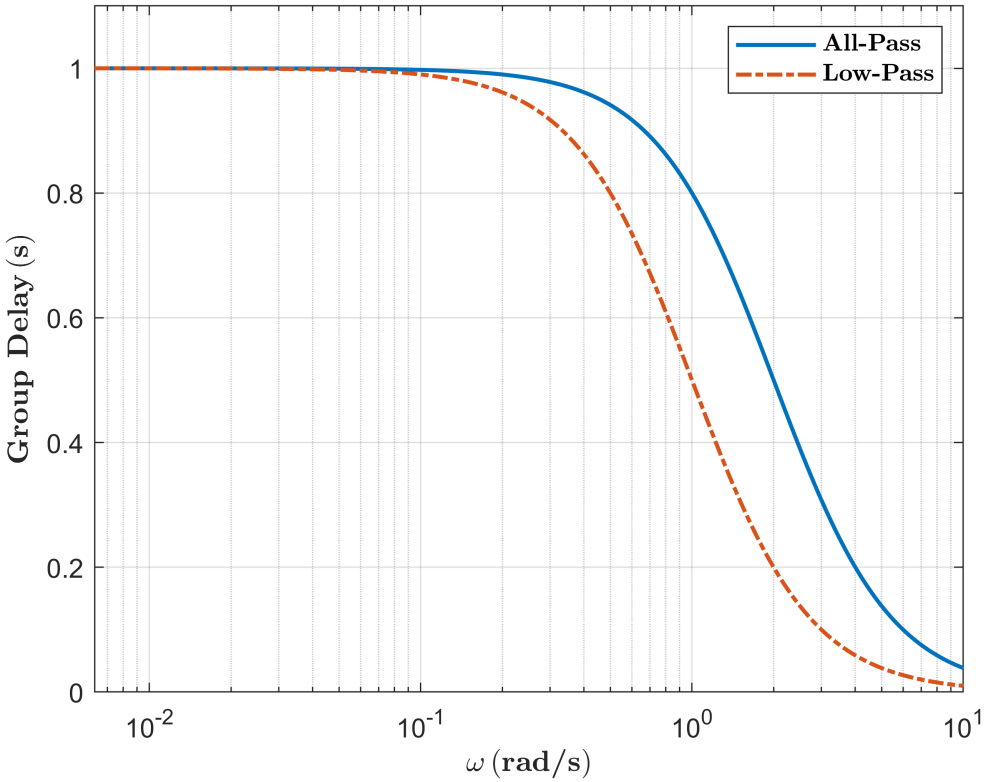

Figure 2.1: All- vs. Low-Pass group delay response of a Maclaurin first-order TDOA.

After truncating all the higher order terms for $n > 1$ the following TDOA is obtained:

$$H(s) = \frac{2 - s\tau}{2 + s\tau} \tag{2.15}$$

which exhibits an all-pass response, since $|H(j\omega)| = 1$ for all frequencies. The group delay is given by

$$\tau_{gd}(\omega) = \frac{\tau}{1 + (\omega\tau/2)^2} \tag{2.16}$$

The quantity $BW_{90} = \omega_L - \omega_H$ is now defined as the *group delay bandwidth*, where ω_L is the low frequency (usually, $\omega_L = 0$) and ω_H is the highest frequency at which $\tau_g = 0.9\tau$, then, from (2.13) and (2.16) we get:

$$BW_{90_{AP}} = 2BW_{90_{LP}} \tag{2.17}$$

where $BW_{90_{AP}}$ and $BW_{90_{LP}}$ are the group delay bandwidths of the all-pass and low-pass approximations, respectively.

This effect is clearly shown in Fig. 2.1, which displays the group delay response of (2.13) and (2.16) for a unit time delay. It becomes evident that the all-pass type approximation is superior to the low-pass type, both with respect to its magnitude response and group delay bandwidth; this wider group delay bandwidth is directly a result of the all-pass response,

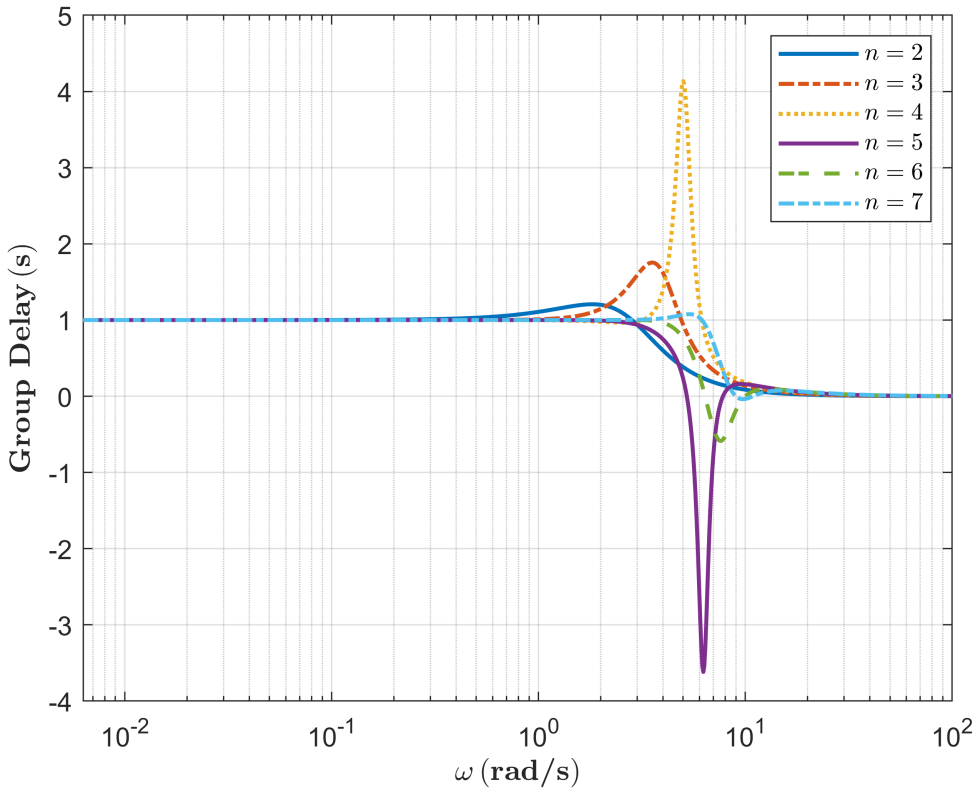

Figure 2.2: Group delay response comparison between different Maclaurin all-pass type approximations using n^{th} degree polynomials.

which is a type of non-minimum phase transfer function. However, if one keeps increasing the order of the Maclaurin all-pass type TDOA by taking into account terms higher than $n > 1$, the resulting group delay response becomes non-monotonic. Furthermore, the transfer function becomes unstable for $n > 4$ [34].

Figure 2.2 shows the group delay response for different Maclaurin all-pass type TDOAs of n^{th} order and $\tau = 1$ s. As can be seen, the response becomes highly non-monotonic as the value of n is increased; moreover, for $n > 4$ it exhibits regions where the group delay becomes negative, this implies a time advance rather than a time delay; something unachievable with a practical real-time causal system.

2.2 Monotonic Approximations

2.2.1 Padé Approximation

The problem of the loss of monotonicity in the group delay response that appears for $n > 1$ using the Maclaurin approximation, can be solved by using the Padé approximation, which may be defined as "the generalization of Taylor polynomials to rational approximation,

that is, rational interpolation at a single point" [31]. For increasing orders the poles of the Padé approximation remain stable and tend to group with each other, although in general its use is recommended for $n \leq 10$ [34], depending on the application.

The general form is as follows [30]:

$$S^{[n,m]}(x) = \frac{R_n(x)}{Q_m(x)} \tag{2.18}$$

where $R_n(x)$ and $Q_m(x)$ are polynomials in x of order n and m, respectively. The approximation becomes most accurate when $m = n$ or $m = n - 1$ [30].

If a Taylor series

$$S(x) = \sum_{N=0}^{\infty} c_N x^N \tag{2.19}$$

is approximated using $m = n$, Eq. (2.18) becomes [30]

$$S^{[n,m]}(x) \approx \frac{r_0 + r_1 x + r_2 x^2 + \cdots + r_n x^n}{1 + q_1 x + q_2 x^2 + \cdots + q_n x^n} \tag{2.20}$$

Thus, $S(x) - S^{[n,m]}(x)$ consists of a power series in which the lowest exponent of x is $2n+1$. All the remaining terms after the subtraction operation are represented by $\mathcal{O}(x^{2n+1})$ [30]:

$$\begin{aligned} S(x) - S^{[n,m]}(x) &= \left(1 + q_1 x + q_2 x^2 + \cdots + q_n x^n\right) \sum_{N=0}^{\infty} c_N x^N \\ &- \left(r_0 + r_1 x + r_2 x^2 + \cdots + r_n x^n\right) \\ &= \sum_{k=2n+1}^{\infty} r_k x^k \equiv \mathcal{O}\left(x^{2n+1}\right) \end{aligned} \tag{2.21}$$

The conclusion derived from (2.21) is that all the x terms, which have powers of $k \leq 2n$ for $k = 0, 1, \cdots, 2n$ must be zero. This results in a linear system of equations in terms of r_k and q_k, making it possible to compute numerical solutions for the coefficients of (2.20).

The Padé TDOA for $S(x) = e^x$, $x = -s\tau$ and $m = n$ can be obtained from [35]:

$$S^{[n,n]}(x) = H(s) = \frac{\sum_{k=0}^{n} \frac{(n+k)!}{k!\,(n-k)!} (-s\tau)^{n-k}}{\sum_{k=0}^{n} \frac{(n+k)!}{k!\,(n-k)!} (s\tau)^{n-k}} \tag{2.22}$$

Notice that for $n = 1$, (2.22) reduces to (2.15).

The second-order Padé TDOA will be referenced many times in the present work, thus,

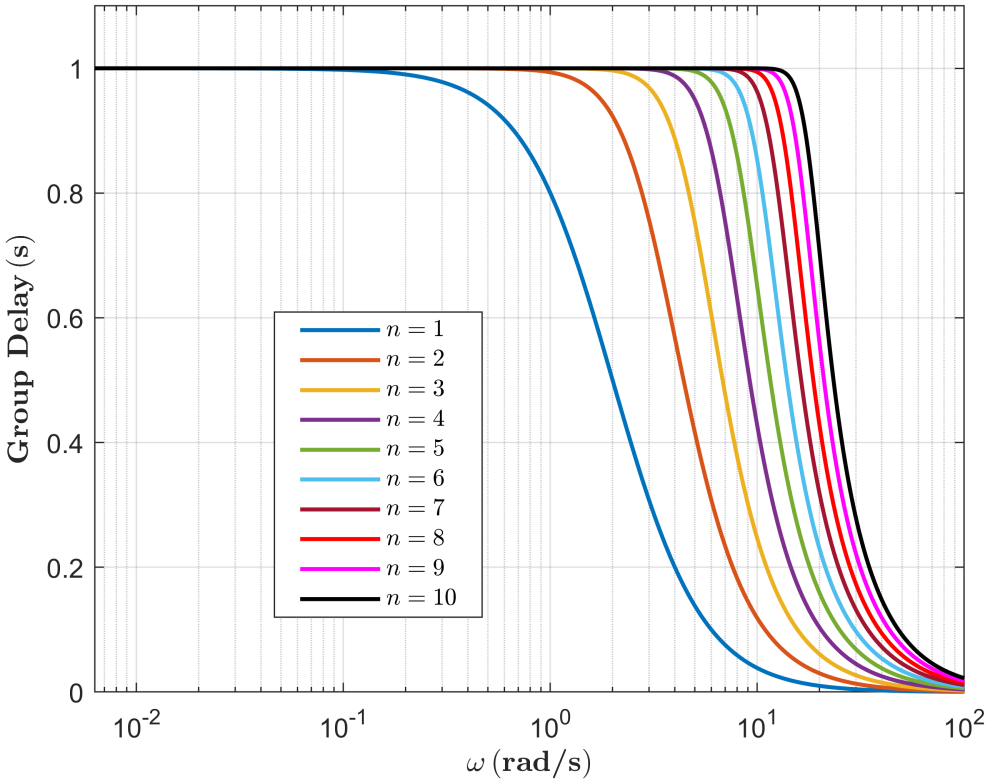

Figure 2.3: Group delay response comparison for Padé TDOAs up to $n = 10$.

it is now introduced:

$$H(s) = \frac{12 - 6s\tau + (s\tau)^2}{12 + 6s\tau + (s\tau)^2} \tag{2.23}$$

Figure 2.3 shows the different group delay responses up to $n = 10$ for the Padé TDOA of Eq. (2.22). As expected, increasing the order of the polynomials increases the bandwidth and the slope of the curve.

2.2.1.1 Relationship with Bessel Polynomials

Bessel polynomials are frequently used in filter design, the main characteristic of these type of filters is that they exhibit linear phase and maximally flat group delay within a specified bandwidth. The canonical form of a Bessel filter is [36]:

$$H(s) = \frac{1}{\sum_{k=0}^{n} a_k s^k} \tag{2.24}$$

where $a_0 = 1$ and

$$a_{k+1} = \frac{2(n-k)}{(2n-k)(k+1)} a_k, \; k = 0, 1, \cdots, n-1. \tag{2.25}$$

In an all-pass transfer function the numerator polynomial has the same coefficients of the denominator polynomial but with alternating signs, therefore, to obtain an all-pass type Bessel TDOA, Eq. (2.24) can be modified as follows:

$$H(s) = \frac{\sum_{k=0}^{n} a_k \left(\frac{-s\tau}{2}\right)^k}{\sum_{k=0}^{n} a_k \left(\frac{s\tau}{2}\right)^k} \tag{2.26}$$

where $a_0 = 1$ and the remaining a_k coefficients are calculated as in (2.25). The time delay division by two is required in order to obtain the same group delay produced by (2.24) at $\omega_L = 0$ for the same value of n, for the reasons described in Section 2.5.

The formula in (2.26) produces exactly the same transfer function as (2.22), it then follows that the all-pass Bessel and Padé TDOAs are equivalent.

2.2.2 Step Response of a TDOA

When analyzed in the frequency domain, the all-pass type TDOAs have some advantages over the low-pass types (as discussed in Section 2.1.1), however, when analyzed in the time domain, the low-pass type TDOAs—generally speaking—will exhibit a smoother and more predictable step response than the all-pass type approximations. This is illustrated in Fig. 2.4, where the step responses of the low-pass Bessel and all-pass Padé TDOAs for $\tau = 1$ s and $n = 4$ are shown. It can be seen that, even though the low-pass Bessel TDOA presents a longer rise time than the all-pass Padé TDOA, it might be better suited for signals with very fast transition times if the preservation of the wave shape integrity of the delayed signal is a design parameter of upmost importance. Different all-pass approximations might achieve a better step response than the Padé approximation, however, this usually means that the group delay response will exhibit a more narrow bandwidth.

It should be clear now that the selection of a particular approximation becomes a trade-off between step response, flatness and bandwidth of the group delay response.

2.2.3 The Laguerre Formula

Another monotonic all-pass TDOA can be attained with the so-called *Laguerre Formula* [37]:

$$H(s) = \left(\frac{2 - s\tau/n}{2 + s\tau/n}\right)^n \tag{2.27}$$

where $n \in \mathbb{Z}^+$.

It contains only one pole of multiplicity n and its name derives from the fact that it resembles the Laplace transform of Laguerre functions [37]. Its group delay response exhibits

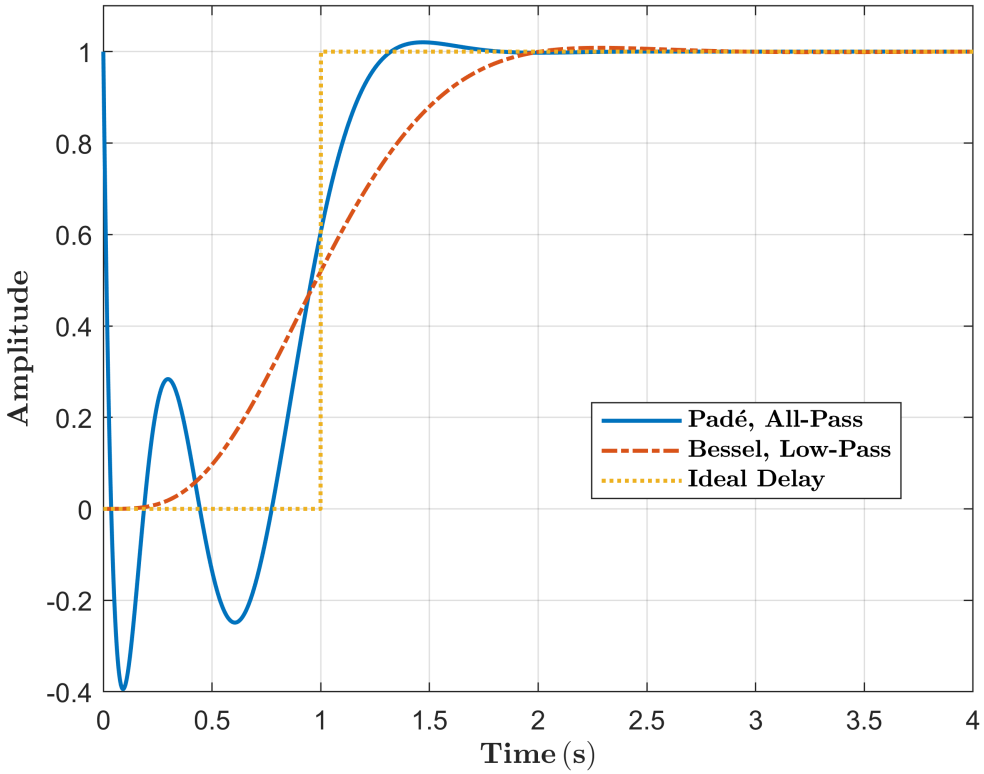

Figure 2.4: Step response comparison for all-pass Padé and low-pass Bessel TDOAs, $n = 4$, $\tau = 1$ s.

a more gentle slope and a narrower bandwidth than the Padé approximation of the same order. Essentially, the Laguerre formula can be conceptualized as the cascade connection of an n number of identical stages implementing first-order Padé approximations, with the total desired delay divided equally among each stage. Its group delay response can be observed in Fig. 2.11 and, as can be seen, the group delay bandwidth achieved with this approximation is very narrow, however, the strength of this type of TDOA lies on its behavior in the time-domain; since all of its poles are equal and real it will provide a step response with no overshoot even though the variations before the step initiates are still present and even more accentuated in the Laguerre Formula TDOA when compared to the Padé TDOA. This is shown along with the step response of a Padé approximation of the same order ($n = 8$) in Fig. 2.5.

2.2.4 The Padé-Kautz Approximation

The Padé-Kautz approximation, commonly known as the Kautz shift operator due to its primary application in time-delay system analysis and control [38], obtains its formulation based on Kautz functions [39, 40]. Simply speaking, it follows the same logic of the Laguerre Formula described in the previous section (2.2.3), but rather than being comprised of an n number of equal first-order Padé sections, it consists of the product of M identical second-order Padé approximations as given by [40]

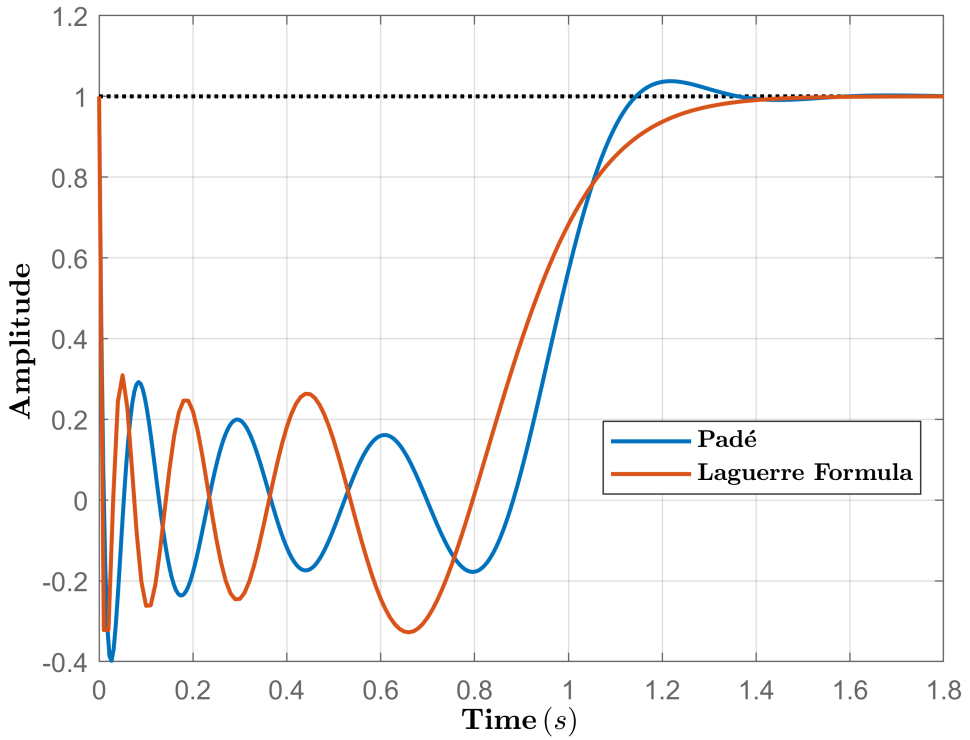

Figure 2.5: Step response comparison between Padé and Laguerre Formula TDOAs, $n = 8$, $\tau = 1$ s.

$$H(s) = \left[\frac{12 - 6s\tau/M + (s\tau/M)^2}{12 + 6s\tau/M + (s\tau/M)^2}\right]^M \tag{2.28}$$

where $\{n, M \in \mathbb{Z}^+ \mid n = 2M\}$.

The results are similar to a regular Padé approximation but with a smaller bandwidth (see Fig. 2.6), nevertheless, the step response exhibits less overshoot; this becomes more evident at higher values of n as can be seen in Figure 2.7.

2.3 Non-Monotonic Approximations

If some amount of ripple in the pass band of the group delay response becomes acceptable in a particular application, the following approximations can achieve a larger bandwidth than those previously presented in Sections 2.1.1-2.2.3 given the same value of n.

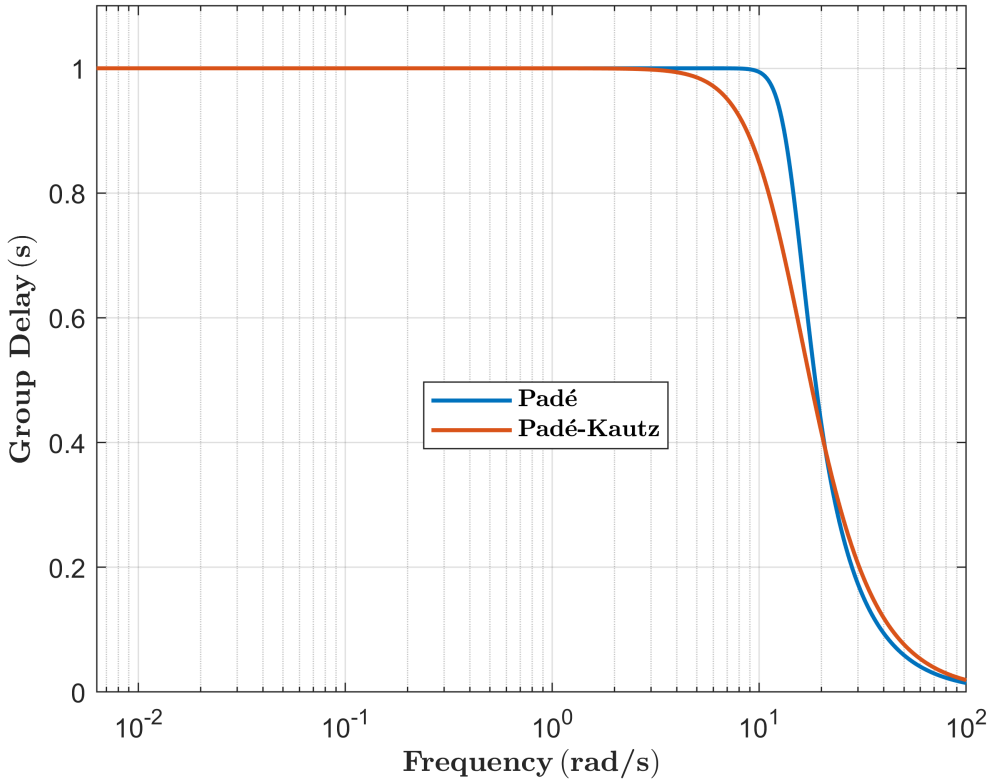

Figure 2.6: Group delay response comparison between Padé and Padé-Kautz TDOAs, $n = 8$, $\tau = 1$ s.

2.3.1 The Piché Product Formula

The ideal delay exponential operator can be expressed with the following identity:

$$e^{-s\tau} = \frac{\cosh(s\tau/2) - \sinh(s\tau/2)}{\cosh(s\tau/2) + \sinh(s\tau/2)} \tag{2.29}$$

whilst the hyperbolic sine and cosine functions can be expanded in terms of a product series as

$$\sinh\left(\frac{s\tau}{2}\right) = \prod_{k=1}^{\infty}\left[1 + \frac{(s\tau)^2}{(2k-1)^2\pi^2}\right] \tag{2.30a}$$

$$\cosh\left(\frac{s\tau}{2}\right) = \frac{s\tau}{2}\prod_{k=1}^{\infty}\left[1 + \frac{(s\tau)^2}{4k^2\pi^2}\right] \tag{2.30b}$$

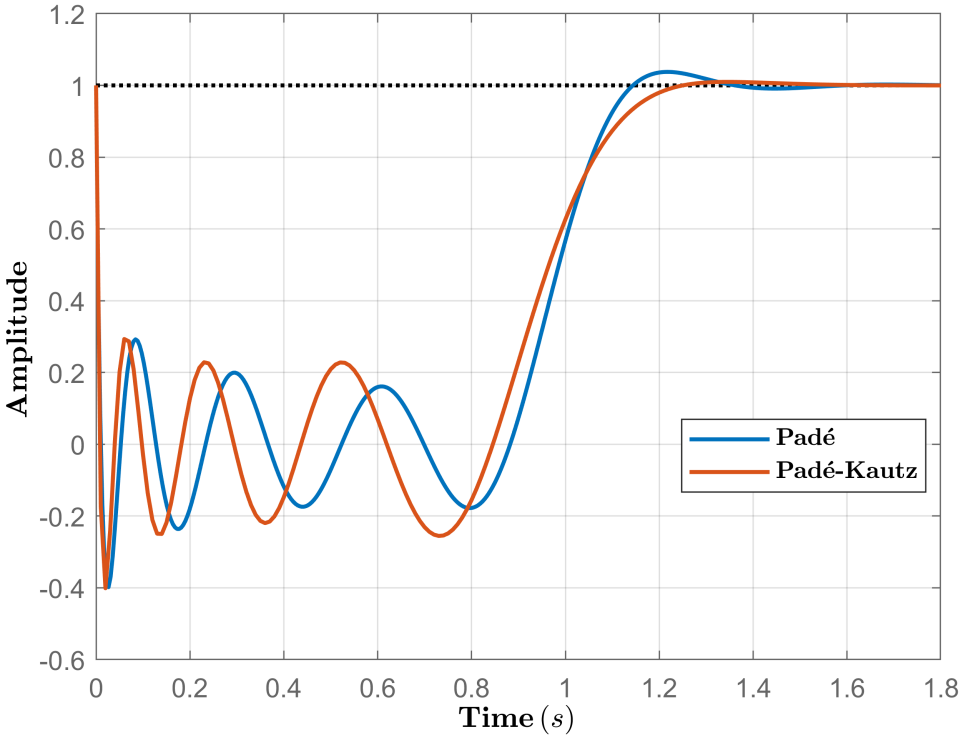

Figure 2.7: Step response comparison between Padé and Padé-Kautz TDOAs, $n = 8$, $\tau = 1$ s.

By employing (2.29) and (2.30) the Piché Product formula is obtained [35]:

$$e^{-s\tau} = \frac{\prod_{k=1}^{\lfloor n/2 \rfloor} \left[1 + \frac{(s\tau)^2}{(2k-1)^2 \pi^2}\right] - \frac{s\tau}{2} \prod_{k=1}^{\lfloor (n-1)/2 \rfloor} \left[1 + \frac{(s\tau)^2}{4k^2\pi^2}\right]}{\prod_{k=1}^{\lfloor n/2 \rfloor} \left[1 + \frac{(s\tau)^2}{(2k-1)^2 \pi^2}\right] + \frac{s\tau}{2} \prod_{k=1}^{\lfloor (n-1)/2 \rfloor} \left[1 + \frac{(s\tau)^2}{4k^2\pi^2}\right]} \tag{2.31}$$

where the notation $\lfloor \cdot \rfloor$ represents the floor function and means take the integer part.

Figure 2.8 shows plots for different values of n up to six. As can be seen, the amount of ripple and the level of the final last peak increases considerably as the order n of the approximation increases.

2.3.2 Stubbs-Single Approximation

Stubbs and Single [41] presented an approximation based on the following formulation:

$$e^{-4\zeta\tau s} = \lim_{r \to \infty} \left[\frac{1 - 2\zeta s\tau/r + (s\tau/r)^2}{1 + 2\zeta s\tau/r + (s\tau/r)^2}\right]^r \tag{2.32}$$

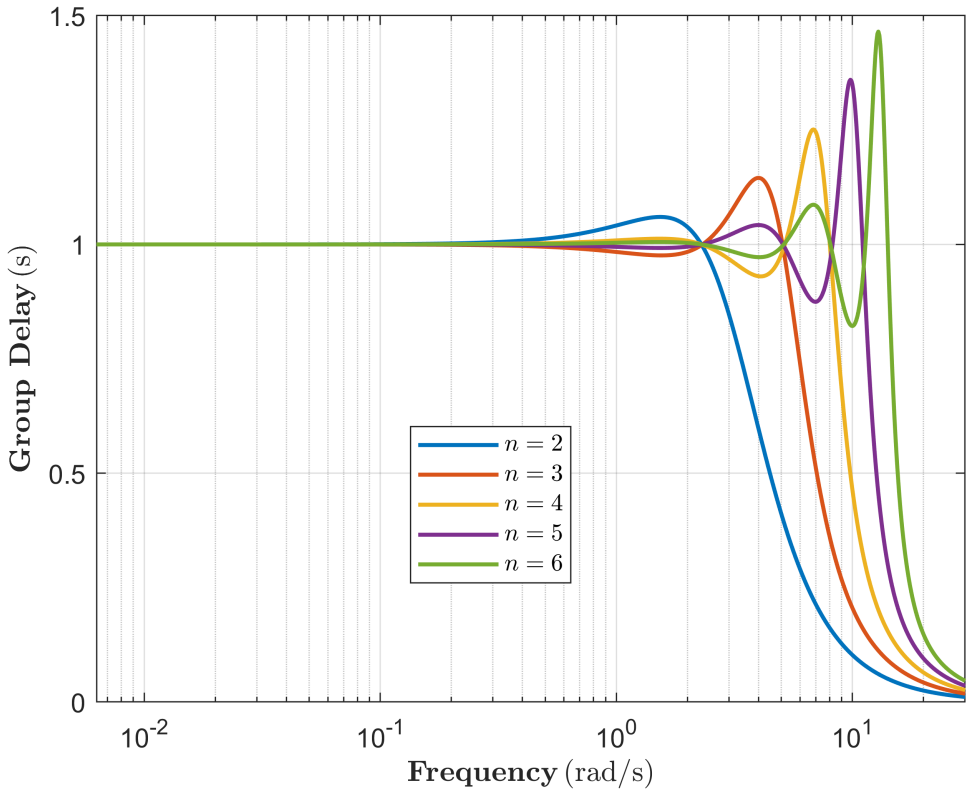

Figure 2.8: Group delay response of the Piché Product formula TDOA, $\tau = 1$ s.

indicating that the resulting delay is equal to $4\zeta\tau$. In practice, r must adopt a finite value. If $r = 1$, (2.32) reduces to the canonical form of a second-order all-pass transfer function:

$$H(s) = \frac{1 - 2\zeta s\tau + (s\tau)^2}{1 + 2\zeta s\tau + (s\tau)^2} \tag{2.33}$$

which produces $\tau_{gd} \approx 4\zeta\tau$ for low frequencies.

The *phase error* $\delta(\omega)$ that exists between the phase $\phi_0(\omega)$ of a pure time delay and the phase $\phi(\omega)$ of a TDOA, as obtained from (2.7), is defined as

$$\delta(\omega) = \phi(\omega) - \phi_0(\omega) \tag{2.34}$$

It is possible to select a value for ζ that is able to produce maximum phase displacement and minimum phase error. In the specific case of (2.33), the optimum value $\zeta = \sqrt{3}/2$ is given in [41] and was determined by means of a semi-graphical method.

In a pure time delay the value of $\phi_0(\omega)$ varies linearly with respect to frequency, but the same thing can not be said of $\phi(\omega)$, therefore, Stubbs and Single [41] point out that if the TDOA consists of a product of two second-order all-pass transfer functions with different values of ζ and τ, it is possible to make the phase error $\delta_1(\omega)$ of the first transfer function to partially cancel out the phase error $\delta_2(\omega)$ of the second one by proper selection of ζ_1, ζ_2,

τ_1 and τ_2. This process can be extended to an M number of second-order function products, resulting in a TDOA of order $n = 2M$:

$$H(s) = \prod_{k=1}^{M} \frac{1 - 2\zeta_k s\tau_k + (s\tau_k)^2}{1 + 2\zeta_k s\tau_k + (s\tau_k)^2} \tag{2.35}$$

and

$$\tau_{gd}(\omega) \approx \sum_{k=1}^{M} 4\zeta_k \tau_k \tag{2.36}$$

for low frequencies.

Design values for ζ_k and τ_k, as presented in [41] for $M = 2, 4$, are shown in Table 2.1.

$\boldsymbol{M}$	$\boldsymbol{\zeta_1}$	$\boldsymbol{\zeta_2}$	$\boldsymbol{\zeta_3}$	$\boldsymbol{\zeta_4}$	$\boldsymbol{\tau_1/\tau_2}$	$\boldsymbol{\tau_1/\tau_2}$	$\boldsymbol{\delta_{MAX}}$ (rad)
2	$\sqrt{3}/2$	$2/5$	-	-	1.68	-	0.021
4	$\sqrt{3}/2$	$2/5$	1	$1/2$	1.68	1.14	0.016

Table 2.1: Design values for a Stubbs-Single TDOA [41]

An important remark needs to be made: for the case of $M = 1$, the delay time value τ can be expressed in terms of the group delay by means of (2.36) as

$$\tau = \frac{\hat{\tau}}{4\zeta} \tag{2.37}$$

where $\hat{\tau}$ is a fixed value for the group delay at $\omega = 0$. It was already mentioned that $\zeta = \sqrt{3}/2$ is the optimum value when $M = 1$, in this case, if (2.37) is substituted in (2.35), the latter reduces to the same transfer function of (2.23), which means that the Padé and Stubbs-Single TDOAs are equivalent for $n = 2$ if the value of τ in (2.35) is selected in such a way that the resulting group delay of both TDOAs becomes the same at $\omega = 0$. As a consequence, the Stubbs-Single approximation is only relevant for $M \geq 2$.

The Stubbs-Single approximation provides a very large amount of group delay bandwidth, but it also exhibits a very high level of ill-defined ripple.

2.3.3 Hepner Approximation

The following formulation based on the approximation of a tangent function, which then was used to approximate and ideal delay was developed by Hepner [42]:

$$\tan\left(\frac{\omega\tau}{2}\right) \approx L\left(\frac{\omega\tau}{2}\right) \frac{\left[\left(\frac{\omega\tau}{2}\right)^2 - \pi^2\right]}{\left[\left(\frac{\omega\tau}{2}\right)^2 - \pi^2\right]\left[\left(\frac{\omega\tau}{2}\right)^2 - V^2\right]} \tag{2.38}$$

where V is a user selectable pole and L is a factor, in terms of V, that makes $\tan(\omega\tau/2) = 1$ when $\omega\tau = \pi/2$.

It can be shown [42] that (2.38) can be rewritten in such a way that it represents the phase of the following polynomial, which will serve to find the characteristic equation for the transfer function of the TDOA:

$$4\pi^2V^2 - 8L\pi^2 s\tau + \left(4V^2 + \pi^2\right) s^2\tau^2 - 2Ls^3\tau^3 + s^4\tau^4 \tag{2.39}$$

where

$$L = \frac{-3\pi^2 + 48V^2}{-60\pi^2} \tag{2.40}$$

and the value of V is obtained by a trial and error. After the optimal values for V and L are found, equation (2.39) becomes the denominator of the desired transfer function, the numerator will be the same but with alternating signs in order to produce an all-pass response.

Variations of (2.38) with more or less poles and zeros can serve to find other polynomials of even degree, for odd degree polynomials the procedure is very similar to the one just described, but the following equation is used [42]:

$$\tan\left(\frac{\omega\tau}{2}\right) \approx L\left(\frac{\omega\tau}{2}\right) \frac{\left[\left(\frac{\omega\tau}{2}\right)^2 - \pi^2\right]\left[\left(\frac{\omega\tau}{2}\right)^2 - Z^2\right]}{\left[\left(\frac{\omega\tau}{2}\right)^2 - \pi^2\right]\left[\left(\frac{\omega\tau}{2}\right)^2 - \left(\frac{3\pi}{2}\right)^2\right]} \tag{2.41}$$

where Z is a user selectable zero. Again, an expression for L such that $\tan(\omega\tau/2) = 1$ when $\omega\tau = \pi/2$ is found and the value of Z is obtained by trial and error. Adding more or less zeros to (2.41) achieves different odd order polynomials.

Transfer functions up to $n = 6$ are shown in Table 2.2 [42].

$\boldsymbol{n}$	$\boldsymbol{H(s)}$
2	$\dfrac{11.51 - 5.756s\tau + (s\tau)^2}{11.51 + 5.756s\tau + (s\tau)^2}$
3	$\dfrac{102.3 - 51.31s\tau + 10.36(s\tau)^2 - (s\tau)^3}{102.3 + 51.31s\tau + 10.36(s\tau)^2 + (s\tau)^3}$
4	$\dfrac{1193 - 595.3s\tau + 130.8(s\tau)^2 - 15.08(s\tau)^3 + (s\tau)^4}{1193 + 595.3s\tau + 130.8(s\tau)^2 + 15.08(s\tau)^3 + (s\tau)^4}$
5	$\dfrac{17933 - 8977s\tau + 2019(s\tau)^2 - 266.9(s\tau)^3 + 20.46(s\tau)^4 - (s\tau)^5}{17933 + 8977s\tau + 2019(s\tau)^2 + 266.9(s\tau)^3 + 20.46(s\tau)^4 + (s\tau)^5}$
6	$\dfrac{311490 - 155594s\tau + 35944(s\tau)^2 - 4927(s\tau)^3 + 454(s\tau)^4 - 24.96(s\tau)^5 + (s\tau)^6}{311490 + 155594s\tau + 35944(s\tau)^2 + 4927(s\tau)^3 + 454(s\tau)^4 + 24.96(s\tau)^5 + (s\tau)^6}$

Table 2.2: Transfer functions up to $n = 6$ for the Hepner approximation [42].

2.3.4 Approximations Using Equiripple Type Functions

Equiripple type functions are commonly used in the design of filters to obtain larger magnitude response bandwidths, whilst still being able to exert some control over its ripple characteristics. Conversely, in the design of TDOAs the main focus lies on using such functions to control the ripple characteristics of the group delay response in order to extend its bandwidth, whilst keeping a flat magnitude response over the entire frequency span. Group delay bandwidth and ripple are directly related, which means that, given a fixed value for n, increasing the bandwidth also implies increasing the amount of ripple.

Some of these type of approximations are now discussed.

2.3.4.1 Elliptic

Consider the following second-order transfer function:

$$H(s) = \frac{1 - KWs\tau + W(s\tau)^2}{1 + KWs\tau + W(s\tau)^2} \tag{2.42}$$

Kiseda and Ford [43] suggest that its group delay can be forced to adopt the form of an elliptic function by differentiating its phase with respect to the angular frequency and making it equal to the desired response:

$$\frac{d\phi}{d\omega} = \left[\frac{KW + KW^2(\omega\tau)}{1 + (K^2W^2 - 2W)(\omega\tau)^2 + W^2(\omega\tau)^4}\right] = \frac{-1}{\sqrt{1 - k^2\sin^2(\omega\tau)}} \tag{2.43}$$

To obtain equations for coefficients W and K in terms of the ripple factor k, the denominator of the right hand term is then expanded by means of a binomial series and only the the first three terms are retained; the resulting expressions become [43]

$$W = \frac{1 + 2k^2}{12} \tag{2.44a}$$

$$K = \frac{6}{1 + 2k^2} \tag{2.44b}$$

It is no surprise that if the amount of ripple is set to zero ($k = 0$), equation (2.42) reduces to the second-order Padé TDOA of (2.23).

The fourth order TDOA is defined as the following product [43]:

$$H(s) = \frac{1 - KWs\tau + W(s\tau)^2}{1 + KWs\tau + W(s\tau)^2} \times \frac{1 - LMWs\tau + MW(s\tau)^2}{1 + LMWs\tau + MW(s\tau)^2} \tag{2.45}$$

Following a similar procedure as before, the right hand side denominator of (2.43) is expanded with a binomial series and only the first five terms are retained. The resulting system of equations is very complex so obtaining closed form expressions for W, K, L and M might not be possible. Numerical solutions for different k values can be found in [43].

2.3.4.2 Chebyshev

The use of Chebyshev rational polynomials can achieve a group delay response which exhibits equiripple in its pass-band, just as the type one would observe from the magnitude response of low-pass filters that employ Chebyshev polynomials.

The group delay as a function of s can be expressed as [44]

$$\tau_{gd}(s) = \tau_{gd}(0) - k\tau_{gd_R}(s) \tag{2.46}$$

where $\tau_{gd}(0)$ is the DC group delay, k is the ripple factor, and $\tau_{gd_R}(s)$ is a Chebyshev rational function given by

$$\tau_{gd_R}(s) = \frac{1}{2}\left(\prod_{v=1}^{n}\frac{z-z_v}{-z-z_v} + \prod_{v=1}^{n}\frac{-z-z_v}{z-z_v}\right) \tag{2.47}$$

and

$$z^2 = \frac{s^2+1}{s^2} \tag{2.48a}$$

$$z_v^2 = \frac{s_v^2+1}{s_v^2},\ v = 1, 2, \cdots, n \tag{2.48b}$$

If a series of conditions are satisfied and values for k and n are specified, the poles of the TDOA can be determined by numerically solving the n number of equations produced by [44]

$$\frac{\left(z_\mu^2-1\right)^{3/2}}{z_\mu^2} + k\prod_{\substack{v=1\\ \mu\neq v}}^{n}\frac{-z_\mu - z_v}{z_\mu - z_v} = 0,\ \mu = 1, 2, \cdots, n \tag{2.49}$$

Tables with pole values for $2 \leq n \leq 10$ and prescribed values of k can be found in [44].

As can be seen from Fig. 2.9 for $n = 4$, $n = 5$, $k = 0.1$ and $\tau = 1$ s, the amount of ripple is perfectly defined. It can be observed that this type of approximation is not capable of achieving $\tau_{gd}(0) = \tau$ whilst producing an equiripple characteristic around τ, if $\tau_{gd}(0) = \tau$ is a requirement, the transfer function must be normalized; the result is that all the variations will develop either above the value $\tau_{gd}(\omega) = \tau$ (for $n = even$) or below it (for $n = odd$).

A similar approach which uses Chebyshev equiripple type functions to obtain a low-pass TDOA can be found in [45].

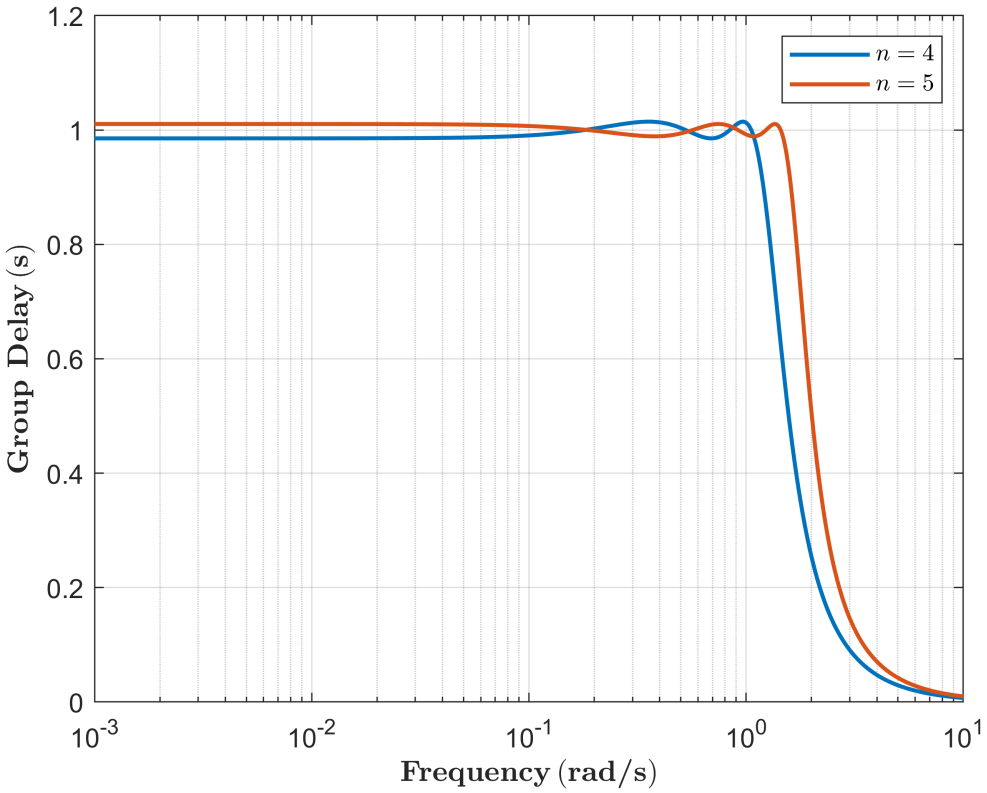

Figure 2.9: Group delay response comparison of the Chebyshev TDOA: $k = 0.1$ and $\tau = 1$ s.

2.3.4.3 Equiripple Optimization

Another way to obtain a group delay response which exhibits equiripple in the group delay response, can be accomplished by defining a target transfer function and employing numerical optimization to compute the coefficients for some specified amount of group delay ripple [35].

2.3.5 Error Minimization Approximations

Some approximations can be accomplished by minimizing the amount of error based on a specific metric or method, this allows the possibility to find coefficients for the best approximation within a prescribed bandwidth.

2.3.5.1 Chebyshev Norm

Hausner and Furlani [46] proposed an approximation which uses a Chebysev norm. Given a maximum allowable error ϵ, a specified group delay bandwidth, and the order of the approximation n, it is possible to obtain the best Chebyshev approximation in the form of an all-pass transfer function. While the results do not exhibit an equiripple response, the

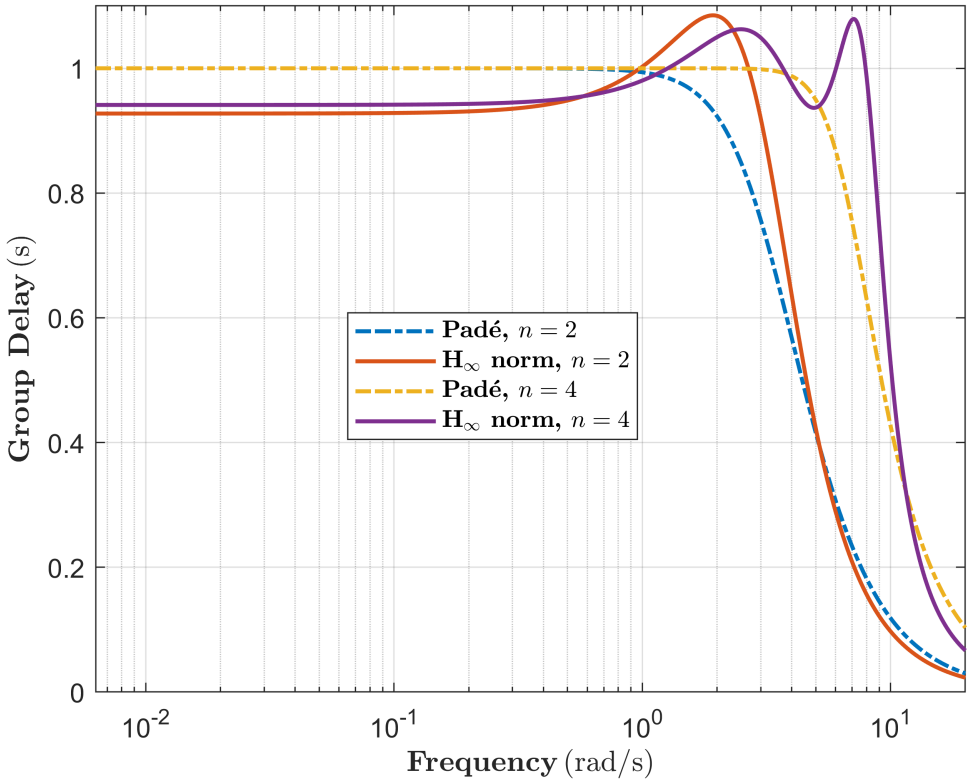

Figure 2.10: Group delay response of the H_∞ norm approximation with $n = 4$, $\tau = 1$ s. Traces of Padé approximations of the same order are included for comparison purposes

amount of ripple is directly relatable to the level of error ϵ selected, which in turn defines the bandwidth of the approximation.

TDOA coefficients for different values of ϵ up to $n = 12$ can be found in [46]. Figure 2.11 shows plots for $\epsilon = 0.005$ and $\epsilon = 0.020$, $\tau = 1$ s and $n = 4$.

2.3.5.2 H_∞ Norm Minimization

Al-Amer and Al-Sunni [47] employ the minimization of an H_∞ norm to obtain rational approximations for $e^{-s\tau}$. When compared to the Padé approximation, this method can achieve a lower error over a specified frequency range; for instance, the 2nd order approximation can achieve the same error as a 3rd order Padé approximation, whilst a 3rd order approximation is able to attain a lower error than a 4th order Padé approximation. Event though it is capable of providing a very large bandwidth it also presents a very high amount of ripple. Figure 2.10 shows the group delay response for $n = 2$ and $n = 4$, Padé approximations of the same order are included for comparison purposes.

Transfer functions up to $n = 4$ are shown in Table 2.3 [47].

n	$H(s)$
1	$\dfrac{1.7838 - s\tau}{1.7838 + s\tau}$
2	$\dfrac{9.732644 - 4.513319s\tau + (s\tau)^2}{9.732644 + 4.513319s\tau + (s\tau)^2}$
3	$\dfrac{77.300063 - 41.150766s\tau + 7.614365(s\tau)^2 - (s\tau)^3}{77.300063 + 41.150766s\tau + 7.614365(s\tau)^2 + (s\tau)^3}$
4	$\dfrac{921.489126 - 433.667527s\tau + 105.120715(s\tau)^2 - 10.833948(s\tau)^3 + (s\tau)^4}{921.489126 + 433.667527s\tau + 105.120715(s\tau)^2 + 10.833948(s\tau)^3 + (s\tau)^4}$

Table 2.3: Transfer functions up to $n = 4$ obtained by H_∞ norm minimization [47].

2.4 Comparison

The approximations mentioned up to this point are just some of those reported in the literature, summaries and reviews of more of them can be found in [48, 49], and other sources. It is important, however, that their characteristics are compared, therefore, some of the approximations mentioned in the previous sections are now plotted in Fig. 2.11. All of them correspond to a fourth order TDOA with $\tau = 1$ s. Notice the vertical axis scale, which has been limited to $0.9 - 1.025$ s to make it easier to appreciate the ripple characteristics. Some important conclusions can be observed:

The Padé approximation provides the largest bandwidth whilst still being able to retain a maximally flat group delay response, thus, the Padé approximation should be favored whenever possible if the design requirements allow it, if the bandwidth requirements are stronger the order will have to be increased, or an approximation which exhibits ripple will have to be used (or both).

From the traces displayed in Fig. 2.11, it can be seen that the Stubs-Single approximation achieves the largest bandwidth but with a large amount of ill-defined ripple characteristics, followed by Hausner $\epsilon = 0.020$, Chebyshev $k = 0.05$ and Hepner approximations. One of the best compromises between bandwidth and ripple is the Hausner $\epsilon = 0.0005$ approximation, followed by the Elliptic $k = 0.02$ type. Other approximations, such as those obtained by Piché and by means of H_∞ norm minimization, are not shown in the figure due to the fact the they exhibit much higher levels of ripple extending well beyond the scale range of the plot.

As will be discussed in the following section, even-order approximations are preferred since their implementation usually requires roughly the same amount of circuitry (particularly amplifiers) of an even-order approximation of lower degree (e.g. a fourth-order approximation usually takes about the same amount of components as a third-order approximation).

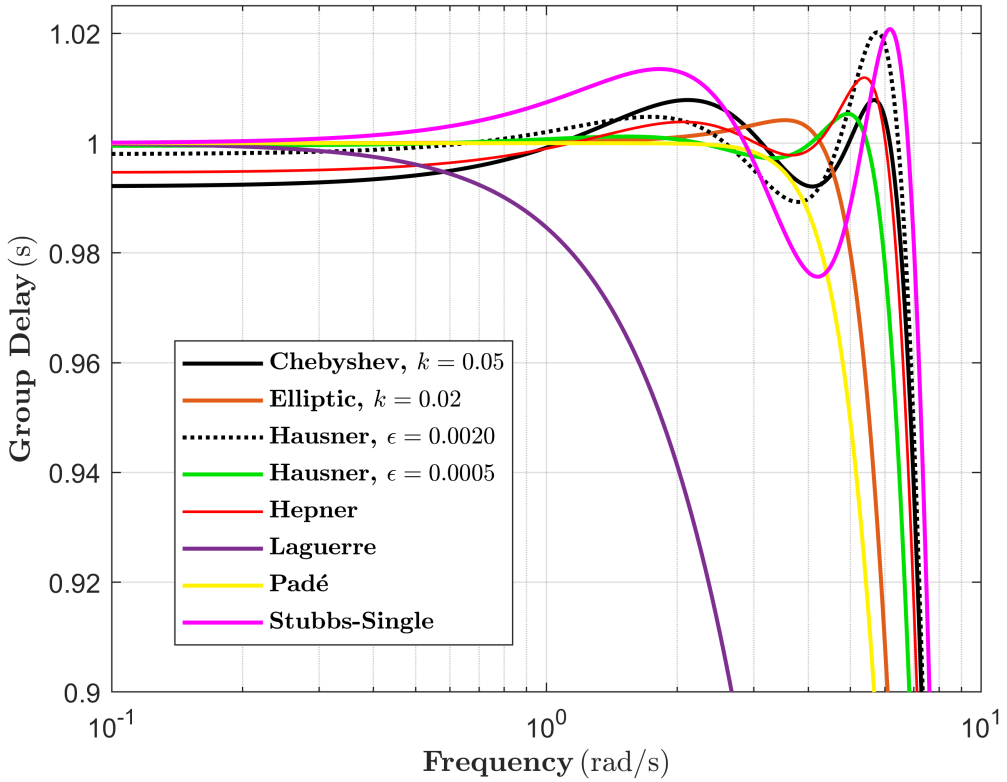

Figure 2.11: Group delay response comparison for different TDOAs, $n = 4$, $\tau = 1$ s.

2.5 Implementation With All-Pass Filters (APF)

Now that the fundamental theory has been laid out, we move on to the matter of how to electronically implement the TDOAs described in the previous sections. In the past, analog computing techniques employing generic circuit blocks were mainly used to develop TDOAs [50, 51, 52, 53, 54], with the possibility of being implemented with any type of active elements ranging from vacuum tubes to operational amplifiers, nevertheless, this involves a complicated design process resulting in a large component count. With the advent of the operational amplifier (OpAmp) in integrated form, the tendency has shifted towards a synthesis using cascade connections of first and/or second-order active all-pass filters (APFs), which greatly simplifies the design process and reduces the amount of components. The latter is the approach followed in this work.

Several factors should be taken into account when selecting a specific circuit, the most important are: number of active and passive elements, the circuit's sensitivity to component value variations, and component value spread. With regards to active components, those circuits which minimize the amount of OpAmps are preferred, but there is an important caveat: in general, commercial OpAmps are only available in single, dual and quad OpAmp-per-package presentations. Commonly, the package size of an integrated circuit (IC) containing a single OpAmp will be the same as the one containing two OpAmps, whilst quad opamp ICs tend to be double the size of single and dual OpAmp ICs. This usually

means that it takes roughly the same amount of PCB real estate and number of ICs to use a single rather than a dual OpAmp IC circuit; moreover, using four OpAmps also requires a single IC, albeit a larger one. Thus, since—generally speaking—the number of OpAmps equals the order n of the TDOA being implemented, it is evident that it makes more sense to use *even*- rather than *odd*-order approximations when cost is no issue.

With regards to passives the dominant factor is capacitors. Capacitors are usually of higher tolerance than resistors and they are also physically larger, less values are commercially available, and they tend to be more expensive (precision capacitors can represent the largest expense in a circuit), consequently, those circuits which use less capacitors are to be favored. In general terms, the order n of the TDOA equals the number of capacitors.

Component value spread is also very important, that is the relationship between the values of different components, not surprisingly, this becomes the biggest nuisance when it comes to capacitors. In this sense, a circuit which uses capacitors of the same value is better; first, because it reduces production costs, secondly, the required values might not always be commercially available, and thirdly, if a required capacitor value becomes too large, the size of the capacitor will also be physically larger and a different dielectric might have to be used; in many cases these type of dielectrics, which achieve higher capacitance values, are less accurate, produce more harmonic distortion, are more sensitive to temperature variations, etc... With regards to resistors, the conditions are less constricting since many values are commercially available and very low tolerances can be attained.

Only first- and second-order APFs will be required to realize any of the TDOAs presented in the previous sections since they can be synthesized as a cascade connection of these circuits, for example, a fifth-order TDOA may be synthesized using a first-order and two second-order active all-pass sections, and so on.

At this point, it becomes useful to define some equations in terms of the zeros and poles of the all-pass transfer function. Equation (2.8) which describes a TDOA can be expressed in its zero-pole form as

$$H(s) = \prod_{k=1}^{n} \frac{(s - s_{z_k})}{(s - s_{p_k})} \tag{2.50}$$

where s_{z_k} and s_{p_k} represent the k^{th} zero and pole, respectively. In a low-pass filter (LPF) transfer function every zero s_{z_k} is located at infinity [32], however, in an all-pass transfer function $s_{z_k} = -s_{p_k}$, that is

$$H(s) = \prod_{k=1}^{n} \frac{(s + s_{p_k})}{(s - s_{p_k})} \tag{2.51}$$

The group delay can be expressed as a series in terms of its poles, in the case of a LPF it is:

$$\tau_{gd}(\omega) = -\sum_{k=1}^{n} \frac{s_{p_k}}{\omega^2 + s_{p_k}^2} \tag{2.52}$$

whilst for an APF:

$$\tau_{gd}(\omega) = -2\sum_{k=1}^{n} \frac{s_{p_k}}{\omega^2 + s_{p_k}^2} \tag{2.53}$$

where it is clearly seen that an APF achieves twice the delay of a LPF of the same order and with the same pole locations. These equations will be used throughout the entire discussion of the following sections.

2.5.1 First-Order APF Formulation

A first-order APF transfer function has the general form:

$$H(s) = \frac{\omega_0 - s}{\omega_0 + s} \tag{2.54}$$

where ω_0 is commonly referred to as the cut-off frequency, resonant frequency or the undamped natural frequency as in the case of second-order systems.

As can be seen, equation (2.54) has a single zero and pole at $|\omega_0|$, thus, by means of (2.53) its group delay is simply

$$\tau_{gd}(\omega) = \frac{2\omega_0}{\omega^2 + \omega_0^2} \tag{2.55}$$

What we seek is to transform (2.54) into the form of a first-order TDOA as

$$H(s) = \frac{a - s\tau}{a + s\tau} \tag{2.56}$$

From inspection, it can be seen that this is accomplished by making

$$\omega_0 = \frac{a}{\tau} \tag{2.57}$$

where a is a constant coefficient obtained by any of the approximations described in the previous sections. The group delay becomes

$$\tau_{gd}(\omega) = \frac{2a\tau}{\tau^2\omega^2 + a^2} \tag{2.58}$$

whilst the delay at DC is

$$\tau_{gd} = \frac{2\tau}{a} \tag{2.59}$$

where $\tau_{gd}(0)$ has been re-written as τ_{gd} for simplicity.

2.5.2 Second-Order APF Formulation

A second-order APF transfer function has the general form:

$$H(s) = \frac{\omega_0^2 - BWs + s^2}{\omega_0^2 + BWs + s^2} \tag{2.60}$$

where ω_0 is the the un-damped natural frequency and BW is the bandwidth given by

$$BW = \frac{\omega_0}{Q} \tag{2.61}$$

where Q is the quality factor.

Equation (2.60) produces two poles, thus, by means of (2.53) its group delay will be

$$\tau_{gd}(\omega) = -2\left[\frac{s_{p_1}}{\omega^2 + s_{p_1}^2} + \frac{s_{p_2}}{\omega^2 + s_{p_2}^2}\right] \tag{2.62}$$

where

$$s_{p_1} = -\frac{BW}{2}\left[1 + \sqrt{1 - 4Q^2}\right] \tag{2.63a}$$

$$s_{p_2} = -\frac{BW}{2}\left[1 - \sqrt{1 - 4Q^2}\right] \tag{2.63b}$$

It can be seen that for $Q > 1/2$ the poles will be complex conjugates, otherwise they will be real.

Equation (2.60) must be forced to adopt the from of a second-order TDOA as

$$H(s) = \frac{a - bs\tau + (s\tau)^2}{a + bs\tau + (s\tau)^2} \tag{2.64}$$

By inspection and comparing to Eq. (2.60):

$$\omega_0 = \frac{\sqrt{a}}{\tau} \tag{2.65a}$$

$$BW = \frac{b}{\tau} \tag{2.65b}$$

where a and b are constant coefficients obtained from any of the approximations reviewed in the previous sections.

Combining equations (2.61), (2.65a) and (2.65b), we get

$$Q = \frac{\sqrt{a}}{b} \tag{2.66}$$

so equations (2.63a) and (2.63b) become

$$s_{p_1} = -\frac{b}{2\tau}\left[1 + \sqrt{1 - \frac{4a}{b^2}}\right] \tag{2.67a}$$

$$s_{p_2} = -\frac{b}{2\tau}\left[1 - \sqrt{1 - \frac{4a}{b^2}}\right] \tag{2.67b}$$

and if $b < 2\sqrt{a}$ the poles will be complex conjugates, otherwise they will be real.

2.5.3 Higher Order APF formulation

Any of the numerator and denominator polynomials used for the TDOAs in this work can be factorized into a product of first- and second-order polynomials, thus, an APF of order $n > 2$ can be implemented as the product of first- and second-order all-pass transfer functions. The general formula to synthesize any TDOA of arbitrary n such that $n \in \mathbb{Z}^+$ with a cascade of APF transfer functions is:

$$H(s) = \prod_{k=1}^{\lfloor n/2 \rfloor} \frac{a_k - b_k s\tau + (s\tau)^2}{a_k + b_k s\tau + (s\tau)^2} \cdot \left[\frac{a_0 - s\tau}{a_0 + s\tau}\right]^{n \bmod 2} \tag{2.68}$$

where the notation $\lfloor \cdot \rfloor$ represents the floor function and means take the integer part.

Chapter 3

Electronic Implementation in the Time Domain

3.1 Introduction

The previous chapter described the different types of approximations for the time delay operator (TDOA), which are required to perform travelling wave separation in the time domain. This chapter deals with the realization of the stabilized equations presented in Section 1.4 using electronic circuitry.

First, circuits to implement any of the TDOAs of Chapter 2 by means of active All-Pass Filters (APF) are presented. Afterwards, two methods to realize the complete circuitry required to obtain $p'(t)$, $\rho_0 c_o u'(t)$, $a'(t)$ and $b'(t)$ are discussed, namely: the Active Network Synthesis Method (ANSM) and the Analog Computing Method (ACM), the former, uses a product of transfer functions for $p'(t)$ and $\rho_0 c_0 u'(t)$ in the frequency domain, which are then synthesized by means of active network synthesis theory; the latter approach, treats each individual operation required to compute $p'(t)$ and $\rho_0 c_0 u'(t)$ as a separate element; something which is more akin to the techniques used in analog computing systems to solve a variety of different problems. Figure 3.1 shows a design flow chart of the process just described. Starting from the number of microphones being used, the TDOA order and type (e.g., Chebyshev, Padé, etc...) is selected for $H_1(s)$ and $H_2(s)$, afterwards, either the ANSM or the ACM are used to attain the required circuits to obtain a complete TWSS.

Both methods have some advantages over the other: the ANSM is particularly useful when low order TDOAs are used, which generally yields smaller circuits than the ACM. However, it is difficult to implement if some parameters (such as α, β, or τ) are required to be variable; in most cases, this means that the circuit has to be synthesized with a particular set of fixed values, otherwise, adjusting a single parameter without changing the rest becomes truly impractical, also, the transfer function might be very difficult to realize with a small number of op-amps and a low component value spread when a particular set of values is selected; this is also true when the order of the TDOA is high. On the other hand, the ACM

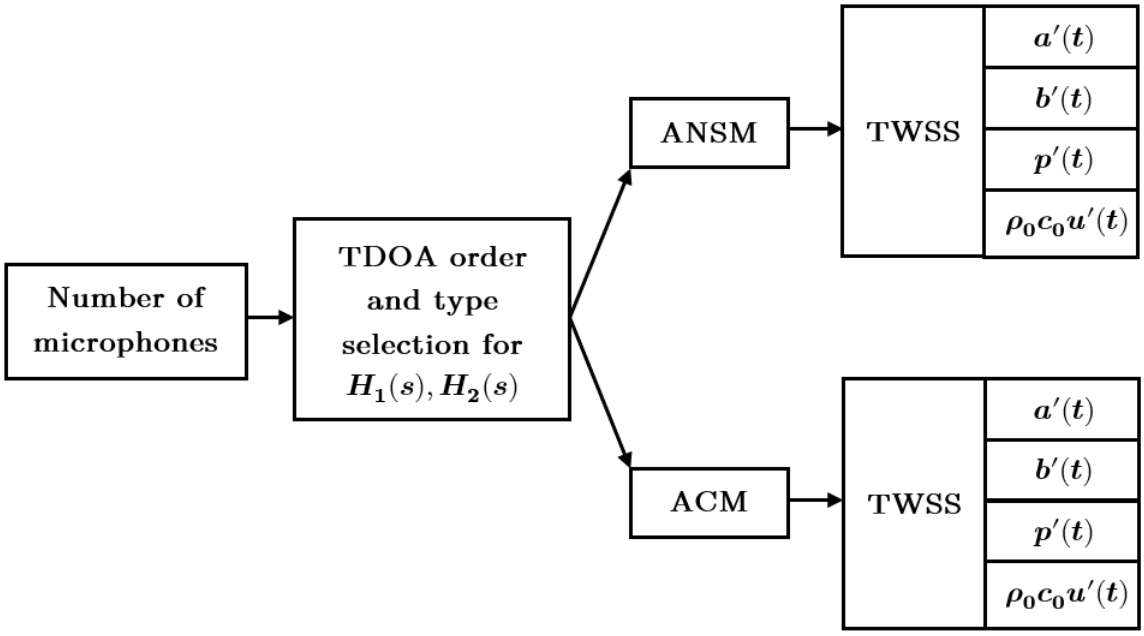

Figure 3.1: Design flow chart for implementation of a complete TWSS.

makes the design easier and allows more flexibility to make some of its parameters variable, and TDOAs of any practical order can be selected. The downside is that, in most cases, a larger and more complex circuit is required.

3.2 The Active All-Pass Filter (APF)

Most of the TDOAs presented in Chapter 2 are of the all-pass type and can be synthesized as a product of first- and second-order transfer functions, therefore, one of the most effective ways to implement them with electronic circuitry is by using active All-Pass Filters (APF). In the following sections, some of these filters along with their transfer functions and design equations are presented.

3.2.1 First-Order Active APF Circuits

The first-order active APF is very well known and it is available in two circuit configurations: inverting and non-inverting. Both achieve the same group delay response, however, in the case of the inverting configuration, the output signal will exhibit opposite polarity with regards to the input signal. Both circuits require a single op-amp, three resistors, and one capacitor. Figure 3.2 shows the circuits in both configurations

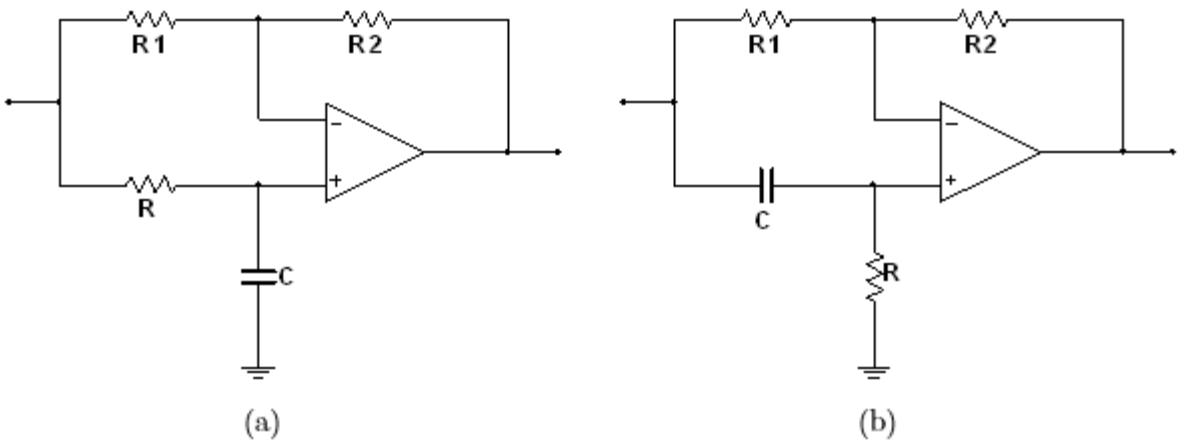

Figure 3.2: First-order APF circuits: (a) non-inverting and (b) inverting .

For the non-inverting circuit the transfer function when $R_1 = R_2$ is

$$H(s) = \frac{1 - RCs}{1 + RCs} \tag{3.1}$$

and for the inverting circuit it is

$$H(s) = -\frac{1 - RCs}{1 + RCs} \tag{3.2}$$

where, from inspection and comparing to Eq. (2.54), it can be seen that

$$\omega_0 = \frac{1}{RC} \tag{3.3}$$

and from (2.57) the design equation becomes

$$RC = \frac{\tau}{a} \tag{3.4}$$

The design procedure is very simple: after the a coefficient has been obtained based on a particular approximation, the value of C is user-selected and R is computed from (3.4). The values of R_1 and R_2 are arbitrary as long as both are equal and their current consumption lies both within the input source (not shown in Fig. 3.2) and the op-amp's output current driving capabilities. The current flowing through R and C should also be taken into account in that regard.

3.2.2 Second-Order Active APF Circuits

There are basically two approaches to design a second-order APF circuit: the first involves the use of a band-pass filter (BPF), and the second is achieved by direct synthesis;

both of these methods will be discussed.

3.2.2.1 The Band-Pass Approach

A BPF can be used to synthesize an APF due to the following property:

$$\frac{\omega_0^2 - BWs + s^2}{\omega_0^2 + BWs + s^2} = 1 - 2\frac{BWs}{\omega_0^2 + BWs + s^2} \tag{3.5}$$

where the last term on the right hand side represents the transfer function of an active BPF with a DC gain of two. This method has the advantage that it is quite simple to implement, however, it requires at least two operational amplifiers: one to implement the the BPF itself, and other to implement the sum operation.

There are many circuit topologies available to implement a BPF, one of the most popular is the Multi-Feedback or Rauch filter shown in Fig. 3.3, which realizes a second-order BPF with a single op-amp. Its transfer function is given by [55]

$$H(s) = -\frac{R_2 C_1 s}{1 + R_1 (C_1 + C_2) s + R_1 R_2 C_1 C_2 s^2} \tag{3.6}$$

where the negative sign indicates that this is an inverting filter and

$$\omega_0 = \frac{1}{\sqrt{R_1 R_2 C_1 C_2}} \tag{3.7a}$$

$$Q = \frac{\sqrt{R_2/R_1}}{\sqrt{C_1/C_2} + \sqrt{C_2/C_1}} \tag{3.7b}$$

$$H_{0_{BP}} = -2Q^2 \tag{3.7c}$$

where $H_{0_{BP}}$ is the DC gain.

To simplify the design, it is common to impose $C_1 = C_2 = C$, so Equations (3.7a) and (3.7b) reduce to [55]:

$$\omega_0 = \frac{1}{\sqrt{R_1 R_2} C} \tag{3.8a}$$

$$Q = \frac{1}{2}\sqrt{\frac{R_2}{R_1}} \tag{3.8b}$$

The complete circuit required to produce the APF is shown in Figure 3.4.

From the results obtained in Section 2.5.2, and using Equations (3.8a) and (3.8b) we

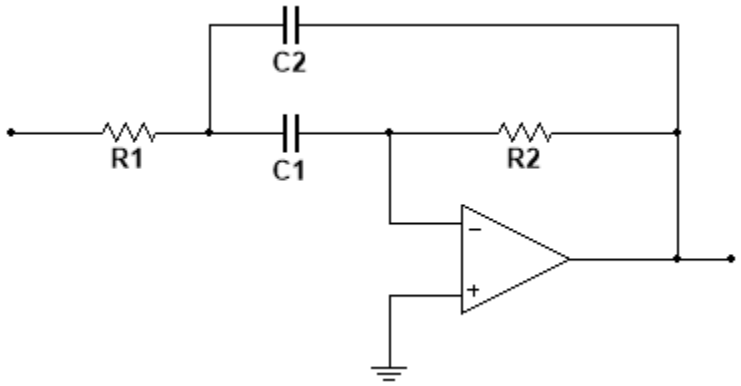

Figure 3.3: Second-order MFB-BPF.

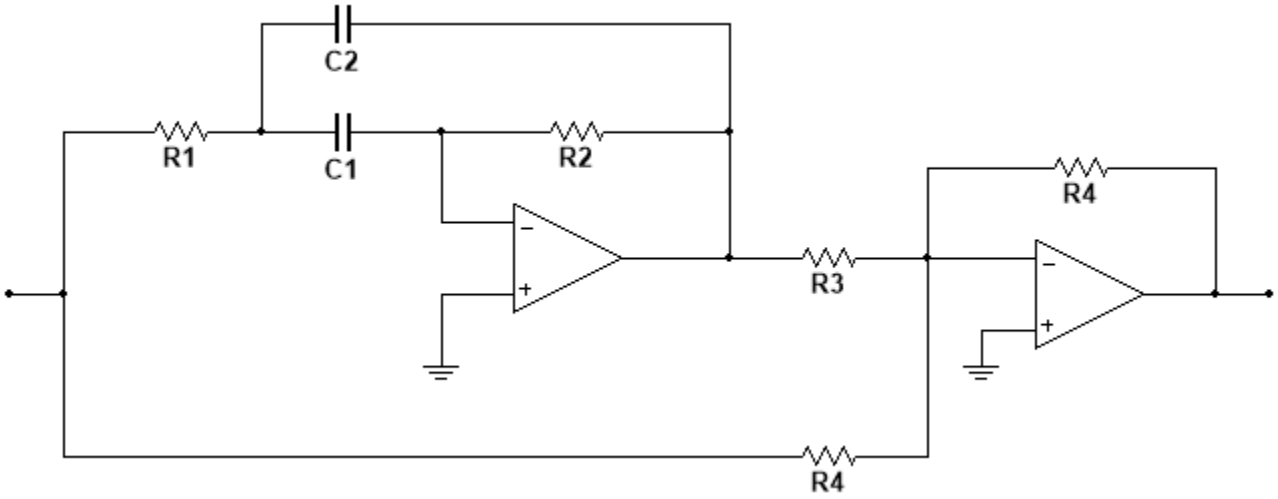

Figure 3.4: Second-order APF using a Band-pass MFB filter, the two resistors labeled R_4 must be of equal value.

can obtain the following design equations:

$$R_1 = \frac{a}{b}\frac{\tau}{2C} \tag{3.9a}$$

$$R_2 = \frac{1}{b}\frac{2\tau}{C} \tag{3.9b}$$

$$\frac{R_4}{R_3} = \frac{b^2}{a} \tag{3.9c}$$

Usually, once the coefficients a and b are extracted from an approximation, the capacitor value C is selected and values for R_1 and R_2 are computed from (3.9a) and (3.9a). Either R_4 or R_3 can be selected, and the remaining resistor is computed from (3.9c). It is important to note that the circuit in Fig. 3.4 produces an inverting APF.

3.2.2.2 Direct Synthesis

A big disadvantage of the band-pass approach is that it requires at least two operational amplifiers, which can demand a lot of ICs if the order of the TDOA is large. To overcome this, an alternative which can produce a wide array of circuits makes use of active network synthesis techniques. With this approach a specific circuit can be synthesized to implement an all-pass transfer function, or the BPF and the sum operation can be performed with a single op-amp. The overarching principle in the present work will be to reduce the component count of the final circuit, particularly the number of ICs, therefore, only those circuits which are capable of implementing a second-order APF with a single op-amp will be discussed. Generally speaking, as the value of Q of the all-pass transfer function increases the circuit will become more sensitive to variations in component values, to overcome this the number of op-amps has to increase, fortunately, most TDOAs require relatively low Q values.

A second-order APF using a single op-amp can be implemented with a Single Amplifier Biquad (SAB) circuit, the term "Biquad" is an abbreviation of *biquadratic* due to the fact that these type of circuits are able to produce a transfer function comprised of the ratio of two quadratic polynomials.

Deliyannis SAB

The Deliyannis SAB is capable of performing the MFB-BPF and the sum operation in a single op-amp as shown in Fig. 3.5 which, aside from the addition of R_3 and R_4, bears a striking resemblance to the circuit of Fig. 3.3,. The general transfer function is given by [56]

$$H(s) = K\frac{\dfrac{1}{R_1R_2C_1C_2} - \left[\dfrac{R_4}{R_3}\dfrac{1}{R_1C_2} - \dfrac{1}{R_2C_p}\right]s + s^2}{\dfrac{1}{R_1R_2C_1C_2} + \dfrac{1}{R_2C_p}s + s^2} \tag{3.10}$$

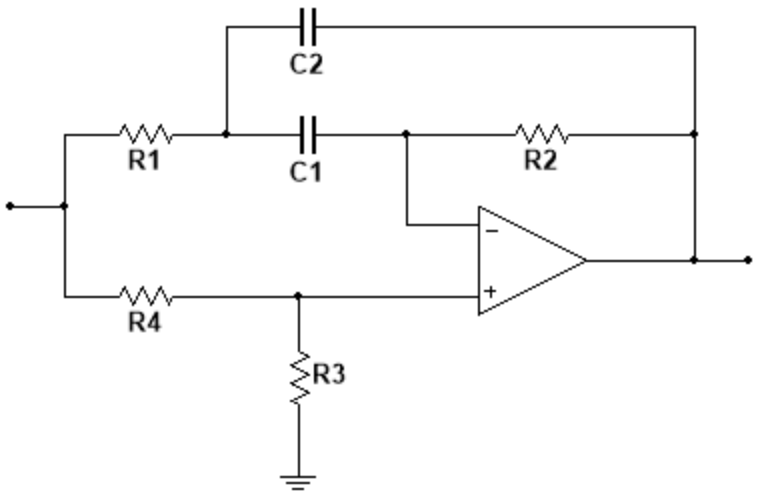

Figure 3.5: Second-order Deliyannis SAB APF.

where $C_p = C_1 \parallel C_2$. If $C_1 = C_2 = C$ is imposed, Equation (3.10) reduces to [56]:

$$H(s) = K \frac{\dfrac{1}{R_1 R_2 C^2} - \left[\dfrac{R_4}{R_3}\dfrac{1}{R_1 C} - \dfrac{2}{R_2 C}\right] s + s^2}{\dfrac{1}{R_1 R_2 C^2} + \dfrac{2}{R_2 C} s + s^2} \tag{3.11}$$

Unsurprisingly, the design equations for R_1, R_2 and R_4/R_3 are the same as (3.9a) and (3.9a), given the similarity of both circuits; but the big difference is in the K term present in (3.11) representing the DC gain, which is given by [56]

$$K = \frac{R_3}{R_3 + R_4} \tag{3.12}$$

This means that this APF will always exhibit a gain of less than one. To correct this issue, a voltage divider formed by R_5 and R_6 is introduced at the output of the op-amp as shown in Fig. 3.6. The feedback path is then taken from the voltage divider, which attenuates the op-amp's output signal being fed back to the inverting input. Since an op-amp operating with negative feedback always tries to make the voltages at both of its inputs equal, the op-amp's output will have to rise in order to compensate for the loss being introduced by the voltage divider, thus, with this method it is possible to obtain a larger gain at the output of the op-amp. Nevertheless, the Thevenin equivalent resistance formed by R_5 and R_6 should be as small as possible—without exceeding the op-amp's current drive capabilities—when compared to R_2 and the reactance of C_2 in order not to disturb the time constants and the response of the circuit. The new DC gain $H_{0_{AP}}$ is determined by

$$H_{0_{AP}} = \frac{K}{\gamma}, \quad \gamma = \frac{R_6}{R_5 + R_6} \tag{3.13}$$

where γ is the attenuation factor introduced by the output voltage divider.

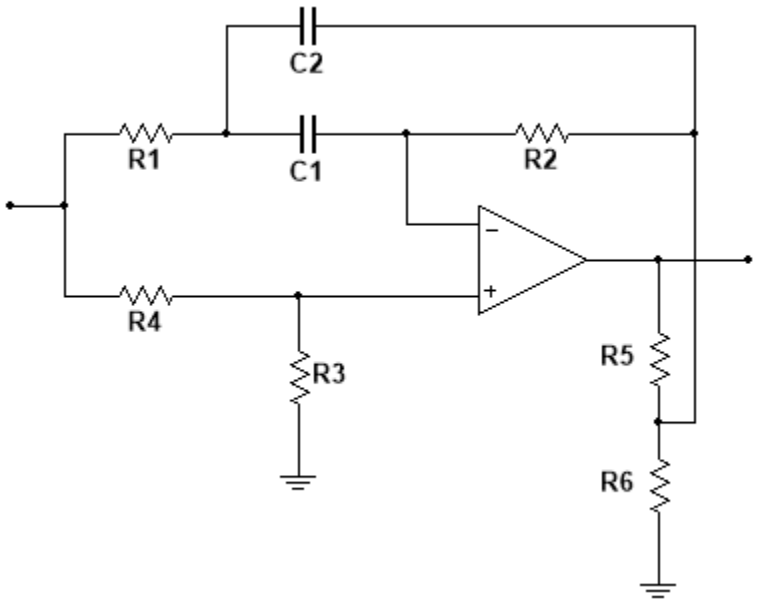

Figure 3.6: Second-order Deliyannis SAB APF with gain.

As the value of Q increases, the ratio R_2/R_1 will also increase, which means that component spread will be higher, setting a limit on the maximum resistance values admissible for a design [56]. Not only that, but the Gain-Sensitivity Product (GSP), defined as the circuit's sensitivity to variations on op-amp open-loop gain, will also increase as the value of Q increases; for this particular circuit, provided that $C_1 = C_2$, the expression is given by [57]

$$\text{GSP} = 2Q^2 \tag{3.14}$$

For these reasons, this circuit is usually recommended for $Q \leq 2$ [57].

The Bridged-T All-Pass SAB

Another SAB based on a Sallen-Key circuit, which can be used for APFs with mid-Q values ($Q \leq 20$) was presented by Moschytz [58, 59], and it is shown in Fig. 3.7. The transfer function is given by [57]

$$H(s) = \frac{\dfrac{1}{R_1 C_1 C_2 R_p} - \left[\dfrac{R_3}{R_2 R_p C_1} - \dfrac{1}{R_1 (C_1 \parallel C_2)}\right] s + s^2}{\dfrac{1}{R_1 C_1 C_2 R_p} + \left[\dfrac{R_3}{R_2 R_p C_1} - \dfrac{1}{R_1 (C_1 \parallel C_2)}\right] s + s^2} \tag{3.15}$$

where $R_p = R_4 \parallel R_5$, and

$$\text{GSP} = Q\frac{R_p}{R_5}\left(1+\frac{R_3}{R_6}\right)^2\sqrt{\frac{R_1C_2}{R_pC_1}} \tag{3.16}$$

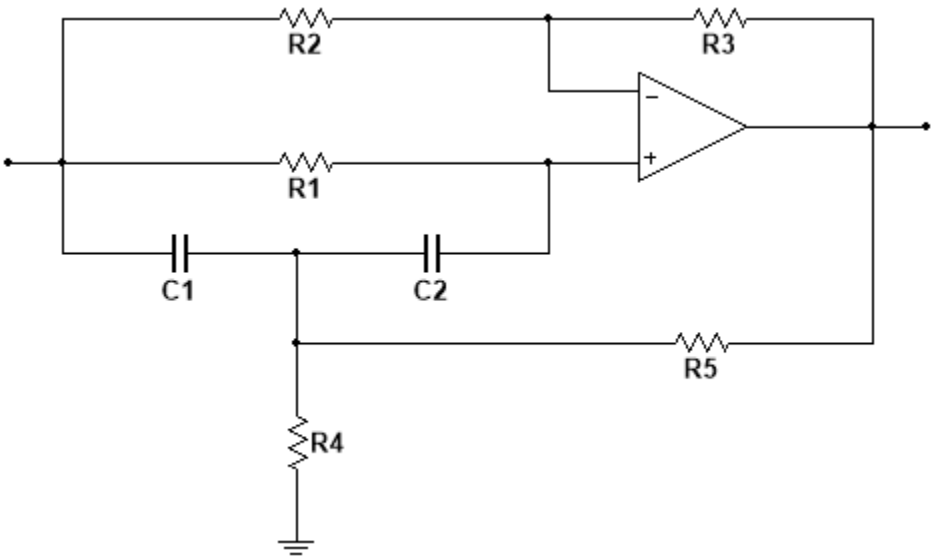

Figure 3.7: Second-order Bridged-T All-Pass SAB.

A very elaborate algorithmic procedure along with the required equations to design this APF circuit is available in [57]. If R_2 is user-selected, it was found by means of a minimization routine in MATLAB® that the capacitor ratio $C_2/C_1 = 1/2$ achieves the lowest GSP, but great care must be taken since ratios lower than 1/2 will produce negative or complex resistor and GSP values; due to component tolerances it is of paramount importance to insure that C_2/C_1 always remains sufficiently greater than 1/2.

As presented in this section, this circuit is incapable of producing a gain higher than 1, however, a practically identical circuit, which includes an extra resistor from the inverting input to ground, was published in [60] and allows for gains higher or equal to 1. Design equations and a sensitivity analysis was presented and discussed when compared to a 2 op-amp topology. It was shown that the 1 op-amp circuit becomes sensitive with moderate values of Q, fortunately, most of the TDOAs discussed in Chapter 2 exhibit low Q values, especially at low orders.

3.3 Active Network Synthesis Method (ANSM)

In Chapter 1, stabilized Equations (1.9) corresponding to $P'(\omega)$ and $\rho_0 c_0 U'(\omega)$ were obtained. These expressions can be rewritten as transfer functions in the s domain as follows:

$$H_P(s) = \frac{\alpha H_{1_P}(s)}{1 + \beta H_{2_P}(s)} \tag{3.17a}$$

$$H_U(s) = \frac{\alpha H_{1_U}(s)}{1 - \beta H_{2_U}(s)} \tag{3.17b}$$

where

$$H_P(s) = P'(s) / [P_1(s) + P_2(s)] \tag{3.18a}$$

$$H_U(s) = \rho_0 c_0 U'(s) / [P_1(s) - P_2(s)] \tag{3.18b}$$

and $H_{1_P}(s)$, $H_{2_P}(s)$, $H_{1_U}(s)$, $H_{2_U}(s)$ are TDOAs of the form shown in Eq. (2.68). Although not strictly necessary, the following simplifications can be made: $H_{1_P}(s) = H_{1_U}(s) = H_1(s)$ and $H_{2_P}(s) = H_{2_U}(s) = H_2(s)$.

After $H_1(s)$ and $H_2(s)$ are selected, $H_P(s)$ and $H_U(s)$ are completely defined and can be implemented by means of active network synthesis techniques, this process constitutes the ANSM. When the order of the transfer functions is low the synthesis process is relatively simple, but as the order increases (by selecting higher order TDOAs), the synthesis becomes considerably more complicated resulting in a larger and more complex circuit, hence, the ANSM is not usually recommended for high order TDOAs.

Two special cases become very relevant for the ANSM, namely, the first- and second-order circuits, the order refers to the highest order TDOA being used rather than the order of $H_P(s)$ and $H_U(s)$. These circuits will be discussed in the following sections.

3.3.1 First-Order Circuit

By proper selection of the TDOAs, reduced circuits can be attained. A particularly useful choice is $H_1(s) = 1/(1 + s\tau)$, which corresponds to a first-order low-pass Padé $[0, 1]$ or Maclaurin approximation for $e^{-s\tau}$, and $H_2(s) = (1 - s\tau)/(1 + s\tau)$, which corresponds to a first-order all-pass Padé approximation for $e^{-2s\tau}$. With these choices the following transfer functions are obtained:

$$H_P(s) = \frac{\alpha}{1 + \beta + (1 - \beta) s\tau} \tag{3.19a}$$

$$H_U(s) = \frac{\alpha}{1 - \beta + (1 + \beta) s\tau} \tag{3.19b}$$

Some important observations can be made: in the case of Eq. (3.19a) it is valid to set $\beta = 1$ since the pole disappears and the transfer function results in a constant; the same cannot be said of Eq. (3.19b), because that would reduce the transfer function to that of an unstable ideal integrator. As discussed in Section 1.4 the optimum value for α is

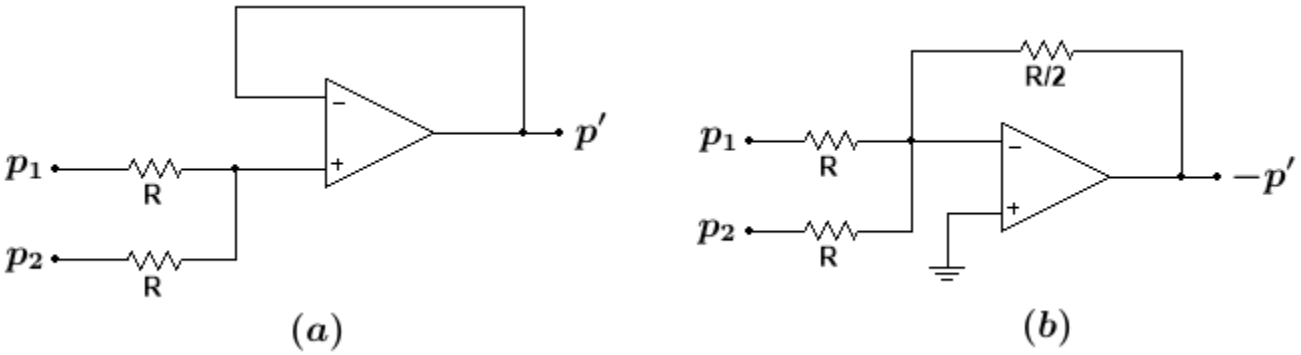

Figure 3.8: Summing amplifier with a gain of 1/2, (*a*) non-inverting and (*b*) inverting configurations.

$\alpha_{opt} = (1+\beta)/2$, hence, Eqs. (3.19) reduce to:

$$H_P(s) = 1/2 \tag{3.20a}$$

$$H_U(s) = \frac{1}{2}\frac{1+\beta}{1-\beta} \cdot \frac{\dfrac{1-\beta}{(1+\beta)\tau}}{\dfrac{1-\beta}{(1+\beta)\tau} + s} \tag{3.20b}$$

With Eqs.(3.18) and (3.20) it is possible to obtain $p'(t)$ by taking the average of the sound pressures being sensed by both microphones, whilst $\rho_0 c_0 u'(t)$ can be obtained by subtracting $p_2(t)$ from $p_1(t)$ and sending the difference through a first-order low-pass filter, with a pole located at $\omega_0 = (1-\beta)/[(1+\beta)\tau]$ and a DC gain of $H_{U_0} = (1/2)[1+\beta]/[1-\beta]$.

The circuit required for $p'(t)$ is a summing amplifier with a gain of 1/2, it can be of the inverting or non-inverting types depending on the application requirements as shown in Fig. 3.8. For $\rho_0 c_0 u'(t)$ a subtraction operation followed by a low-pass filter is required, this can be accomplished with a standard differential amplifier and an active first-order low-pass filter but, in order to keep the op-amp count low, both can be combined into a single op-amp circuit as shown in Fig. 3.9.

The circuit in Fig. 3.9 is a first-order active low-pass filter with differential inputs, and its transfer function is

$$H(s) = \frac{R_2}{R_1}\frac{1/(R_2 C)}{1/(R_2 C) + s} \tag{3.21}$$

By comparing Eqs. (3.21) and (3.20b) it is possible to obtain the following relationships:

$$R_1 C = 2\tau \tag{3.22a}$$

$$\frac{R_2}{R_1} = \frac{1}{2}\frac{1+\beta}{1-\beta} \tag{3.22b}$$

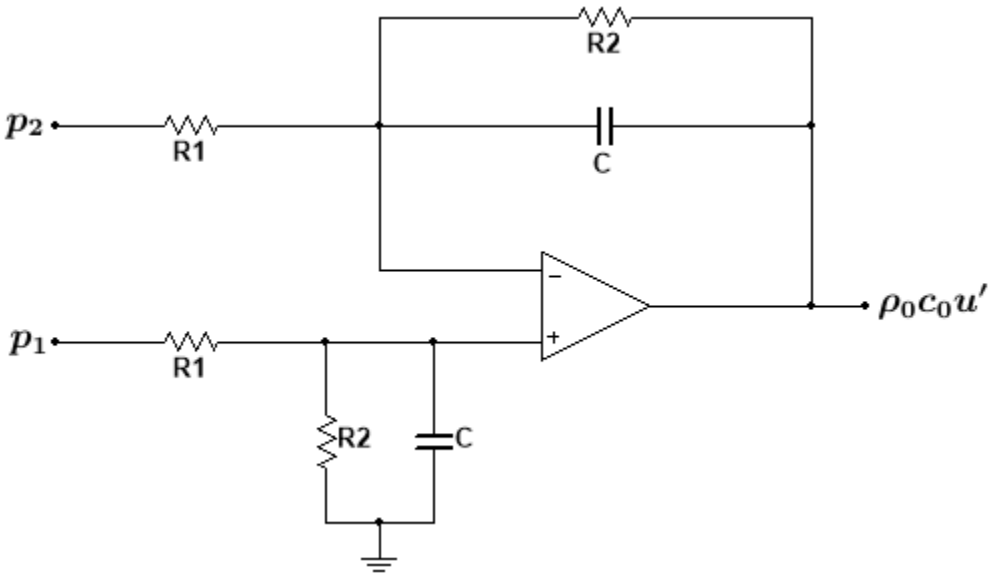

Figure 3.9: First-order active low-pass filter with differential input used to obtain $\rho_0 c_0 u'(t)$.

Thus, the delay time is determined by the product R_1C. For the design process it is convenient to first select a commercial capacitor value and compute R_1 from (3.22a), afterwards, the value of R_2 is obtained from (3.22b) for a particular value of β.

The remaining elements needed to obtain $a'(t)$ and $b'(t)$ are a summing and a differential amplifier with a gain of 1/2 as required by Eqs. (1.10). The complete circuit is shown in Fig. 3.10, the total op-amp count is 4, which means that it can be implemented with a single IC. Notice that the inputs to the $\rho_0 c_0 u'(t)$ circuit were reversed in order to obtain $-\rho_0 c_0 u'(t)$ at its output, this is convenient in order to reduce the number of resistors in the $a'(t)$ circuit by using a summing rather than a differential amplifier, since the latter uses more resistors than the former. If the $\rho_0 c_0 u'(t)$ signal will be used, it is preferred that it should be in-phase, in such case, the inputs can be reverted to their original order and the summing amplifier at the $a'(t)$ output should be replaced by a differential amplifier, which would involve 2 extra resistors and the same number of op-amps. In any case, the great advantage of this circuit is its simplicity, the downside is that, since low-pass type TDOAs were employed, the magnitude response of the outputs will drop as the frequency increases.

A somehow similar circuit to that of Fig. 3.10 but using 5 op-amps was presented in [28, 27], however, a direct relationship between β, τ, and the component values of the circuit was not established, since the approach followed in the cited references was to use first-order truncation of a Taylor series expansion for the exponential delay operators in the non-stabilized Equations (1.4). Also, the use of 5 op-amps requires at least 2 ICs, which results in a larger circuit; reducing the main appeal of a first-order approximation which is simplicity.

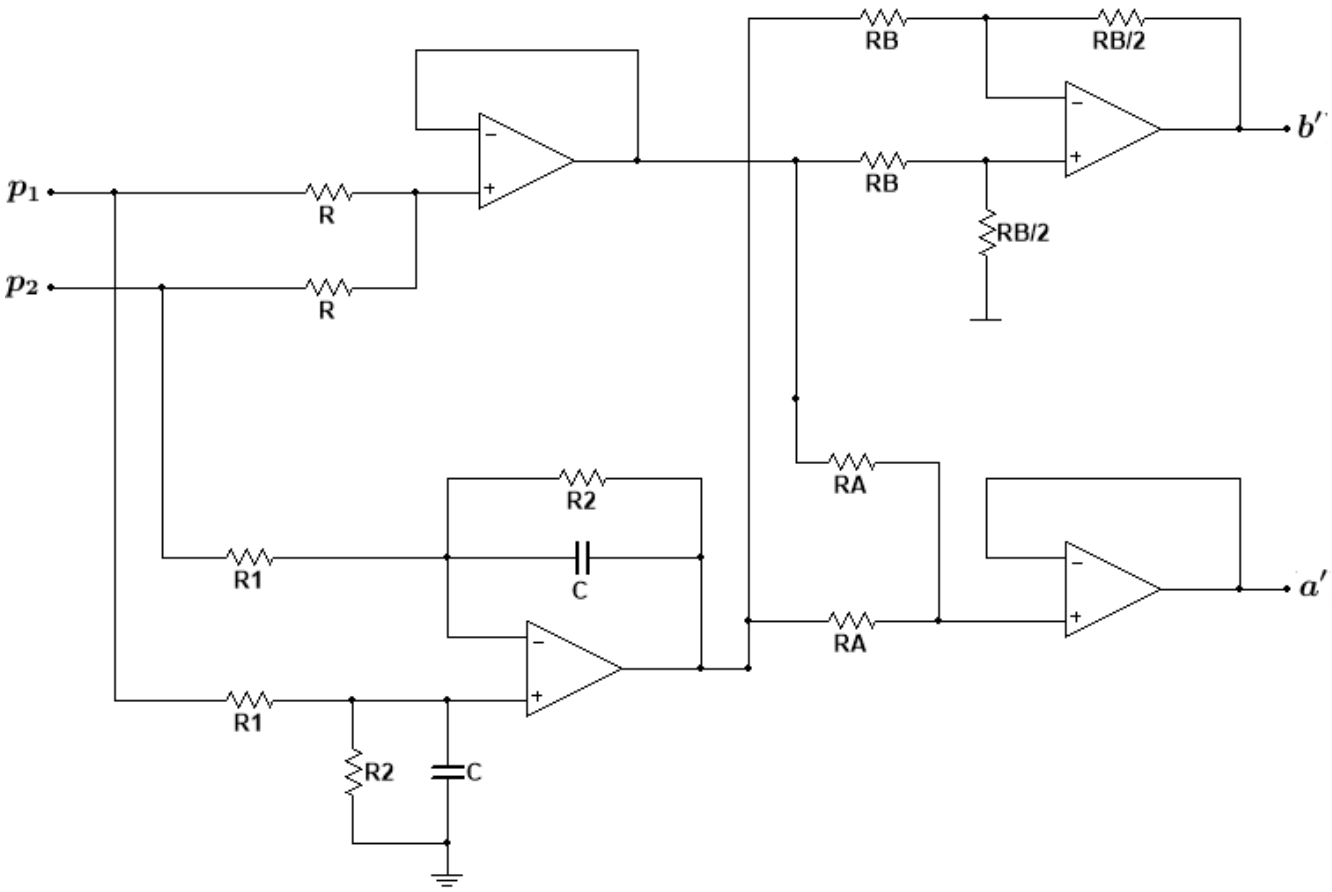

Figure 3.10: First-order circuit used to obtain the forward and backward travelling wave components.

3.3.2 Second-Order Circuit

If $\alpha = \alpha_{opt} = (\beta + 1)/2$, the following transfer functions for the second-order case are obtained:

$$H_P(s) = \frac{1}{2} \cdot \frac{a_2/4 + (b_2/2)\, s\tau + (s\tau)^2}{a_2/4 + [(b_2/2)(1-\beta)/(1+\beta)]\, s\tau + (s\tau)^2} \cdot \frac{a_1 - b_1 s\tau + (s\tau)^2}{a_1 + b_1 s\tau + (s\tau)^2} \tag{3.23a}$$

$$H_U(s) = \frac{1}{2}\frac{1+\beta}{1-\beta} \cdot \frac{a_2/4 + (b_2/2)\, s\tau + (s\tau)^2}{a_2/4 + [(b_2/2)(1+\beta)/(1-\beta)]\, s\tau + (s\tau)^2} \cdot \frac{a_1 - b_1 s\tau + (s\tau)^2}{a_1 + b_1 s\tau + (s\tau)^2} \tag{3.23b}$$

where $\{a_1, b_1 \in \mathbb{R}\}$ and $\{a_2, b_2 \in \mathbb{R}\}$ are TDOA coefficients corresponding to $H_1(s)$ and $H_2(s)$, respectively. The most evident difference between the first- and second-order transfer functions is the increased complexity of the latter.

By inspecting Eqs. (3.23) it can be seen that the DC gain for both $H_P(s)$ and $H_U(s)$ is the same as in the first-order case. The next step consists on synthesizing the right hand terms of Eqs. (3.23): the last term on the right is a standard all-pass TDOA of the type discussed in Chapter 2 and can be synthesized with a second-order all-pass filter, however,

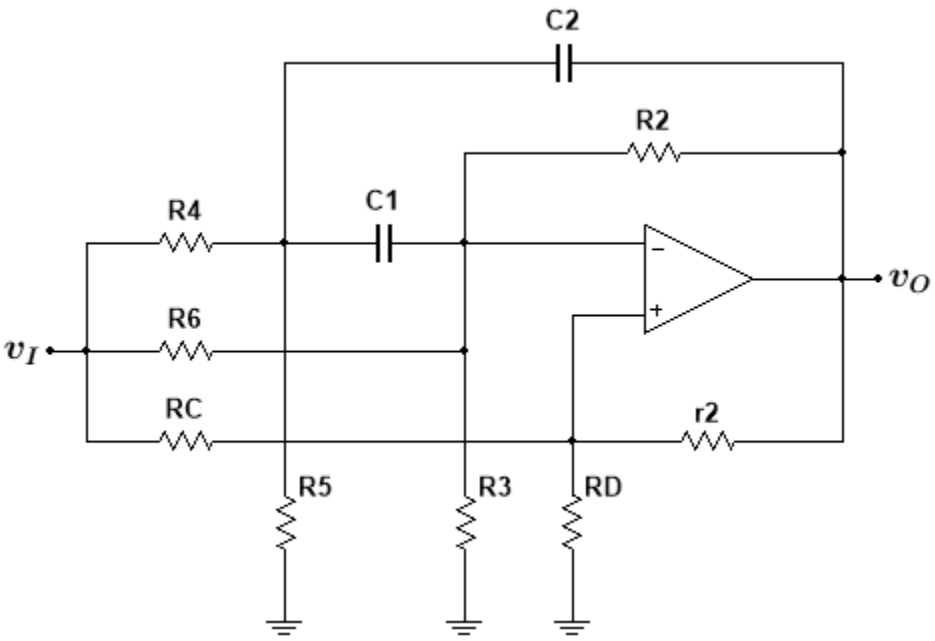

Figure 3.11: Single-Amplifier General Biquad.

the first right hand transfer function is not a standard form and is more challenging to synthesize.

The Single-Amplifier General Biquad of Fig. 3.11, which was developed by Friend *et al* [61] and "is often considered as an extension of the network proposed by Deliyannis [62]" [63] is able to synthesize the following transfer function:

$$H(s) = K\frac{f_0 + f_1 s + f_2 s^2}{d_0 + d_1 s + s^2} \tag{3.24}$$

The final configuration of the circuit in Fig. 3.11 may vary depending on the value of the coefficients in Eq. (3.24). The equations required to compute the value for each component are very lengthy and cumbersome; they can be found in [63]. Instead, MATLAB® scripts developed to compute the component values of the circuits in Figs. 3.12 and 3.13, which correspond to the first right-hand transfer term of $H_P(s)$ and $H_U(s)$ using Padé coefficients are available in Appendix A.

The circuit of Fig. 3.12 is quite easy to realize, however, the one in Fig. 3.13 poses a much greater challenge for a variety of reasons: the DC gain increases and the quality factor Q of the denominator polynomial gets closer to 0 as the value of β gets closer to 1, this places a heavy burden on the circuit, which results in a large component value spread and high sensitivity; in some cases, it might not even be possible for the circuit to meet the design requirements if the value of β is high. The value of R_b should be extremely small (less than 10 Ω) for the value of R_C not to become extremely large and for the circuit to perform properly, also, the total resistance seen by the right hand terminal of r_2 must be

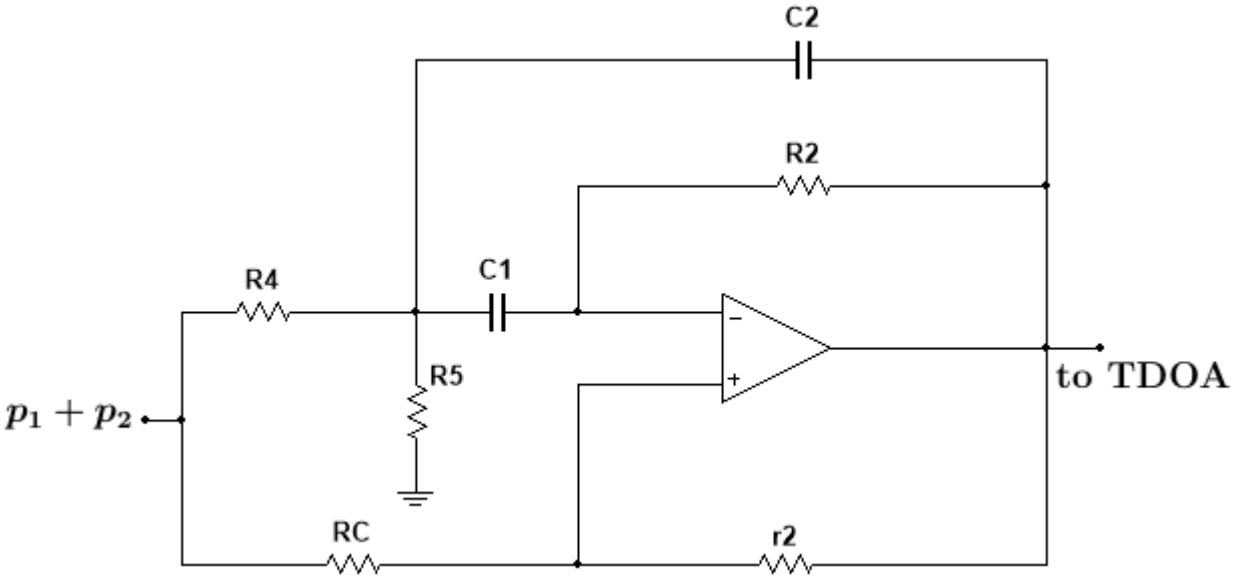

Figure 3.12: Single-Amplifier General Biquad for $H_P(s)$.

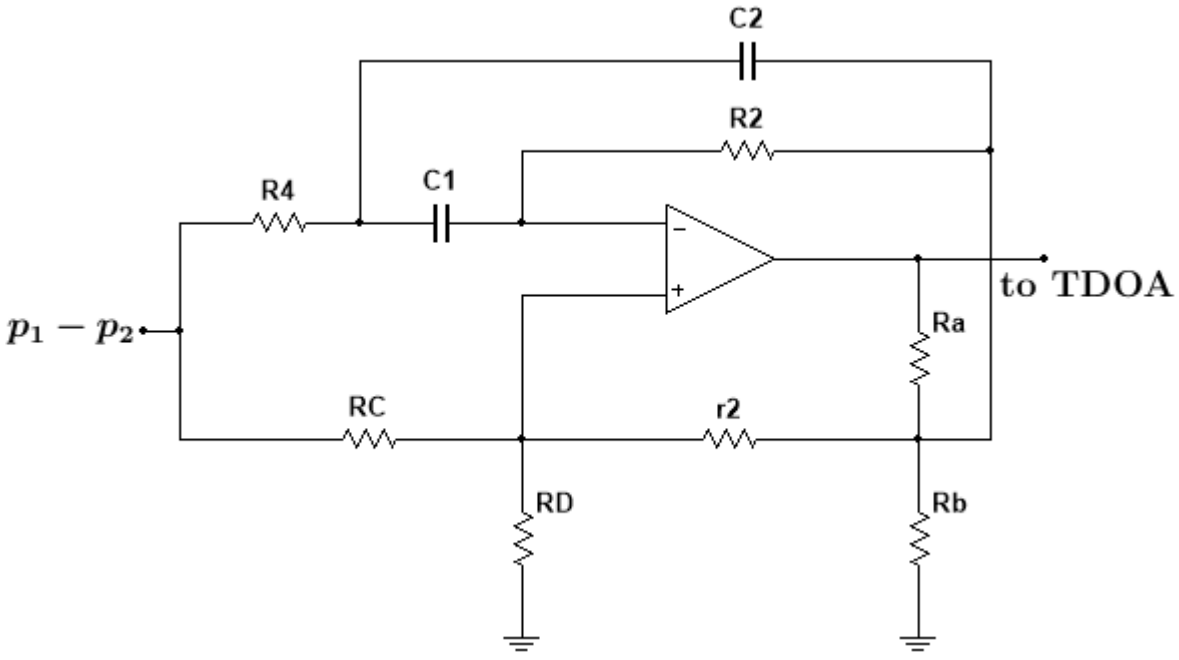

Figure 3.13: Single-Amplifier General Biquad for $H_U(s)$.

small when compared to the value of r_2. For these reasons, it is highly recommended that the circuit should exhibit a DC gain of 1 or close to it, which means that the rest of the gain has to be provided by the previous stage (which, in most cases, would be a differential amplifier) or a subsequent stage. The value of β must not be very high, simulations show that the maximum recommended value of β should be in the vicinity of 0.85. Also, a lot of component values for both circuits (Figs. 3.12 and 3.13) depend on the value of β, which means that it is extremely difficult to make β user-adjustable. Many of these complications might be resolved—particularly in the case of the $H_U(s)$ circuit synthesis—if a different circuit topology is selected, however, such circuits generally require a larger number of op-amps. Some resources where Multiple-Amplifier General Biquad circuits can be found are: [63, 64, 65, 66, 67].

Finally, once the circuits for $p'(t)$ and $\rho_0 c_0 u'(t)$ have been synthesized, the only remaining circuits required to obtain $a'(t)$ and $b'(t)$ are a summing and a differential amplifier with a gain of $1/2$ as required by Eqs. (1.10).

3.4 Analog Computing Method (ACM)

As described in the previous section the ANSM is capable of producing reduced circuits but, as the TDOA order is increased, the circuits become more complex and user adjustability of parameters becomes harder to implement. The Analog Computing Method (ACM) represents a different alternative which works on the expanded equations for $P'(s)$ and $\rho_0 c_0 U'(s)$, and allows the possibility to synthesize each operation as a separate element rather than trying to reduce the circuit to a product of transfer functions. The method derives its name from the somehow similar approach followed by analog computing techniques when solving differential equations using electronic circuits, which normally focus on realizing each operator of the equation rather than on synthesizing a transfer function as a whole. The advantage of the ACM is that it allows for a simpler design process, user adjustability of parameters such as β and τ, and the possibility to implement TDOAs of any practical order using all-pass filters. On the other hand, this usually means that the resulting circuits will be larger than those obtained by the ANSM using the same TDOA order, especially when very low-order TDOAs are selected. Thus, the ACM is most efficacious for TDOA with $n \geq 2$.

The expanded recursive equations from which the circuits will be derived using the ACM are the following:

$$P'(s) = \alpha_{opt} \left[P_1(s) + P_2(s) \right] H_1(s) - \beta P'(s) H_2(s) \tag{3.25a}$$

$$\rho_0 c_0 U'(s) = \alpha_{opt} \left[P_1(s) - P_2(s) \right] H_1(s) + \beta \rho_0 c_0 U'(s) H_2(s) \tag{3.25b}$$

The only adjustable parameter will be β. Since $\alpha_{opt} = (1+\beta)/2$, only β has to be adjustable and a proper circuit should be able to provide the corresponding α_{opt} for a given value of β. Fig. 3.14 shows the functional block diagram required to implement a fully

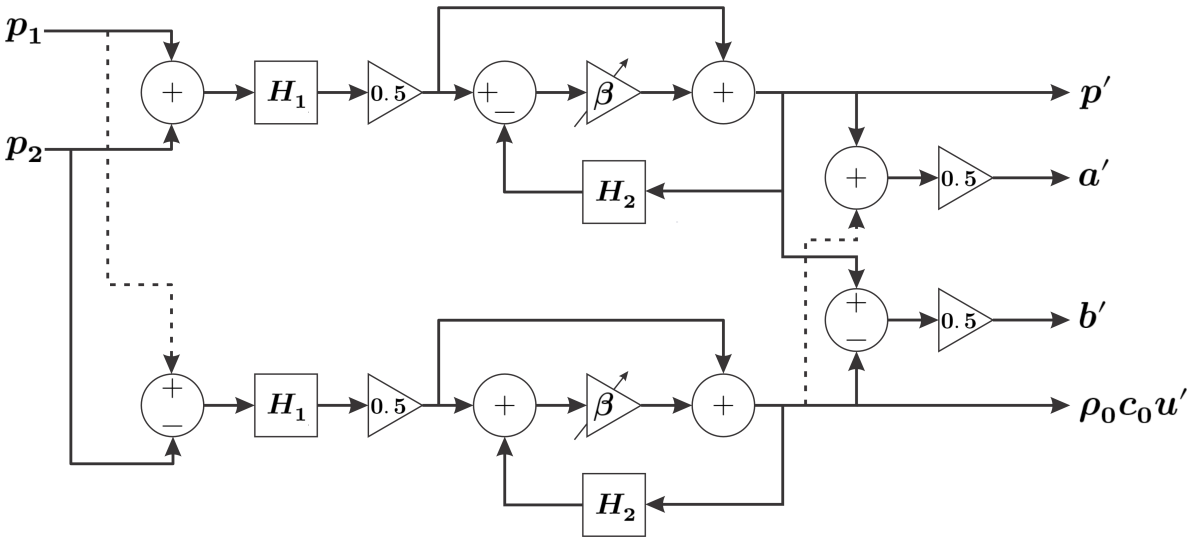

Figure 3.14: Circuit block diagram using the ACM [1].

working circuit. The main focus of the following discussion will be placed on the section required to adjust β, to make things clearer Fig. 3.15 shows a possible way to synthesize such circuit, the inverting variant is shown in Fig 3.16, both circuits will serve to explain how β is user-adjustable while α_{opt} automatically adopts its required value for the selected value of β. These circuits are now described.

The components labeled J1 to J3 are jumper terminals (which can be replaced by relays or break-before-make switches), when each of the first two jumper pins are shorted together and the third is left open, the circuit works normally as described in the the diagram of Fig. 3.14, otherwise, when the second and third pins of each jumper are shorted together and the first is left open, the circuit works in β *calibration mode*. To analyze the circuit superposition will be employed. Consider the circuit of Fig. 3.15 required to produce p' when all jumper terminals have their first and second pins shorted together and the third pin is left open, that is, when the circuit is working in normal mode. First, we will consider the contribution from the output of H_1, which means that the output from H_2 is considered a short to ground. The signal at the non-inverting input of op-amp U1 will be $v_{I_{\mathrm{U1}}} = [p_1 + p_2]\, H_1/2$, thus, the 0.5 attenuation represented in Fig. 3.16 by an amplifier block is actually implemented by the 2:1 resistive voltage divider at the input of U1. Op-amp U1 is working as a non-inverting amplifier with a gain $A_1 = 1 + [R2 + R3]\,/R_1$, R_1 and R_2 are fixed resistors, whilst R_3 is a potentiometer; the value of R_1 is selected to be close or equal to that of R_3, whilst R_2 should be smaller than the other two and its value will determine the minimum allowed value for β. The output at U1 will be $v_{O_{\mathrm{U1}}} = [p_1 + p_2]\, H_1\,(1 + [R2 + R3]\,/R_1)\,/2$, so the equation for β is given by:

$$\beta = \frac{1 + [R_2 + wR_3]\,/R_1}{2} \tag{3.26}$$

where $0 \leq w \leq 1$ represents the wiper position of potentiometer R_3. Simultaneously, the output from H_1 also feeds the 2:1 resistor divider connected at the input of op-amp U2, this resistor arrangement provides a 1/2 attenuation to the outputs of U1 and H_1, hence, the

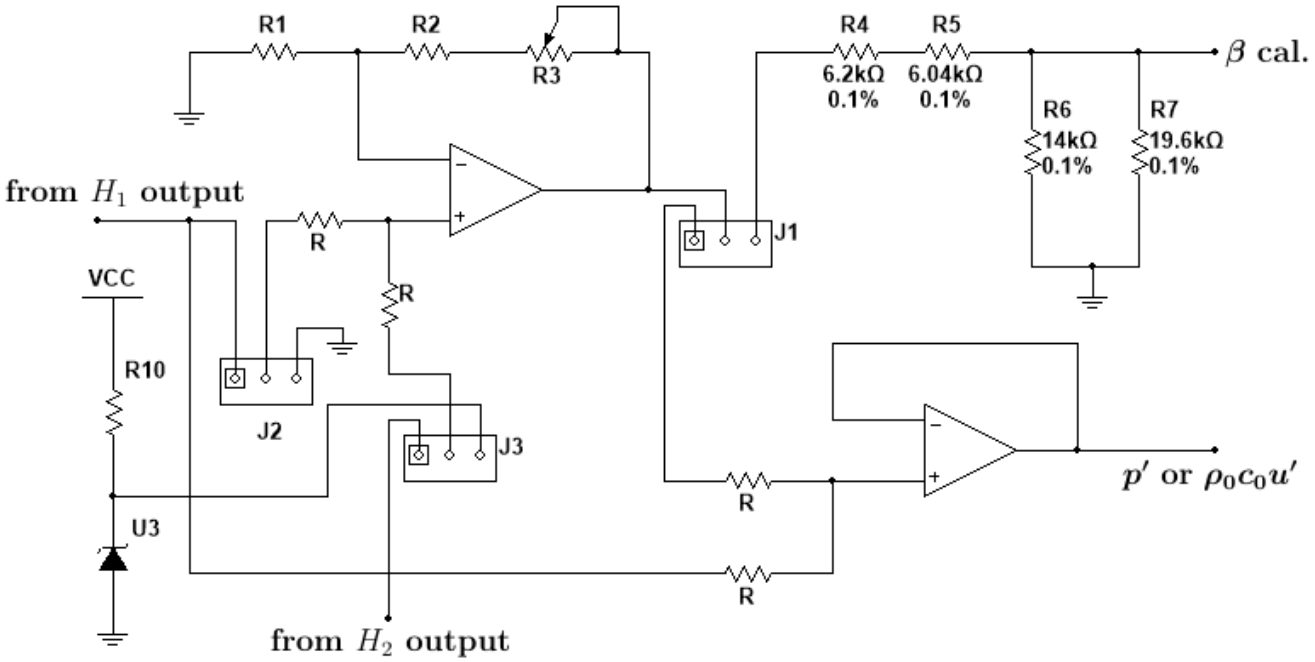

Figure 3.15: Circuit block for adjustable β.

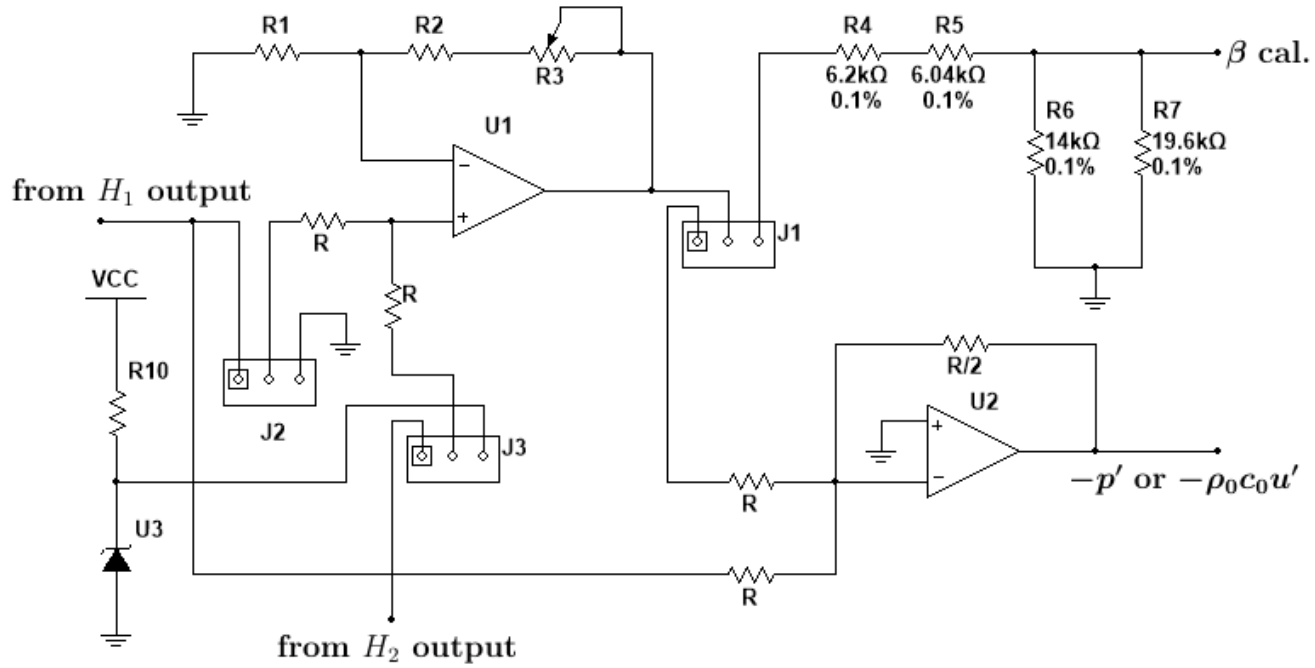

Figure 3.16: Circuit block for adjustable β (inverting).

output of op-amp U2 will be $v_{O_{\mathrm{U2}}} = v_{O_{\mathrm{U1}}}/2 + [p_1 + p_2]\, H_1/2 = \alpha_{opt}\, [p_1 + p_2]\, H_1$.

For illustration purposes a numerical example will be given: suppose $R_1 = R_3 = 2$ kΩ and $R_2 = 200\ \Omega$, now say that the wiper of pot R_3 is located at 80% of its full value, that is $w = 0.80$ and $\beta = 0.95$ from Eq. (3.26), hence, $v_{O_{\mathrm{U1}}} = [p_1 + p_2]\, H_1\, (0.95/2) + [p_1 + p_2]\, H_1/2 = [(0.95 + 1)\, /2]\, [p_1 + p_2]\, H_1$ where it can be seen that $\alpha_{opt} = (0.95 + 1)\, /2 = 0.975$, this is how the circuit obtains the value of α_{opt} automatically when β is adjusted by the user.

To complete the superposition analysis the contribution from H_2 will now be addressed, the output from H_1 is considered a short circuit to ground and the input at op-amp U1 will be $v_{I_{\mathrm{U1}}} = p' H_2/2$, with the corresponding output $v_{O_{\mathrm{U1}}} = p' H_2\, (1 + [R2 + R3]\, /R_1)\, /2 = \beta p' H_2$, the output of U1 is once again fed to a 2:1 resistive voltage divider and the output is $v_{O_{\mathrm{U2}}} = v_{O_{\mathrm{U1}}}/2 = \beta p' H_2/2$, to counter the division by 2, the gain of H_2 must be equal to 2 and we get $v_{O_{\mathrm{U2}}} = \beta p' H_2$. This completes the superposition analysis and shows how the contribution from the outputs of H_1 and H_2 sum up to form Eq. (3.25a). The equivalent circuit required for $\rho_0 c_0 u'\,(t)$ is exactly the same, and the inverting circuit of Fig. 3.16 differs only from the fact that the output is inverted.

An important caveat must be mentioned, the fact that the gain of H_2 has to be raised to 2 so unity gain is achieved after its output is attenuated by 1/2 at the input of U2, does not represent the best gain structure practice. The main consequence of this gain-attenuation scenario is that it reduces headroom since the H_2 stage will saturate earlier, to avoid this complication another circuit arrangement would have to be produced, it would probably involve the usage of inverting amplifiers since their virtual ground property allows isolation between the inputs, however, such type of circuit is not always practical since an extra op-amp has to be introduced at some point to counter the signal inversion. Hence, the circuits discussed thus far represent the best solution devised at the present moment able to produce the desired results with a minimum number of op-amps, but other topologies should be studied in the future to overcome the gain-attenuation issue whilst still being able to provide a non-inverted output with the smallest number of op-amps possible.

Now the procedure to calibrate β is described. The value of β depends on the position of the wiper of R_3, but measuring resistance is neither practical nor does it guarantee that the value of β will be accurately known by just measuring the potentiometer's resistance since the other components of the circuit will also influence the result. For these reasons, one of the most practical ways to approach this issue is to apply a known and precise DC test voltage at the input of the circuit and measure the output produced by U1, such is the purpose of Zener diode symbol U3 which, in fact, is not a Zener diode but rather a precision DC voltage reference IC. When jumpers J1-J3 are set to the β *calibration mode*, that is, when pins 2 and 3 are shorted together and pin 1 is left open, all signals coming from H_1 and H_2 are interrupted but the rest of the circuit is left intact and a stable DC voltage is injected by U3. The resistor voltage divider formed by R_4 to R_7 in Figs. 3.15 and 3.16 produces a 2.5:1 attenuation ratio when a typical DMM (digital multi-meter) with a 10 MΩ input impedance is used to measure the voltage at the terminal β cal. This was done in order to avoid adding an extra op-amp to buffer the output of the divider, so the multi-meter loading of the voltage divider was considered when the resistor values R_4 to R_7 were computed. Moreover, if the

resistors labeled R at the input of U2 are set to 10.2 kΩ each (the value used in this work for experimental validation), the total resistance seen by the output of U1 in β *calibration mode* will be the same that when operating in normal mode, namely, 20.4 kΩ; ensuring that, when calibrating the value of β, the circuit conditions vary as small as possible compared to the normal operating mode. If U3 is a 2.5 V voltage reference, the voltage measured in mV at the β cal terminal will correspond directly to the value of β of the circuit (e.g. if the DMM displays 973 mV it means that $\beta = 0.973$), if U3 is replaced by a reference that produces a voltage other than 2.5 V, the values of R_4 to R_7 will have to change accordingly. Only a single voltage reference is required to calibrate the circuits for p' and $\rho_0 c_0 u'$, this means that the circuits have to be adjusted one at a time.

Finally, to obtain $a'(t)$ and $b'(t)$, a summing and a differential amplifier with a gain of 1/2 each, and with $p'(t)$ and $\rho_0 c_0 u'(t)$ as their inputs are needed to perform the operations required by Eqs. (1.10), in a similar fashion to that of the circuit in Fig. 3.10.

3.5 A or B Using a Single Op-Amp

When maximum simplicity is required without too much precision, a single op-amp can be used to obtain either A or B. Very simple approximate equations for A and B attained by replacing the time delay operators with a Maclaurin series and truncating all the non-linear terms are [24, 28]:

$$A(\omega) = \frac{1}{2}\left[P_2(\omega) + \frac{P_1(\omega) - P_2(\omega)}{j\omega}\right] \tag{3.27a}$$

$$B(\omega) = \frac{1}{2}\left[P_1(\omega) + \frac{P_2(\omega) - P_1(\omega)}{j\omega}\right] \tag{3.27b}$$

The circuits shown in Fig. 3.17 were devised with superposition and are capable of directly obtaining $2a'(t)$ and $2b'(t)$, if the factor of two is to be removed, a simple voltage divider at each op-amp output can be inserted, but it is important to insure that the input resistance of the following stage is high enough as to not load the voltage divider considerably; another option is to pre-attenuate the input signals $p_1(t)$ and $p_2(t)$ before feeding them to each circuit. For these and other reasons, it is convenient to use a line receiver IC like the THAT1286 [68]: it provides differential inputs and conveniently exhibits a −6 dB gain (a factor of 1/2), also, it has a very low output impedance, something which is very important to avoid altering the time constants of the circuit, since any output resistance feeding the inputs will add to R_1 and will alter the time-delay τ. Good component matching is also important for good performance. The design equations for each circuit are the same as Eqs. (3.22).

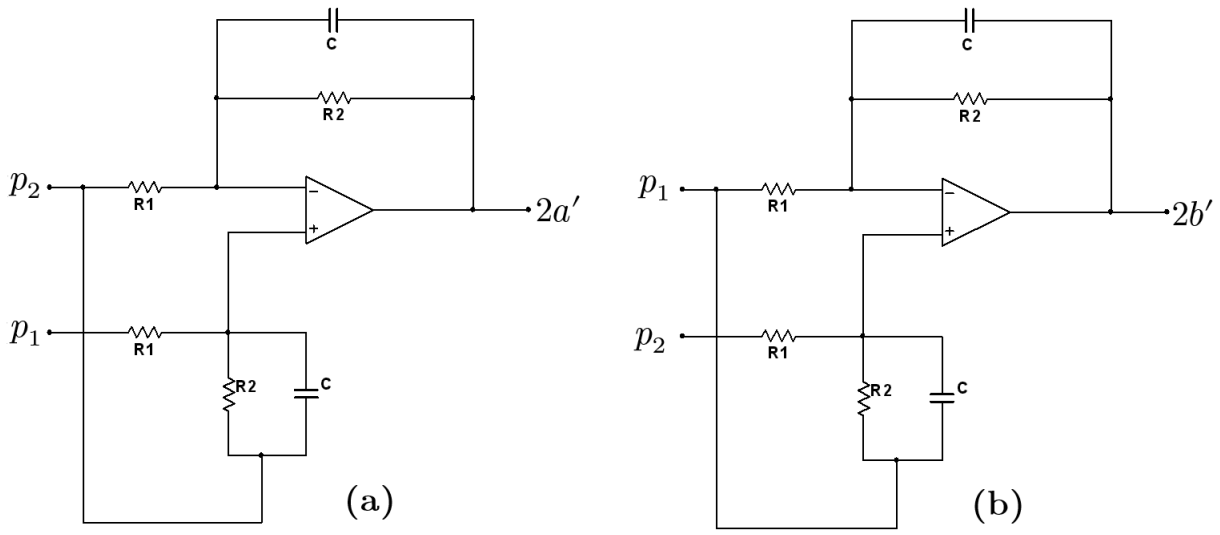

Figure 3.17: One op-amp circuits to obtain: (a) $2a'(t)$ and (b) $2b'(t)$.

3.6 Reconfigurability

If the microphones have to be re-positioned at different distances, if the need to use the same TWSS with different types of tubes arises, or if the environmental conditions vary considerably, the required time delay τ will have to change accordingly. This would require altering the RC time constants of every TDOA circuit block. One possible way to achieve this is by means of digital potentiometer integrated circuits (DP-ICs). These ICs consist of essentially a large number of integrated resistors connected in series. Two of the IC terminals are connected to the two ends of this resistor "ladder", and, by means of programmable electronic switches, it is possible to connect one of the IC terminals to any tap between a combination of resistors; this terminal would be the equivalent to the wiper inside a conventional potentiometer. Hence, DP-ICs are essentially programmable voltage dividers and their main specifications include: the number of steps (number of taps) available, the total resistance from end to end, the number of potentiometers per IC, the potentiometer law (e.g., logarithmic, linear, etc...), and the maximum resistance tolerance. At the time of writing several DP-ICs can be found in the market. A quick survey of readily available DP-ICs revealed that the number of potentiometers per IC is typically 1, 2, 3, 4, or 6; the number of selectable taps or steps range from 32 to 1024, with resistance tolerances as low as 0.025 % and as high as 30 %. The most common programming communication protocols for these ICs are I^2C and SPI; both are supported by the vast majority of popular micro-controllers.

It is important to emphasize that, even though the name of these ICs includes the word "digital" in it, no digital signal processing, nor any AD/DA conversion takes place inside these ICs, the voltages being fed to them always remain in the continuous time domain, it is only the tap selection process that is performed by digital means.

Incorporating DP-ICs and a microcontroller results in an analog-digital hybrid TWSS, which entails several advantages, for example: the inter-microphone distance value could be entered by means of a user interface and the microcontroller would automatically obtain and adjust the time delay τ required for a particular microphone separation. A temperature sensor can be included in the design and periodically monitored by the microcontroller, to take into account the sound speed variations that occur at different temperatures and compensate for these variations accordingly by automatically re-adjusting the value of τ. The potentiometer used to set the value of β could also be replaced by a DP-IC, this would not only allow for the user to enter the desired value for it, but also, it could open up the possibility for dynamic control of β, for example, if the sound field does not vary abruptly (e.g., in the case of an invariable and predictable noise source), the value of β could be made closer to 1 by the microcontroller as to increase the level of separation; if, however, the sound source is more prone to exhibit several transitory components, the value of β could be lowered automatically to reduce the relaxation time T, thus making the system more responsive at the expense of reduced precision.

Since several parameters have to be adjusted in isolation (i.e., without affecting other parameters in the circuit), the circuits obtained by the ACM are the most suitable for this purpose; unlike those obtained by the ANSM which, aside from the simplest configurations (e.g., the first-order circuit), in most cases do not easily allow for the tuning of parameters without major changes to the circuits.

The circuit shown in Figure 3.4 can be modified to implement a variable TDOA. For this purpose, let $R_1 = R$, $R_2 = \xi R$, where $\xi \in \mathbb{R}^+$, $R = R_{fix} + R_{DP}$ and R_{fix} is a fixed value resistor in series with variable resistance R_{DP} controlled by a DP-IC. Also, let $C_1 = \kappa C$, $C_2 = C$, where $\kappa \in \mathbb{R}^+$. This particular choice for the components will become self evident as the design equations are derived.

The transfer function of the circuit in Figure 3.4 is given by Eq. (3.6), comparing it to the canonical form of an all-pass transfer function in Eq. (2.60), it can be seen that

$$\omega_0 = \frac{1}{\sqrt{R_1 R_2 C_1 C_2}} = \frac{1}{RC\sqrt{\kappa\xi}} \tag{3.28}$$

substituting Eq. (2.65a) into (3.28) and solving for τ:

$$\tau = \sqrt{a\kappa\xi}RC \tag{3.29}$$

This result is one of the reasons why the particular selection of components mentioned earlier was performed, that is, because Eq. (3.29) shows that the time delay can be varied linearly by adjusting R, hence, the minimum and maximum time delays: τ_{min} and τ_{max}, respectively, will be:

$$\tau_{min} = \sqrt{a\kappa\xi}R_{fix}C \tag{3.30a}$$

$$\tau_{max} = \sqrt{a\kappa\xi}\left(R_{fix} + R_{DP_{max}}\right)C \tag{3.30b}$$

Again, comparing Eq. (3.6) with (2.60) and substituting (2.65b), the following association can be made

$$BW = \frac{b}{\tau} = \frac{C_1 + C_2}{R_2 C_1 C_2} = \frac{1+\kappa}{\xi \kappa C} \tag{3.31}$$

substituting Eq. (3.29) into (3.31) and solving for κ we get

$$\kappa^2 + \left(2 - \xi \frac{b^2}{a}\right)\kappa + 1 = 0 \tag{3.32}$$

and has the following solutions:

$$\kappa = \xi \frac{b^2}{2a} - 1 \pm \sqrt{\left(\xi \frac{b^2}{2a} - 1\right)^2 - 1} \tag{3.33}$$

In order to obtain real-valued solutions, the following constrain must be met:

$$\xi \geq \frac{4a}{b^2} \tag{3.34}$$

A convenient value is $\xi = 2$, since $R_2 = \xi R_1$ is implemented with a DP-IC and the steps are scaled in powers of 2. This value for ξ will be high enough for most approximations , however, some TDOAs may produce values dangerously close to 2 (e.g., the H_∞ norm approximation has $4a/b^2 = 1.911$, see Table 2.3) and others may even exceed it, so close attention must be paid to insure ample safety margins to account for component tolerances.

Comparing Eq. (3.5) to (3.6), substituting (3.31) and solving for $|H_{0_{BP}}|$, the following expression can be obtained

$$|H_{0_{BP}}| = \xi \frac{\kappa}{\kappa + 1} \tag{3.35}$$

Equation (3.35) also reveals and important aspect, specifically, that the band-pass gain depends only on the values of κ and ξ, and not on the particular value of R, which is used to adjust the time delay τ, this is a consequence of the particular choice of components set at the start of this analysis. In practice, both capacitors, as well as the R_{fix} and R_{DP} resistor values, must be closely matched to obtain good results.

The output of the band-pass MFB circuit is amplified by an inverting amplifier, which has a gain R_4/R_3, the total gain experienced by the band-pass portion of the circuit must be 2 (see Eq. (3.5)), hence

$$\frac{R_4}{R_3} |H_{0_{BP}}| = 2 \tag{3.36}$$

substituting Eq. (3.35) into (3.36) and solving for R_4/R_3, we get

$$\frac{R_4}{R_3} = \frac{2(\kappa + 1)}{\xi \kappa} \tag{3.37}$$

The complete circuit for $\xi = 2$ is shown in Fig. 3.18. Since $R_2 = \xi R = 2R$, 2 digital

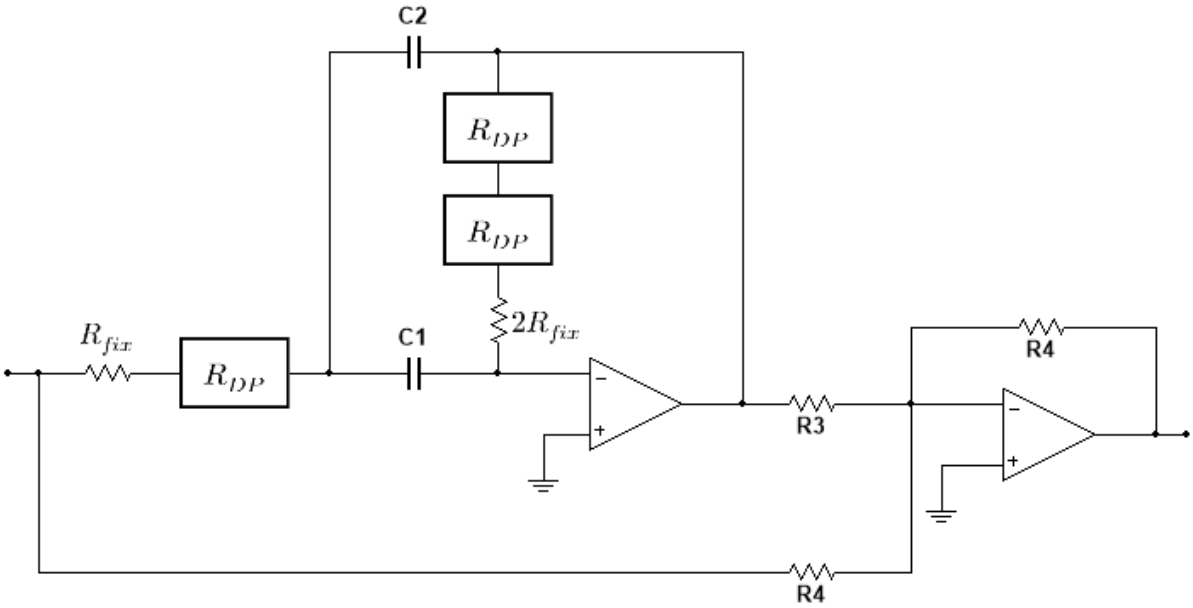

Figure 3.18: Adjustable TDOA using digital potentiometer integrated circuits (DP-ICs), $\xi = 2$.

potentiometers are used for R_2 in order to avoid the loss of tuning range, since, if only one digital potentiometer is used for R_2, R_1 cannot be adjusted further than $R_1 = R_{DP_{max}}/2$, essentially losing half the tuning range. The downside is that this circuit involves using a total of 3 digital potentiometers. If the loss of range can be tolerated, only 1 digital potentiometer can be used for R_2, both fixed resistors would have to be replaced by short circuits, hence, care must be taken that none of the digital potentiometers ever reaches a very low value as to load the previous stage or the output of the op-amp, this circuit is shown in Fig. 3.19.

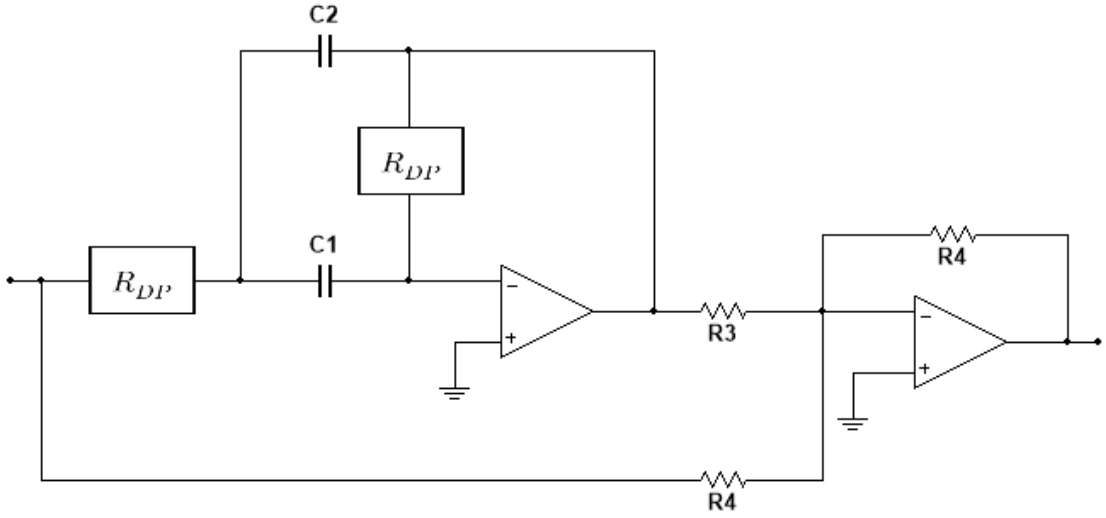

Figure 3.19: Adjustable TDOA using less digital potentiometers, $\xi = 2$.

For illustration purposes a variable second-order Piché TDOA can be implemented as follows: from Eq. (2.31) we get $a = 9.8696044$, 4.9348022, and $4a/b^2 = 1.62$, so $\xi = 2$ will be used. Substituting these values into Eq. (3.33) and taking the smallest solution yields $\kappa = 0.3935$. Selecting $C_2 = C = 12$ nF, then $C_1 = \kappa C = 4.7$ nF. Selecting $R_3 = 1.58$ kΩ, substituting in Eq. (3.37), and rounding to the nearest commercial value we get $R_4 = 5.6$ k. If $R_{fix} = 1$ kΩ and using a DP-IC with at least 3 potentiometers, each with a resistance $R_{DP_{max}} = 10$ kΩ, we get from Eqs. (3.30): $\tau_{min} = 33.4$ μs and $\tau_{max} = 367.9$ μs. These time delay values will be able to accommodate a wide variety of different inter-microphone separations and tube dimensions, as well as changes in environmental conditions.

3.7 Microphone Response Matching

The TWSS's performance will be detrimented if the responses of the microphones being used are mismatched. High quality microphones usually exhibit very similar responses to each other, but less accurate and inexpensive microphones can show significant differences, particularly at low frequencies. Figure 3.20 shows the measured magnitude and phase of two low-cost Behringer ECM8000 measurement microphones. The response is plotted in a frequency span of $100 - 1700$ Hz. This particular range was selected because it roughly corresponds to the operating range of a 4 in diameter tube with $2\delta = 10$ cm microphone spacing, and was determined according to the ASTM E2611-09 standard recommendations and the upper frequency limit set for plane wave propagation for the tube dimensions [29]; also because it clearly shows the differences that occur between both microphones at low frequencies.

A possible way to correct the differences in magnitude and phase between two microphones in the continuous time-domain, can be accomplished by applying a suitable matching transfer function to one of the two microphones. An arbitrary non-minimum phase transfer function can be split into the product of a minimum phase transfer function and an all-pass transfer function [32]:

$$H(s) = H_m(s)\, H_{AP}(s) \tag{3.38}$$

where $H_m(s)$ and $H_{AP}(s)$ represent the minimum phase and all-pass transfer functions, respectively.

Equation (3.38) is quite useful, because it implies that the magnitude and phase can be adjusted separately, since an all-pass transfer function exhibits a flat magnitude response while altering the phase. The approach proposed in this work uses goal-based numerical optimization depending on experimental measurements of two microphones in order to find suitable coefficients for each transfer function: first, the coefficients of the minimum phase transfer function are obtained as to match the magnitude response of both microphones, afterwards, the coefficients of the all-pass transfer function are found in order to match the phase without altering the magnitude response.

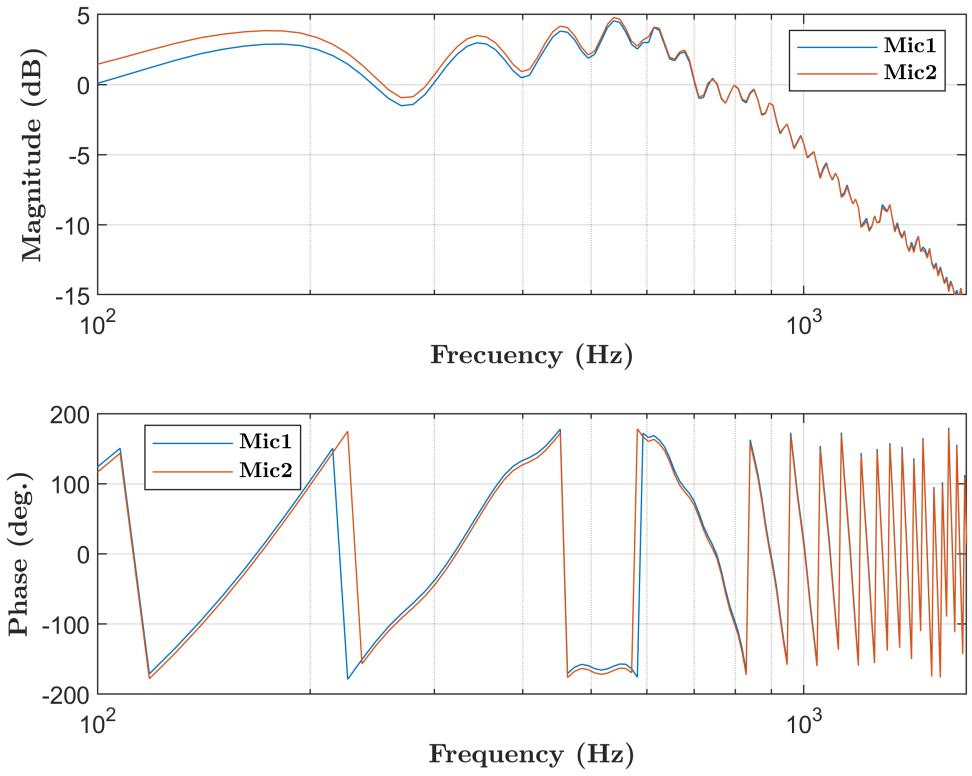

Figure 3.20: Magnitude and phase of each microphone, no correction.

The following prototype functions are used:

$$H_m(s) = H_{m_0} \frac{\sum_{k=0}^{n} a_k s^k}{\sum_{g=0}^{n} b_g s^g} \tag{3.39a}$$

$$H_{AP}(s) = \frac{\sum_{i=0}^{m} (-1)^i d_i s^i}{\sum_{d=0}^{m} f_d s^d} \tag{3.39b}$$

where H_{m_0} is the DC gain, $\{n, m \in \mathbb{Z}^+\}$ correspond to the order of each transfer function, and the coefficients $\{a_k, b_g, d_i, f_d \in \mathbb{R}_*^+\}$ are obtained with numerical optimization. For the microphone responses shown in Figure 3.20 and using $n = 4$, $m = 2$ order minimum phase and all-pass transfer functions, respectively, the optimization routine yielded entirely real poles and zeros.

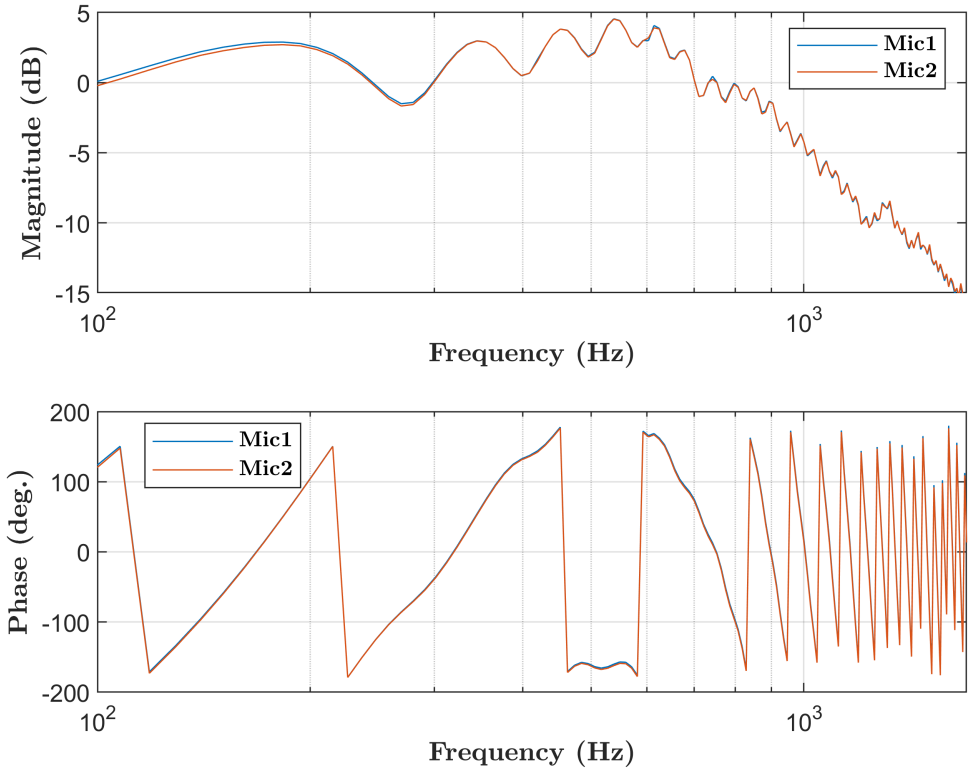

Figure 3.21: Magnitude and phase of each microphone, with correction.

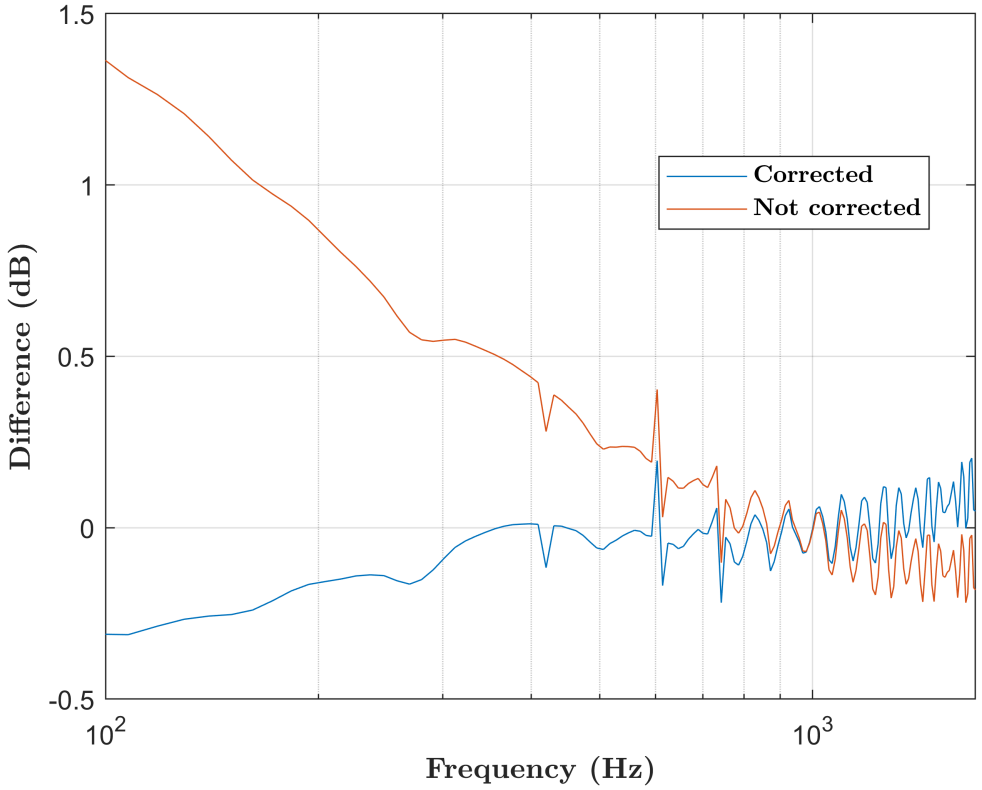

Figure 3.22: Magnitude difference between microphones with respect to frequency.

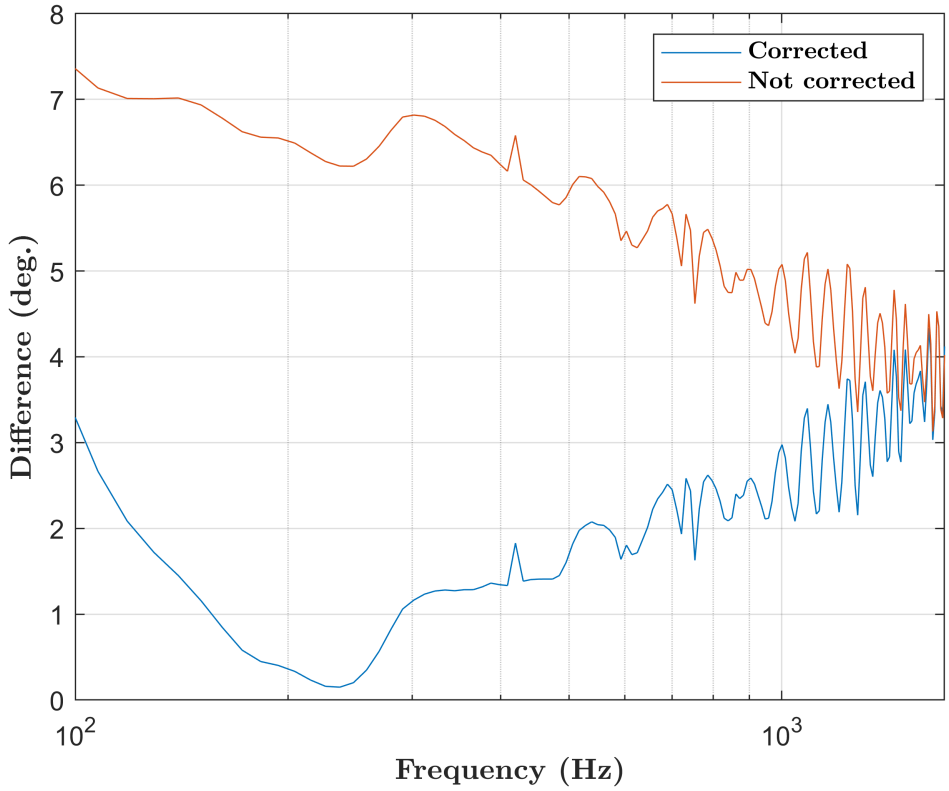

Figure 3.23: Phase difference between microphones with respect to frequency.

Figure 3.21 shows the corrected magnitude and phase response of each microphone after the matching transfer function given by Eqs. (3.38) and (3.39), with the coefficients obtained from numerical optimization, was applied to the DFT of Microphone 2. As can be seen both the magnitude and phase have been closely matched within a small error. Compare the corrected response of Fig. 3.21 to the un-corrected response of Fig. 3.20. Figures 3.22 and 3.23 show the magnitude and phase differences of the corrected and un-corrected responses, respectively, between the two microphones in the operating range of the tube. Higher order transfer functions would probably yield better results, however, the circuit complexity would also increase

One possible way to electronically implement Eq. (3.39a) is with a cascade of Single-Amplifier General Biquad circuit blocks such as the one shown in Fig. 3.11. Likewise, for Eq. (3.39b) any of the circuits discussed in Section 3.2.2 might be used, however, this was not pursued any further in the present work.

Chapter 4

Validation and Results

4.1 Introduction

The circuits required to perform travelling wave separation in the time domain were described in the previous chapter. In this chapter, the experimental validation of the techniques proposed hitherto is presented, for this, two complete Travelling Wave Separation Circuits (TWSC) were fabricated and measured: the first, henceforth referred to as TWSC-1, is a first-order TWSC realized by using the ANSM; the second, henceforth referred to as TWSC-2, is a second-order TWSC with adjustable β realized by means of the ACM. Some experimental results obtained with these circuits were published in [1].

The main application of each circuit is to provide a plug-and-play solution to obtain the forward and backward travelling wave components in a test tube arrangement such as the one shown in Fig. 4.1. Previous knowledge of the distance between microphones and the ambient temperature is necessary, so the circuit must be designed with these set values in mind, or an adjustable circuit such as the one described in Section 3.6 should be used instead. As for the calibration process itself, there is no particular requirement other than to make sure that the microphone gains are as closely matched as possible.

The design goals are as follows:

- Design and implement two TWSCs: a first-order TWSC realized by means of the ANSM, and a second-order TWSC realized by means of the ACM.
- The overarching principle for the first-order circuit (as mentioned in Chapter 3) is simplicity, which was assessed in terms of the number of active elements present in the circuit, and the use of only the indispensable passive components.
- The overarching principle for the second-order circuit is be precision and adjustability, the former will be assessed by its comparison to the equivalent frequency domain separation technique and the TWSC-1 performance.

- The tuning range for β for the TWSC-2 should be at least $0.6 - 1$.
- For TWSC-2, the amplitude deviation should be no larger than ± 0.5 dB in the entire operating range of the tube ($710 - 5680$ Hz), for the TWSC-1, such requirement cannot be specified, since it uses a low-pass approximation, which attenuates the output as the frequency increases.
- Both circuits must have differential (electronically balanced) inputs to provide common-mode rejection of signals and noise.
- Both circuits must have impedance balanced outputs (quasi-balanced) to provide common-mode rejection of signals and noise.

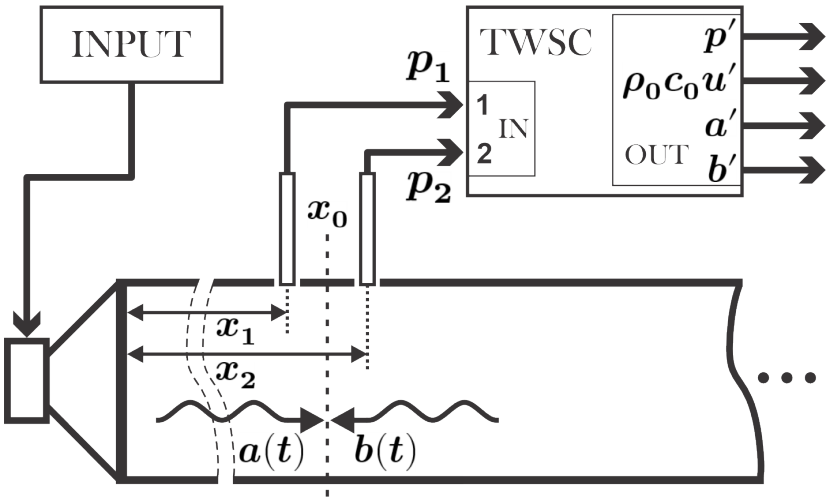

Figure 4.1: Typical arrangement used to obtain the forward- and backward-travelling wave components in a test tube using two microphones. [1]

4.2 Apparatus

The experimental setup consists of an acoustic test tube compliant with the ASTM E2611-09 and ISO 105354–2 standards. The apparatus is shown in Fig. 4.2 and it is the same as the one described in [17] and [1]. It consists of a 35 mm inner diameter aluminum internal tube shielded by a 51 mm inner diameter external tube that provides isolation from environmental noise. With these dimensions, the upper frequency limit at which plane wave propagation still occurs is $5,680$ kHz [29]. Two Brüel & Kjaer type 4938 microphones connected to a Brüel & Kjaer type 2829 power supply were used, the microphones were flush mounted along the tube wall with a distance $2\delta = 24.3$ mm between each other. For this separation, the ASTM E2611-09 standard recommends a lower operational frequency limit of 710 Hz [1]. The first singularity (due to the separation being equal to half a wavelength) occurs at $c_0/4d = 7,076$ Hz [1], which exceeds in good measure the upper frequency

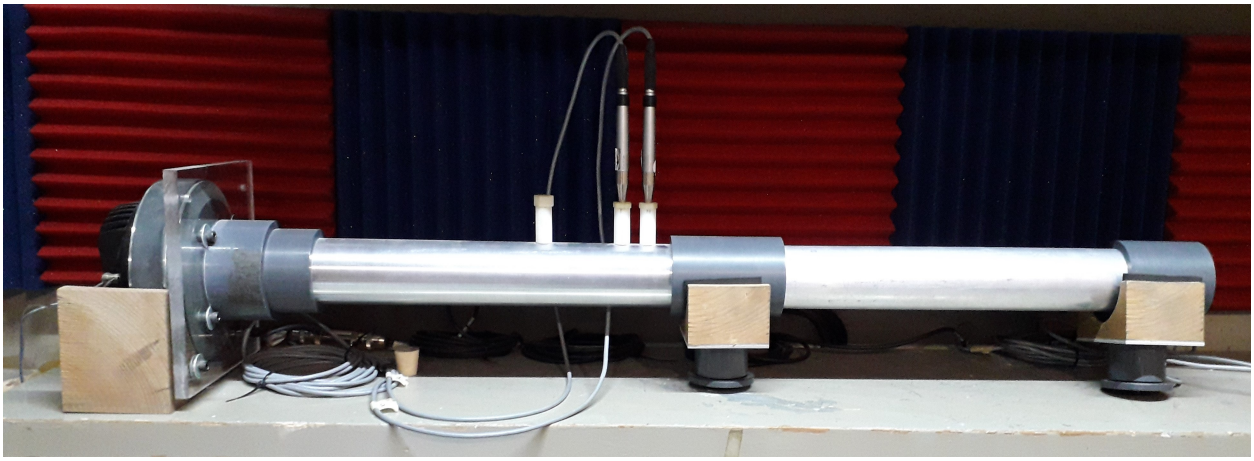

Figure 4.2: Apparatus used to conduct the experiments.

limit determined previously for plane wave propagation. It is assumed that the two microphones exhibit flat frequency responses over the operating frequency range, namely, 710 Hz to 5,680 Hz. The tube is terminated by a strong passive absorbing element, which consists of a 420 mm long aluminum tube filled with cotton blobs of decreasing diameter (increasing cotton-to-free-air ratio), and terminated at the far end with a closed rigid brass cap [1]. A loudspeaker driver located at the upstream end of the tube is fed by a Yamaha AX-380 Stereo Power Amplifier [1]. The setup diagram is shown in Fig. 4.3.

A Behringer UMC404HD audio interface connected to a PC was used to feed a repeated sinusoidal sweep signal of 65536 samples from 160 to 6,300 Hz at a sampling rate of 48 kHz [1]. The temperature at the time of measurement was 21 °C, and the corresponding sound speed was $c_0 = 343.9$ m/s [1], corresponding to $\tau = 35.33$ μs. The magnitude of the reflection coefficient of the absorber, which was measured in compliance with the ISO-10534–2 standard, is shown in Fig. 4.4. The sound pressure signals $p_1(t)$ and $p_2(t)$ that were acquired from the microphones in the test tube were fed to the inputs of the TWSC; the estimated travelling wave signals $a'(t)$ and $b'(t)$ at the output of the TWSC were recorded by the audio interface. In total, 100 sinusoidal sweeps were recorded and time averaged [1]. The same procedure was used to evaluate the two travelling wave separation circuits (TWSC).

4.3 First-Order Travelling Wave Separation Circuit

A first-order circuit using the ANSM and the circuits described in Chapter 3 was designed, simulated, fabricated, and measured experimentally. The circuit diagram is shown in Fig 4.5. It operates on ±15 V DC power supplies. All components are surface mount devices (SMD), resistors are of the thin-film type with 0.1% tolerance, bypass capacitors C_3-C_6 are regular 10% MLCC, but C_1 and C_2 are NP0/C0G 1% tolerance MLCC since they are used to determine the time constant τ of the circuit; capacitors C_7^* and C_8^* were not present in the PCB revision used for this work, but their use is recommended to reduce the risk of very

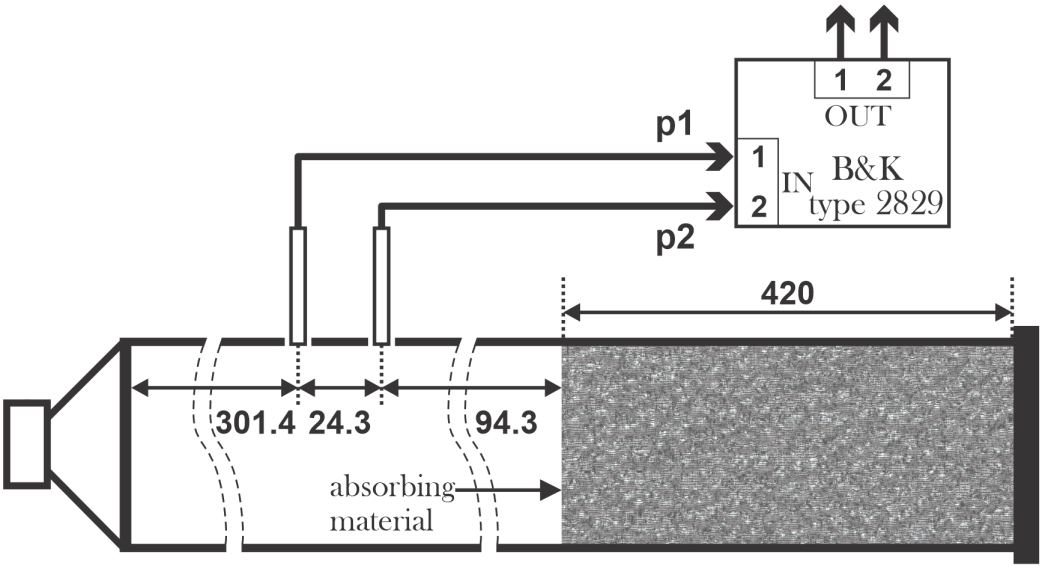

Figure 4.3: Diagram of the apparatus used to conduct the experimental measurements, distances are in millimeters.

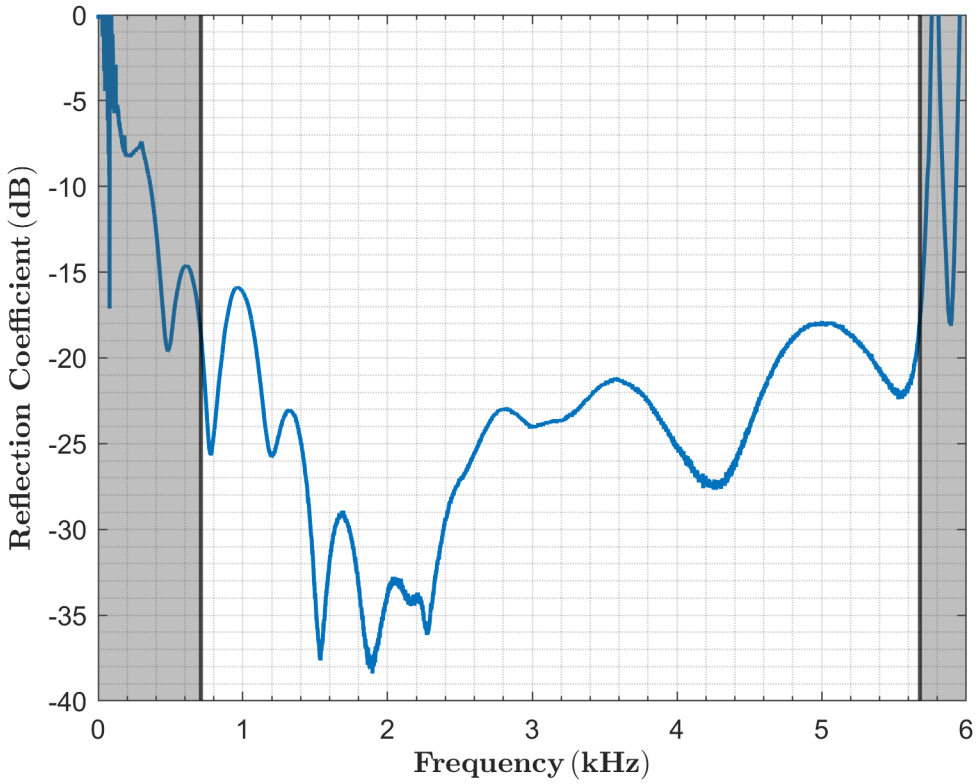

Figure 4.4: Reflection coefficient of the absorber [1].

high frequency oscillations appearing at the output.

All OpAmps labeled U2A to U2D are contained in a single SOIC-14 package with part number MC33079DR2G [69]. This IC was chosen due to its good AC properties and low cost. It consists of 4 bipolar OpAmps capable of operating with up to ±18 V DC supplies. The slew rate is 7 V/μs (typ.) making it capable of amplifying signals up to 80 kHz at full power into a 2 kΩ load when ±15 V DC supplies are used. It has a gain-bandwidth product of 16 MHz and an open-loop unity-gain bandwidth of 9 MHz, which means that plenty of closed-loop gain can be obtained whilst still maintaining an ample bandwidth; the OpAmps are also unity-gain stable. The driving capabilities are very good with loads as low as 600 Ω whilst still exhibiting low THD. On the other hand, the noise voltage and current densities are $e_n = 4.5$ nV/$\sqrt{\text{Hz}}$ and $i_n = 0.5$ $\sqrt{\text{Hz}}$/pA, respectively, which translate into an optimum source resistance $R_{opt} = 9$ kΩ, meaning that, in terms of noise, the OpAmp is most suitable for low to low-mid resistor values [70]. It is also important not to use high valued resistors in the non-inverting configurations (e.g., U2A and U2D) in order to keep common-mode distortion levels as low as possible [71, 72, 73]. The large values of resistors R_8 and R_{10} in amplifier U2B are an exception to the previous recommendations, since they are paralleled by a capacitor, which means that any noise arising from these resistors will be severly attenuated as frequency increases; also, the resistive arms are balanced which means that the amplifier sees the same impedances at both its inputs which reduces common-mode distortion.

Components labeled U2A and U2B are differential line receivers with 0 dB gain, both come in a single SOIC-14 package with part number THAT1280 [68]. Although their use is not strictly necessary, their inclusion is highly recommended for several reasons: first and foremost, they avoid the interaction between the driving sources output resistances and the TWSC by driving the TWSC inputs with a very low output impedance, that would otherwise add to the input resistances of the TWSC (particularly with R_7 and R_9) and alter the time constants of the circuit. Secondly, having a differential input line receiver allows the circuit to be driven with either unbalanced or balanced connections, the latter reduces noise interference, particularly at low frequencies. Thirdly, since the internal resistors of the THAT1280 are laser trimmed the CMRR (common-mode rejection ratio) is usually much higher than the one that could normally be achieved by using OpAmps and discrete resistors.

OpAmps can become unstable when driving capacitive loads, since the OpAmp's open-loop output resistance forms a pole with the load capacitance and introduces extra phase shift in the loop gain response [74]. A shielded audio cable can exhibit several tens of pF/m, consequently, it is capable of developing hundreds of pF depending on its length. To overcome this issue, resistors R_{13}, R_{15}, R_{17} and R_{19} are placed in series with the outputs of each OpAmp, these resistors combined with the load capacitance introduce a zero in the loop gain response that counters the added pole. The absolute value of these resistors is not extremely critical and it is sometimes suggested by the IC manufacturer, however, it must not be very high since a voltage divider is formed between these resistors and the input resistance of the following stage, thus attenuating the signal level. Very high values could also introduce high frequency roll-off in the pass band when long cables are used; more sophisticated solutions to overcome the effect of these resistors are available [75], such as

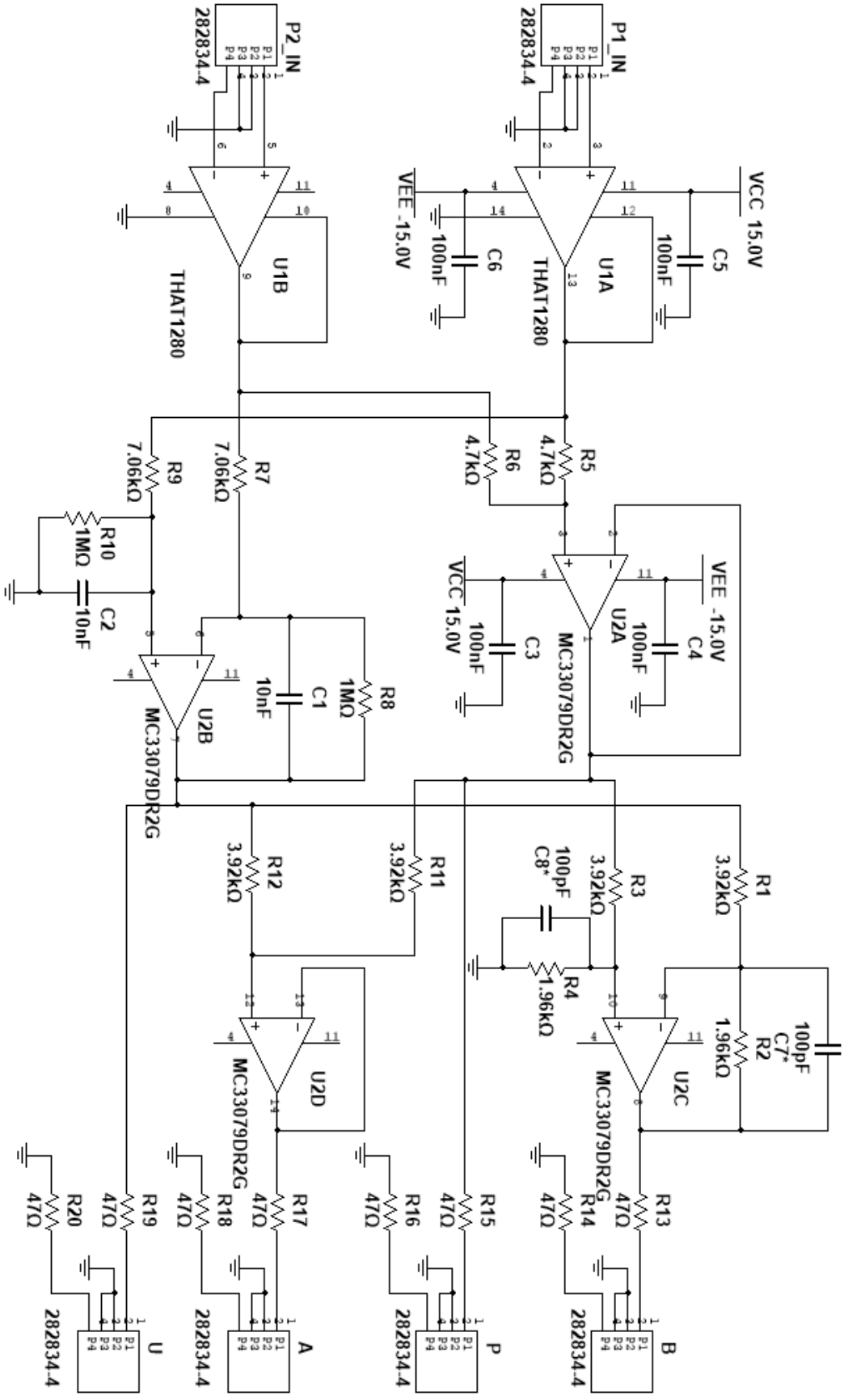

Figure 4.5: TWSC-1 schematic.

placing the resistor inside the feedback loop of the OpAmp [74, 75], however, a simple series resistor as shown in the schematic works well in most cases. Typical values for these resistors range from a few tens of ohms to a couple hundred ohms.

If two conductor shielded audio cables are used, R_{14}, R_{16}, R_{18} and R_{20}, which are meant to be connected between the second conductor (sometimes referred to as "cold") and ground, provide a balanced impedance output, commonly known as a *quasi-balanced* output, which improves induced noise immunity if the receiving stage exhibits a differential input such as those typically found in the line inputs of audio interfaces. The cost of adding these extra resistors is small and the benefit is quite noticeable.

DC blocking capacitors should be placed in series with the outputs (not present in the schematic or in the circuit tested in this work) to ensure that no DC flows into the following stage, however, because simplicity is the main objective of the first-order TWSC, these were not used to avoid having a larger and more cumbersome circuit. This is also justified since both the simulated and experimental measurements showed that the DC voltage at the outputs was low enough as not to create any serious issues.

The complete circuit board is shown in Fig. 4.6, the board dimensions are 100×50 mm with 1 mm thickness. It consists of a double-layer PCB on an FR4 substrate, the bottom layer was used as a ground plane with minimum tracing to avoid interrupting the continuity of the plane, so most of the tracing was done on the top layer.

By introducing the resistor values of R_7 and R_8 (which correspond to R_1 and R_2) into Eq. (3.22b), it can be seen that the value of β is fixed at 0.993. This also translates into a relaxation period $T = 5$ ms and a minimum error $E^2_{min} = -24.6$ dB.

4.4 Second-Order Travelling Wave Separation Circuit

Much of the design philosophy and the component types of the previous circuit were also used for the Second-Order TWSC. The schematic is shown in Fig. 4.7.

As can be seen, the circuit is much more complicated than the first-order TWSC. All TDOAs were synthesized using Delyiannis SABs as those described in Section 3.2.2, the gain setting resistors (e.g., R_{48}, R_{49}, R_{50} and R_{51}), that correspond to R_5 and R_6 in Fig. 3.6, were realized by parallel resistor combinations to achieve more precise values.

The voltage source U6 used to calibrate β consists of a 2.5 V precision voltage reference in a SOT23-3 package with part number LM4040C25MDBZTEP [76]. Resistor R_{11} is used to set the current through the voltage reference U6, its value must be calculated based on the following criteria: when jumpers P_J1, P_J2 and PJ_3 or U_J1, U_J2 and UJ_3 are set in β *calibration mode* (only one set of jumpers corresponding to P or U can be set in calibration mode at a time), that is when the jumpers are shorting the center pin and the pin without a square enclosing it, the output of the voltage reference feeds resistors R_{13} and R_{22} or R_{81} and R_{87} (depending on whether P or U is being calibrated), in either case,

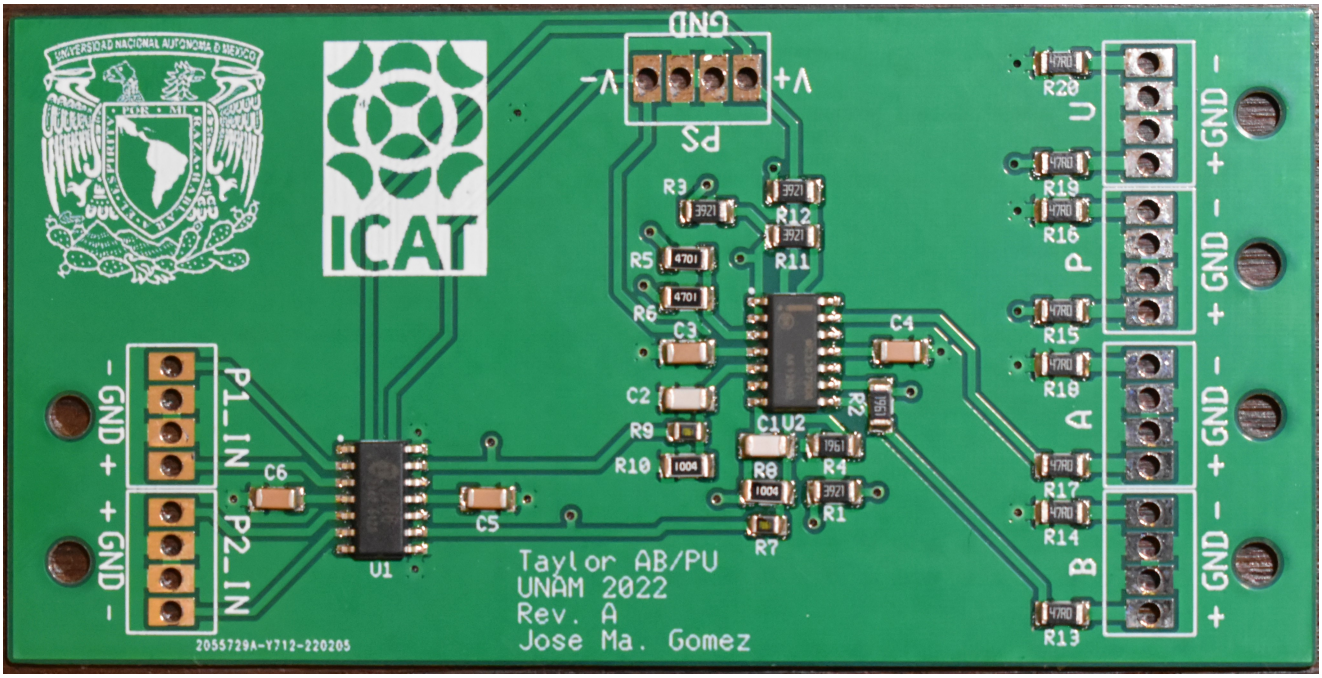

Figure 4.6: TWSC-1 circuit board.

the total load resistance seen by the voltage reference is $R_{load} = 20$ kΩ, and it draws a current $I_{R_{load}} = 2.5/20,000 = 125$ μA. Since the voltage reference changes slightly its value at different currents it is important to consider the current being drawn by the load. The manufacturer states a 2.5 V typical value when the current through the voltage source is $I_Z = 100$ μA [76]. By applying KCL at the node between R_{11} and U6 we get that the total current passing through R_{11} is $I_{R_{11}} = I_Z + I_{R_{load}} = 225$ μA, hence, the resistance should be $R_{11} = (15 - 2.5)/I_{R_{11}} = 55.55$ kΩ; the closest E96 commercial value is 55.6 kΩ, which corresponds to the value shown in the schematic.

An extra MC33079DR2G IC was used, which accounts for 4 extra OpAmps (labeled U3A to U3D), these are not required to obtain a' or b', however, they were added to buffer the signal outputs of p_1, p_2 and $\rho_0 c_0 u'$, and to provide the required circuitry to invert the output of U2C (which is $-p'$) to obtain p'.

Coupling capacitors C_8, C_{11}, C_{14}, C_{18}, C_{19} and C_{21} are used to block any DC from flowing to or from the outputs. Resistors R_{28}, R_{30}, R_{42}, R_{60} and R_{78} serve as a discharge path for the coupling capacitors to ground. The 68 Ω resistors isolate the outputs from capacitive loads as described in the TWSC-1 circuit. These isolation resistors were placed after the discharge resistors to avoid creating an unnecessary voltage divider. Neglecting the small 68 Ω resistors, the total resistance seen by the coupling capacitors will be that of the load (in this work this is determined by the audio interface inputs) in parallel with the 100 kΩ discharge resistors. If it is assumed that the outputs of the TWSC will feed a typical line input stage with input resistances larger than 10 kΩ [71], then, by selecting 10 kΩ as the minimum resistance typically seen by the outputs, the 6.8 μF coupling capacitors will

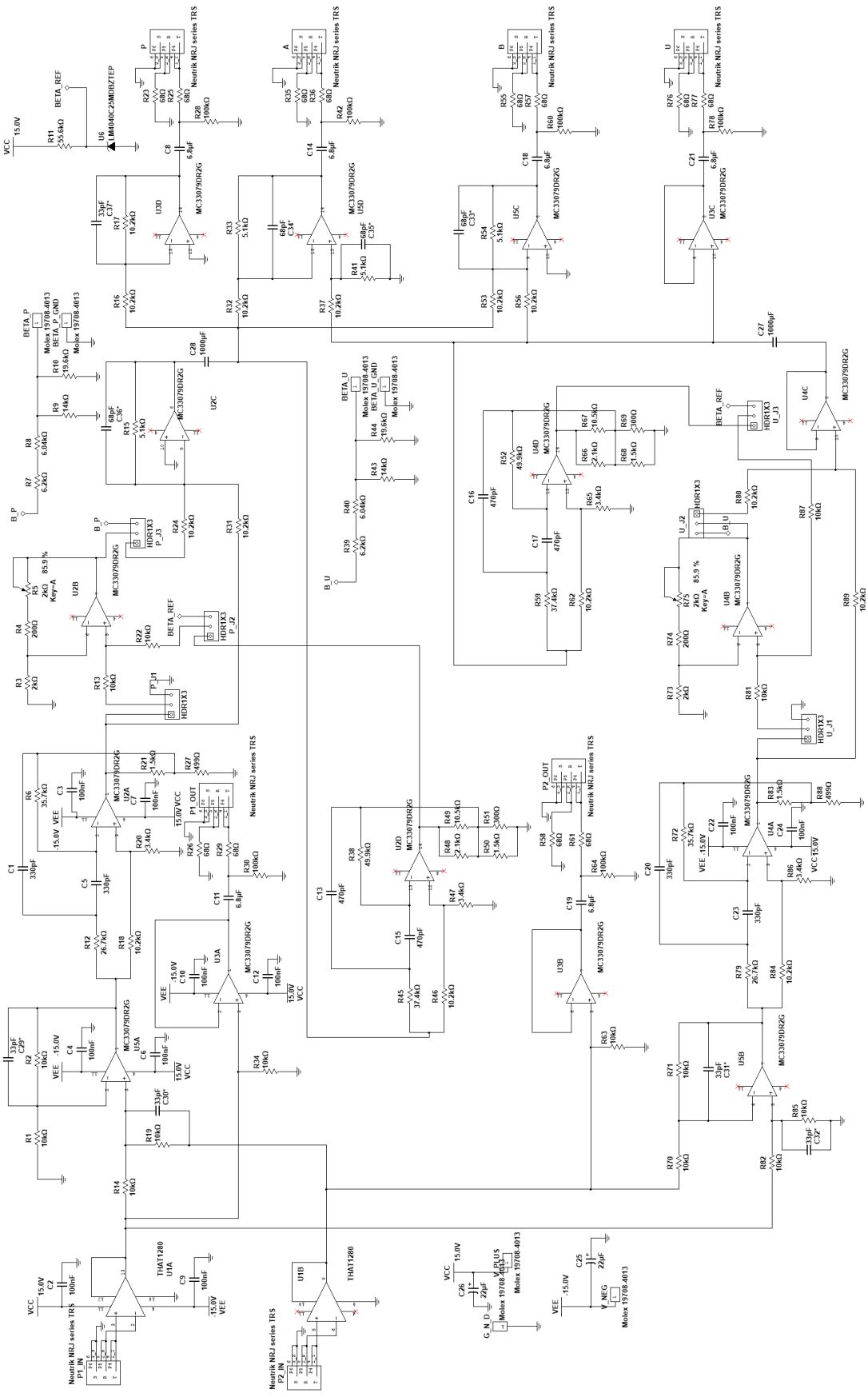

Figure 4.7: TWSC-2 schematic.

see a load of around 9.1 kΩ, forming a high-pass filter with a cut-off frequency at 2.6 Hz and producing a negligible attenuation of 58 μdB at 710 Hz, which corresponds to the lowest frequency limit of the working range of the tube. The coupling capacitors are inside the signal path, it is recommended that, if typical polarized electrolytic capacitors are used, the voltage across them should be no higher than roughly 80 mV at the lowest frequency and at the highest output signal amplitude [71], although this value was stated for a frequency of 20 Hz. The 6.8 μF value displayed in the schematic satisfies the previous requirement, however, at such low capacitance values the use of polypropilene film capacitors is usually preferred over aluminum electrolytics, since the former tend to produce lower levels of distortion [77, 78, 79]. Polypropilene film capacitors are also non-polarized and usually have a voltage rating of at least 50 V, which means that, if 48 V phantom power commonly used to energize condenser microphones is accidentally engaged, the capacitors will not suffer any damage, something that could have disastrous effects on polarized electrolytics.

Capacitors labeled C^*_{29} to C^*_{37} were not used in the current revision of the PCB of this work, but they are recommended to reduce the risk of high-frequency oscillations appearing at the outputs of the OpAmps. Capacitors C_{27} and C_{28} are non-polarized aluminum electrolytics which serve to break the loop formed by H_2 at DC and reduce DC off-set, that can reach considerable levels at high values of β, reducing the headroom of the circuit. Non-polarized capacitors were selected since, in practice, DC off-set voltages can be of either polarity. The largest commercial value available of $1,000$ μF was chosen as to make their capacitive reactances as low as possible at the lowest operating frequency when compared to resistors R_{32}, R_{37}, R_{53} and R_{56}, in order to alter the least possible the sum and difference operations required to obtain a' and b'. Furthermore, electrolytic capacitors have typical tolerances of 20 %, so selecting the largest practical value for them is the best bet to ensure that any differences from their stated value will not have a big impact on the rest of the circuitry.

Components R_5 and R_{75} are 2 kΩ potentiometers in series with fixed resistors R_4 and R_{74} which, together with R_3 and R_{73}, define the value of β according to Eq. 3.26. The minimum adjustable value for β will be around 0.55 (depending on resistor tolerances it might vary slightly). If 10 % tolerance potentiometers and 0.1 % tolerance resistors are used (as in this work), in the worst case scenario (the value of the potentiometers and series resistors at their lowest tolerance limit, resistors R_3 and R_{73} at their highest tolerance limit) the maximum value of β will be 1.005, this ensures that a value of β close to 1 will always be possible to reach.

The completed circuit board is shown in Fig. 4.8, the dimensions are 120 × 150 mm with a thickness of 1.6 mm. It is a dual-layer PCB on an FR-4 substrate. As usual, the bottom layer is a ground plane with the least amount of tracing possible. Figure 4.9 shows the circuit being adjusted in β *calibration mode*, the meter is connected to the $\rho_0 c_0 u'$ circuit's β cal terminal and displays a reading of 978.0 mV, which corresponds to a β of 0.978.

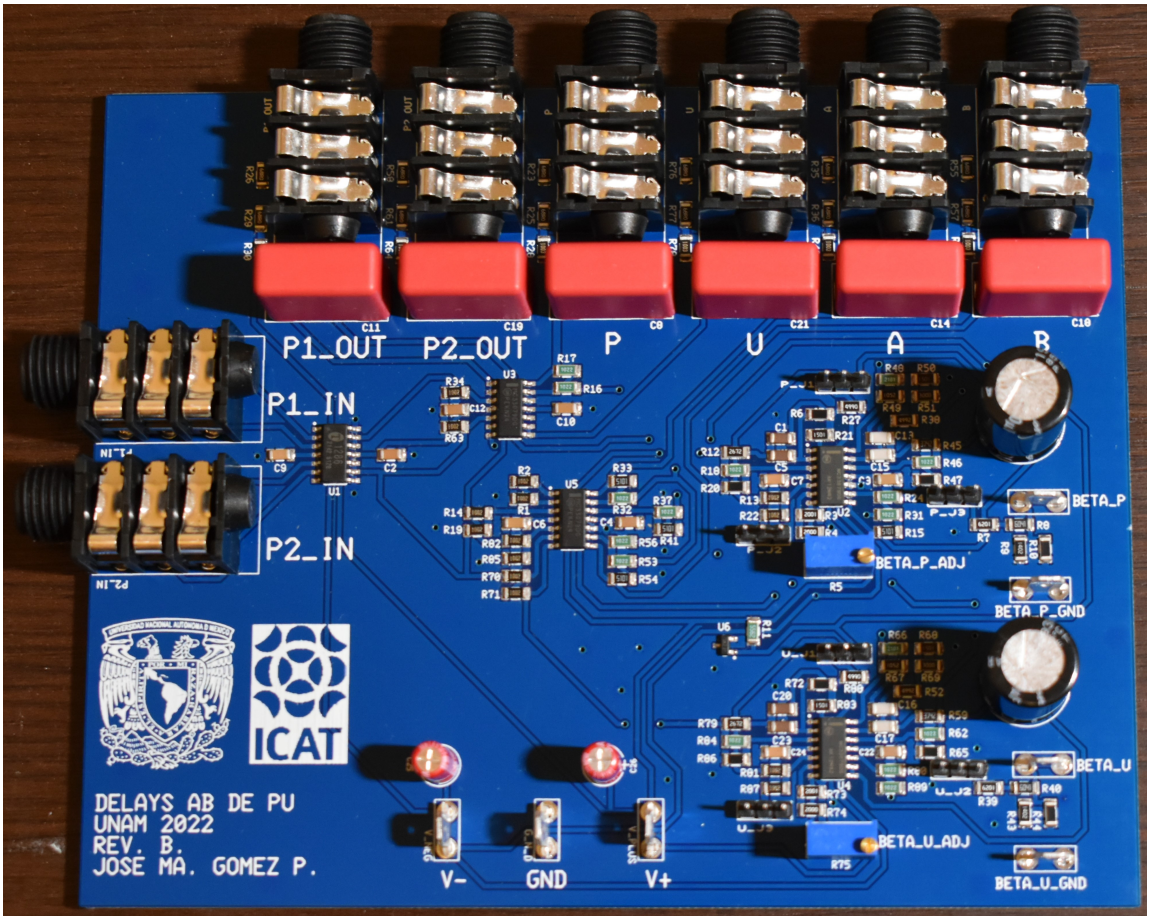

Figure 4.8: TWSC-2 circuit board.

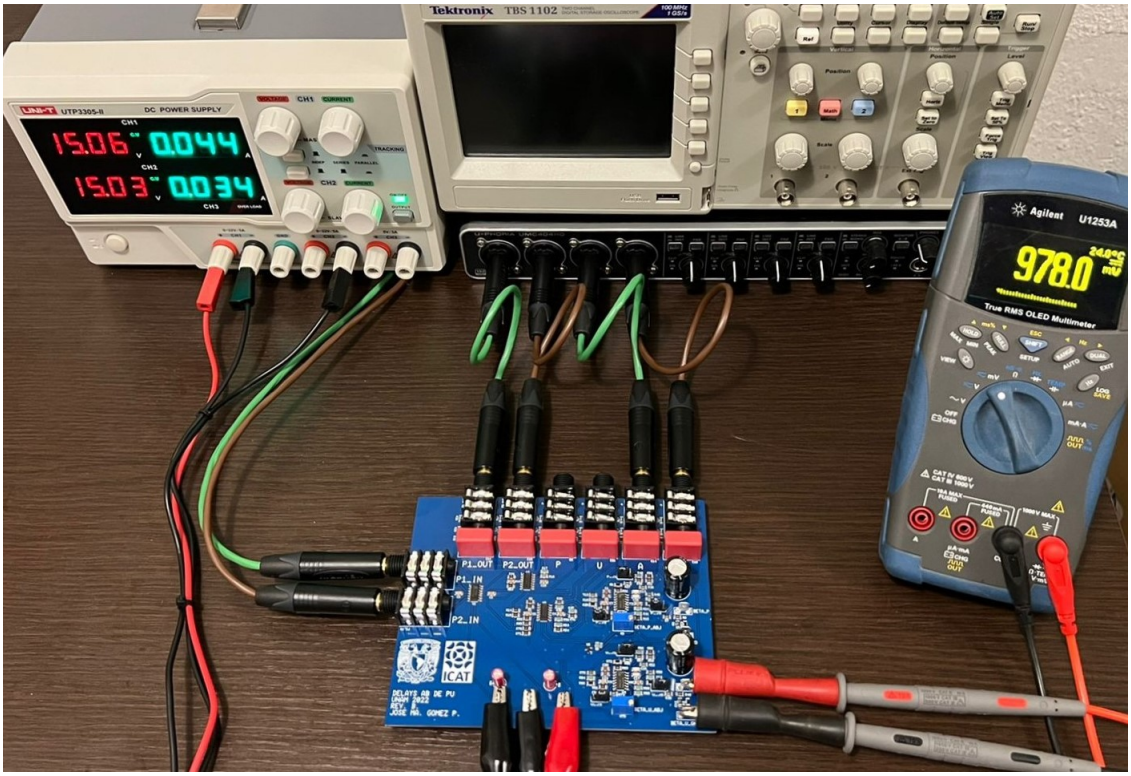

Figure 4.9: TWSC-2 circuit board in β *calibration mode*.

4.5 Results

Table 4.1 shows the parameters for each circuit being tested. The experimental results per frequency range Δf are shown in Table 4.2 as presented in [1]. For comparison purposes, in the table are also included the results obtained in [7, 18] by using a different metric system: the separation index Ψ [7]. For the TWSC-2 a value $\beta > 0.982$ produced an oscillatory response.

The non-optimized setup in [7], which uses a similar procedure to the TWSC-2 but in the frequency domain, reports a separation index of -32 dB in the $2-4$ kHz range using a 3 kHz gated sinusoid excitation signal. Compare that to the -39.0 dB error figure of the TWSC-2 in the same frequency span. However, the separation index metric is not the same as the one being used in this thesis, but it is somehow related and serves as a means to contrast the results to those published in the available literature.

Circuit	$\boldsymbol{\beta}$	$\boldsymbol{\alpha_{opt}}$	$\boldsymbol{E^2_{min}}$ (dB)	**T** (ms)
TWSC-1	0.993	0.997	-24.6	5.0
TWSC-2	0.982	0.991	-20.5	1.9

Table 4.1: Circuit parameters of each circuit being tested.

The normalized travelling wave separation error $E_{WTS}(\omega)$ with respect to frequency for

Δf (kHz)	**TWSC-1** (dB)	**TWSC-2** (dB)	Ψ (dB)
$0.35 - 0.71$	-31.0	-25.2	
$0.71 - 1.42$	-30.4	-32.4	
$1.42 - 2.84$	-20.7	-40.1	-62.1 [18]
$2.84 - 5.68$	-11.6	-30.4	
$0.71 - 5.68$	-11.6	-30.4	-39.1 [7]
$2.00 - 4.00$	-14.9	-39.0	-50.0 [7]

Table 4.2: Experimental results for each circuit being tested as presented in [1] along with the best separation factor figures obtained in [7], [18].

each TWSC is shown in Fig. 4.10. The gray areas represent frequency intervals outside of the working range of the tube.

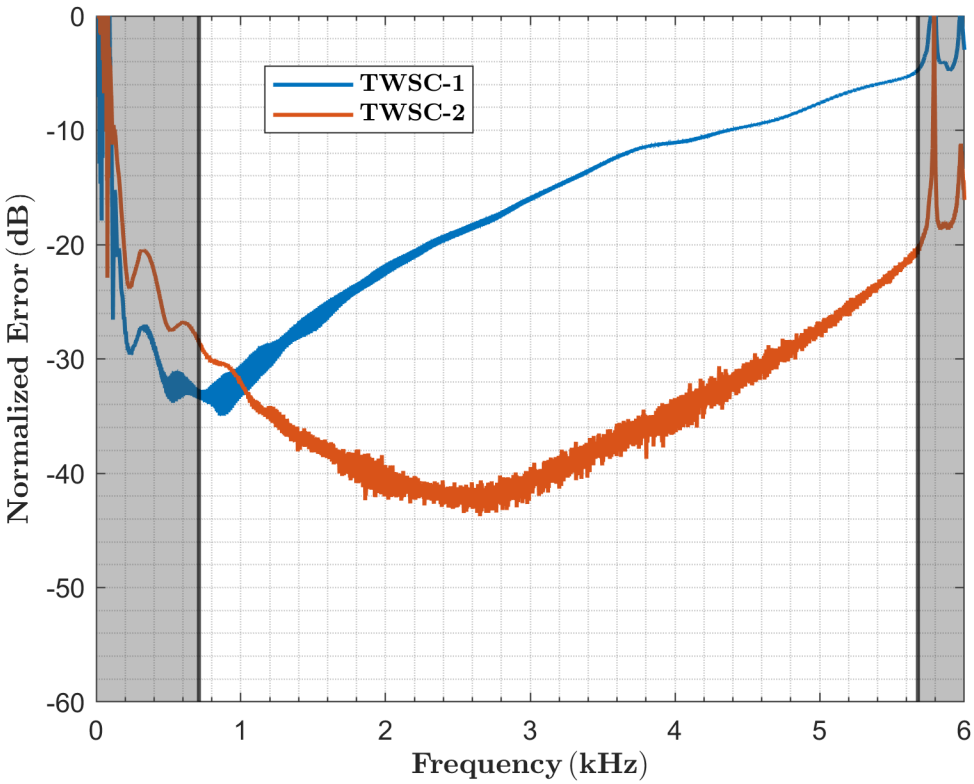

Figure 4.10: Normalized travelling wave separation error $E_{WTS}(\omega)$ for each TWSC [1].

From both Table 4.2 and Figure 4.10 it can be seen that, at very low frequencies, the TWSC-1 circuit performs a bit better than the TWSC-2. This is due to the fact that, at those frequencies, the first-order approximation is still quite accurate and the value of β in the TWSC-1 is also higher than the chosen value for TWSC-2.

These results support the theoretical E^2_{min} values of Table 4.1. As frequency increases the story is quite different, the error of the TWSC-1 circuit increases considerably, whilst the error of the TWSC-2 circuit remains significantly low. The performance degradation

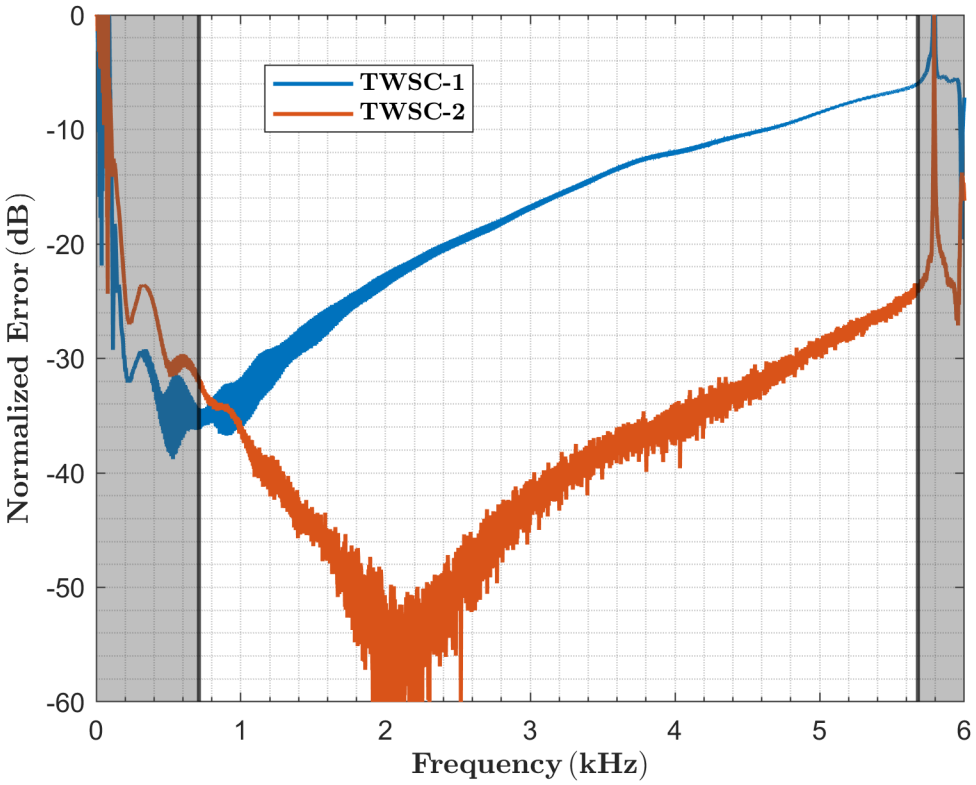

Figure 4.11: Normalized travelling wave separation error of the forward $A'(\omega)$ travelling wave component for each TWSC.

at higher frequencies in the TWSC-2 circuit might be due to the effect of the non-ideal absorber (see Fig. 4.4). Figures 4.11 and 4.12 show the error of only the forward and backward travelling wave components, respectively.

The impulse responses of the measured reference and estimated waves for both TWSC with respect to the input excitation signal (Eqs. (1.19)) are shown in Fig. 4.13. The top plot shows the forward reference $a(t)$ and estimated $a'(t)$ waves, whilst the bottom plot shows the backward reference $b(t)$ and estimated $b'(t)$ waves. The traces display the dynamic response of the loudspeaker and the reflection from the absorbing termination, which occurs around 0.5 ms. The TWSC-1 is less capable of suppressing the estimated backward travelling wave, whilst the TWSC-2 follows more closely the reference wave response.

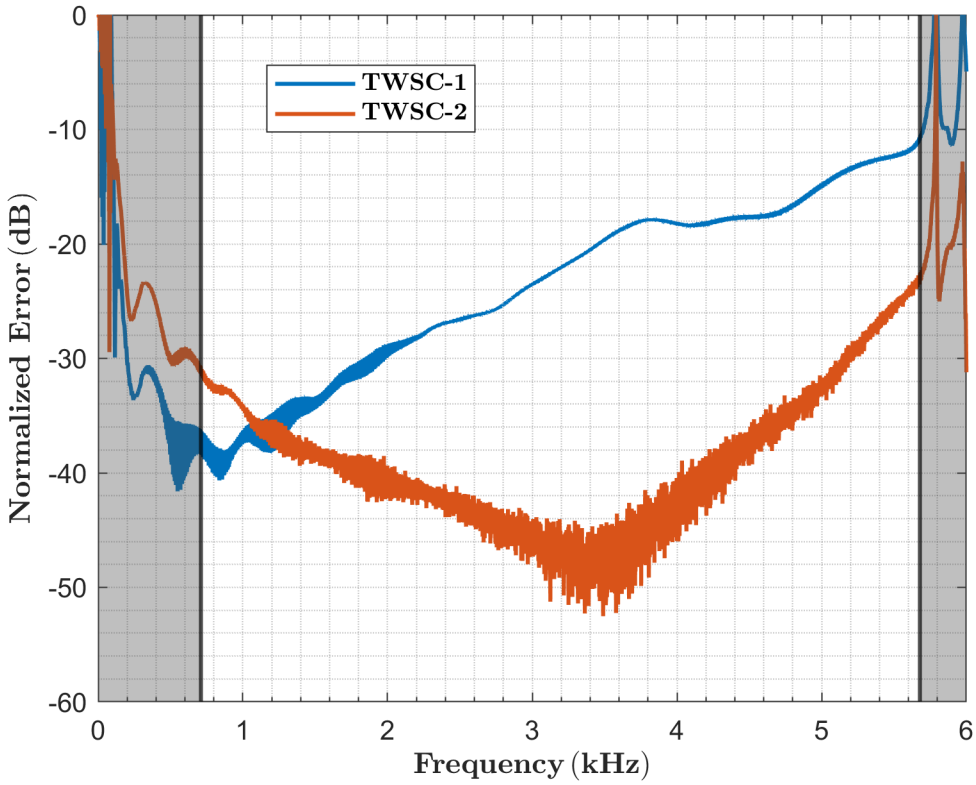

Figure 4.12: Normalized travelling wave separation error of the backward $B'(\omega]$ travelling wave component for each TWSC.

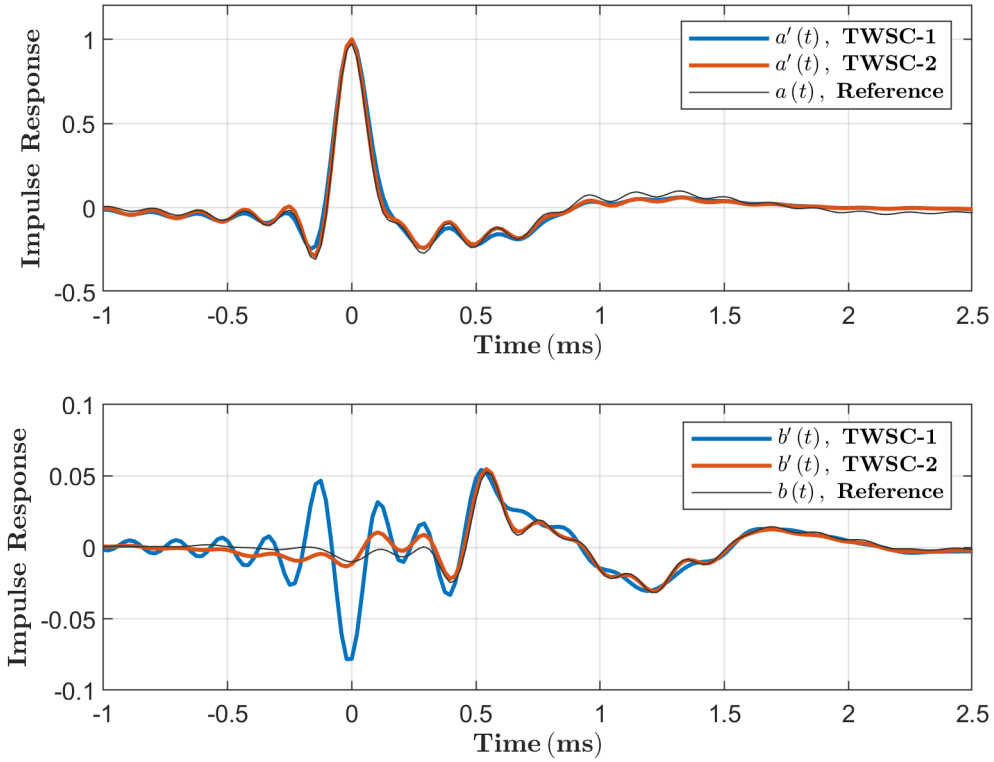

Figure 4.13: Impulse responses of the forward reference $a(t)$ and estimated $a'(t)$ waves (top), and the backward reference $b(t)$ and estimated $b'(t)$ waves (bottom) of both TWSC [1].

The normalized impulse responses of the measured estimated forward and backward wave components $a'(t)$ and $b'(t)$ with respect to the reference forward travelling wave $a(t)$ for both TWSC are shown in Fig. 4.14. These were obtained from the inverse Fourier transforms $A'(\omega)/A(\omega)$ and $B'(\omega)/A(\omega)$ as in Eqs. (1.18). The TWSC-2 again shows its superior capabilities to suppress the backward travelling wave component when compared to the TWSC-1.

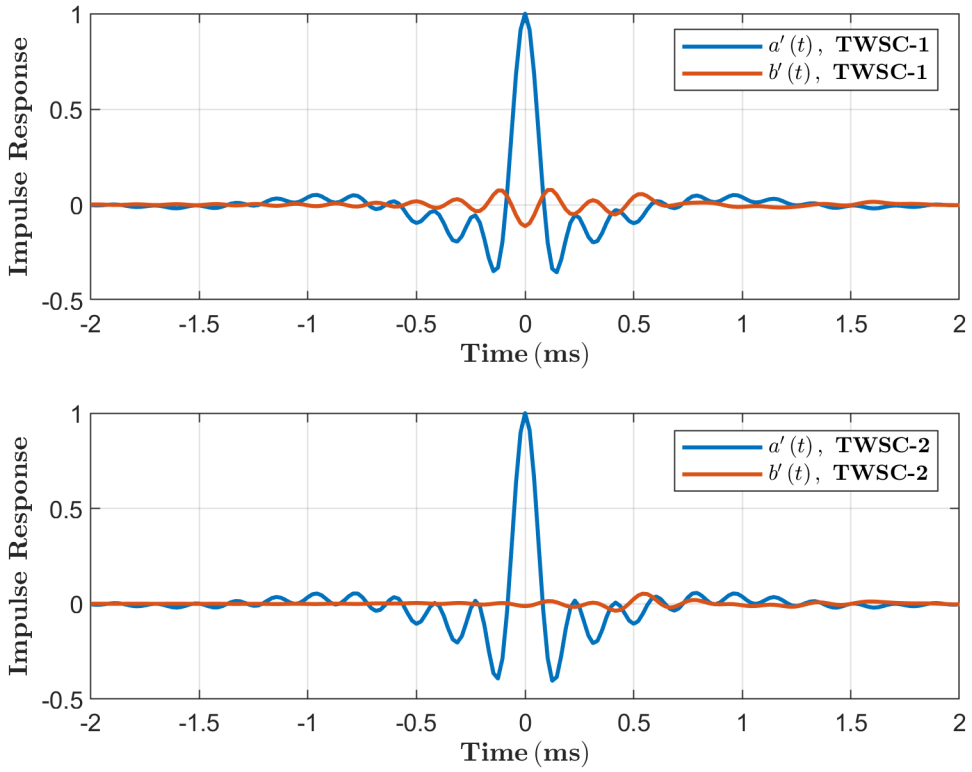

Figure 4.14: Impulse responses of the forward reference $a(t)$ and estimated $a'(t)$ waves (top), and the backward reference $b(t)$ and estimated $b'(t)$ waves (bottom) of both TWSC [1].

Figure 4.15 shows the amplitude error of the estimated forward travelling wave for both TWSC. As expected, the response of the TWSC-1 drops as frequency increases, which is a consequence of the low-pass type TDOA used in its formulation. The TWSC-2 remains well within ± 0.1 dB in the $500 - 5000$ Hz frequency range.

These results show that the circuits are capable of performing travelling wave separation in the time domain with good levels of separation between the forward and backward components, which increase accordingly to the value of β and the order of the TDOA being used. Event though higher levels of separation can be obtained by using more specialized methods such as those proposed in [7] and [18], they require a more convoluted calibration process and optimization than those obtained with the methods proposed in this current work.

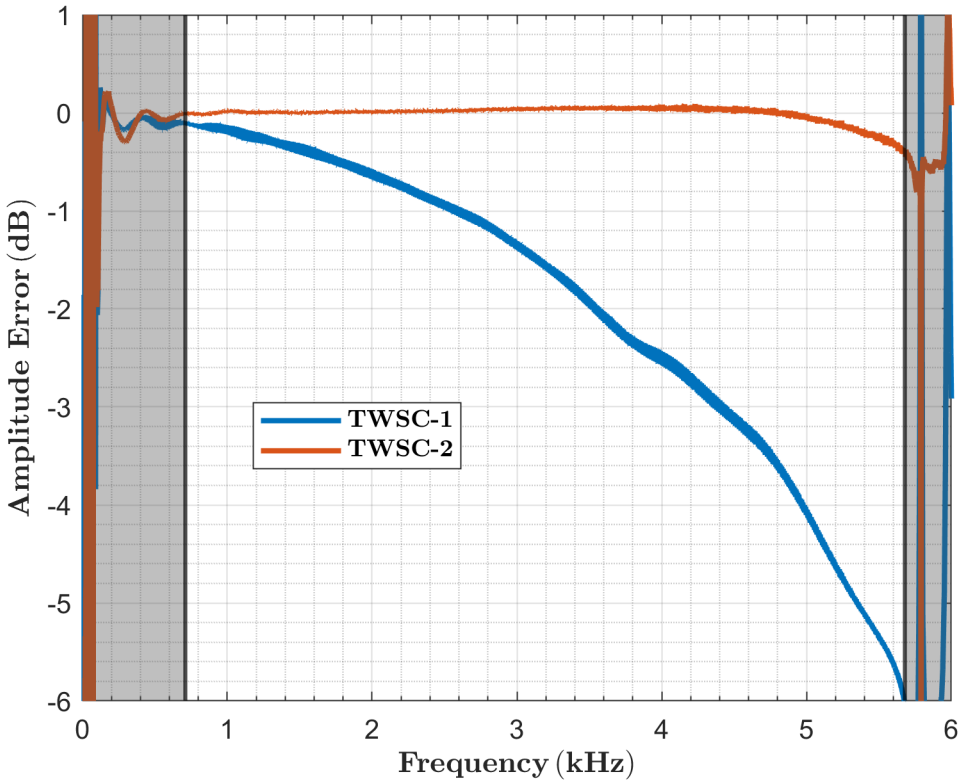

Figure 4.15: Amplitude error for the estimated forward $a'(t)$ wave components for both TWSC [1].

Chapter 5

Conclusions and Future Work

In this work acoustic travelling wave separation in the continuous time-domain using leaky recursion was proposed and implemented using analog electronic circuits. The main travelling wave separation theory using two or three microphones was developed. Afterwards, different approximations (TDOA) for the time delay operator $e^{-s\tau}$ required to perform the wave separation in the time-domain were proposed, and their realization with electronic filters was discussed. Two different methods to obtain fully working circuits for travelling wave separation were developed, namely, the Active Network Synthesis Method (ANSM) and the Analog Computing Method (ACM). The advantages and disadvantages of both methods were discussed. Simple circuits using a single op-amp were also developed. The theory to create circuits which can dynamically adjust their delay and other parameters was laid out. A technique to match the frequency response of two microphones by using transfer function optimization was introduced as well.

Experimental validation was carried out with two Travelling Wave Separation Circuits (TWSC): the first (TWSC-1) is comprised of a first-order approximation with a fixed value for the leaky recursion factor β and realized by means of the ANSM, the second (TWSC-2) is comprised of a second-order approximation with an adjustable β and realized by means of the ACM. Both circuits were evaluated using signals obtained from a setup consisting of an acoustic test tube compliant with the ASTM E2611-09 and ISO 105354–2 standards. The results showed that good levels of travelling wave separation can be attained with both circuits at low frequencies when compared to a reference obtained from a standard frequency-domain separation technique. As frequency rises the second-order circuit obtained much better results than the first-order circuit, however, the simplicity of the first-order circuit makes it appealing for certain applications. These results were published in a peer-reviewed journal [1].

Although higher separation index scores can be achieved with other methods reported in the literature, the system reported in this work has a very short processing time since its fully implemented in continuous time, whilst simultaneously being able to compute the sound pressure and normalized particle velocity at the point of measurement.

The following areas of development require further investigation:

- Experimental validation using three microphones.
- Realization and validation of circuits providing the possibility to adapt to different environmental conditions, test tubes, and varying microphone separations.
- Investigation of the possibility to dynamically vary different parameters such as β and the time delay τ.
- Electronic implementation of suitable transfer functions to match the response of two (or more) microphones.
- Alternative circuits using the ACM, which allow for a better gain structure in the β adjust circuit using the least amount of active elements possible.
- Experimental validation of other circuits such as a second-order TWSC using the ANSM, or the single op-amp circuits.

Bibliography

[1] J. M. Gomez-Perez and F. Orduña-Bustamante, "Acoustic travelling wave separation in the time domain using electronic time delay circuits and leaky recursion," *Applied Acoustics*, vol. 198, p. 108966, 2022.

[2] S.-H. Jang and J.-G. Ih, "On the multiple microphone method for measuring in-duct acoustic properties in the presence of mean flow," *The journal of the acoustical society of America*, vol. 103, no. 3, pp. 1520–1526, 1998.

[3] P. Nauclér and T. Söderström, "Separation of waves governed by the one-dimensional wave equation—a stochastic systems approach," *Mechanical systems and signal processing*, vol. 23, no. 3, pp. 823–844, 2009.

[4] G. Pinero and L. Vergara, "Separation of forward and backward acoustic waves in a car exhaust by array processing," in *1995 International Conference on Acoustics, Speech, and Signal Processing*, vol. 3. IEEE, 1995, pp. 1920–1923.

[5] M. G. Pelletier, G. A. Holt, and J. D. Wanjura, "Simplified three-microphone acoustic test method," *Instruments*, vol. 1, no. 1, p. 4, 2017.

[6] S. Allam and M. Åbom, "Investigation of damping and radiation using full plane wave decomposition in ducts," *Journal of sound and vibration*, vol. 292, no. 3-5, pp. 519–534, 2006.

[7] M. van Walstijn and G. de Sanctis, "Adaptive calibration of a three-microphone system for acoustic waveguide characterization under time-varying conditions," *The Journal of the Acoustical Society of America*, vol. 135, no. 2, pp. 917–927, 2014.

[8] K. H. Groves and B. Lennox, "Directional wave separation in tubular acoustic systems—The development and evaluation of two industrially applicable techniques," *Applied Acoustics*, vol. 116, pp. 249–259, 2016.

[9] P. Naucler and T. Soderstrom, "Separation of one-dimensional waves-a stochastic systems approach," in *2007 Conference Record of the Forty-First Asilomar Conference on Signals, Systems and Computers*. IEEE, 2007, pp. 661–665.

[10] Y. Fujimoto, J. Huang, T. Fukunaga, R. Kato, M. Higashino, S. Shinomiya, S. Kitadate, Y. Takahara, A. Yamaya, M. Saito *et al.*, "A three-microphone acoustic reflection technique using transmitted acoustic waves in the airway," *Journal of Applied Physiology*, vol. 115, no. 8, pp. 1119–1125, 2013.

[11] P. L. Rendón, F. Orduña-Bustamante, D. Narezo, A. Pérez-López, and J. Sorrentini, "Nonlinear progressive waves in a slide trombone resonator," *Journal of the Acoustical Society of America*, vol. 127, no. 2, pp. 1096–1103, 2010.

[12] G. De Sanctis and M. Van Walstijn, "A frequency domain adaptive algorithm for wave separation," in *12th Int. Conference on Digital Audio Effects (DAFx-09), Como, Italy*, 2009.

[13] J. A. Kemp, S. Bilbao, J. McMaster, and R. A. Smith, "Wave separation in the trumpet under playing conditions and comparison with time domain finite difference simulation," *The Journal of the Acoustical Society of America*, vol. 134, no. 2, pp. 1395–1406, 2013.

[14] A. F. Seybert and D. F. Ross, "Experimental determination of acoustic properties using a two-microphone random-excitation technique," *The Journal of the Acoustical Society of America*, vol. 61, no. 5, pp. 1362–1370, 1977.

[15] H. Hou, Y. Huang, and J. Yang, "Acoustic properties test of materials by the dual-microphones broadband impulse method," in *24th International Congress on Sound and Vibration*. London, UK.: ICSV24, 2017, pp. 1–8.

[16] P. A. Nelson and S. J. Elliott, *Active control of sound*. Academic press, 1991.

[17] F. A. Machuca-Tzili, F. Orduña-Bustamante, A. Pérez-López, S. J. Pérez-Ruiz, and A. E. Pérez-Matzumoto, "Modified acoustic transmission tube apparatus incorporating an active downstream termination," *The Journal of the Acoustical Society of America*, vol. 141, no. 2, pp. 1093–1098, 2017.

[18] K. H. Groves, O. Aldughayem, and B. Lennox, "Real-time active suppression of directional acoustic wave components in tubular acoustic systems," *The Journal of the Acoustical Society of America*, vol. 146, no. 6, pp. 4926–4935, 2019.

[19] B. Louis, G. Glass, B. Kresen, and J. Fredberg, "Airway area by acoustic reflection: The two-microphone method," *Journal of Biochemical Engineering*, vol. 115, no. 3, pp. 278–285, 1993.

[20] K. L. Poort and J. J. Fredberg, "Airway area by acoustic reflection: A corrected derivation for the two-microphone method," *Journal of Biomechanical Engineering*, vol. 121, no. 6, pp. 663–665, 1999.

[21] J. A. Kemp, M. van Walstijn, D. Murray Campbell, J. P. Chick, and R. A. Smith, "Time domain wave separation using multiple microphones," *The Journal of the Acoustical Society of America*, vol. 128, no. 1, pp. 195–205, 2010.

[22] J. Guerard and X. Boutillon, "Real-time wave separation in a cylindrical pipe with applications to reflectometry and echo-cancellation," *The Journal of Acoustical Society of America*, vol. 103, no. 5, pp. 3010–3011, 1998.

[23] F. Orduña-Bustamante, "Procesamiento digital de las señales de una sonda de dos micrófonos para mediciones acústicas en un ducto," in *XL Congreso Nacional de Física*, Monterrey, NL, México, 1997.

[24] F. Orduña-Bustamante, M. A. Escobar-Reina, and J. I. Cervantes-Cruz, "El multímetro acústico: un sensor de ondas de sonido en ductos," in *Memorias del Congreso de Instrumentación SOMI XVI*, Querétaro, México, 2001.

[25] M. A. Escobar-Reina and F. Orduña Bustamante, "Realización electrónica digital de un multímetro acústico," in *Memorias del Congreso de Instrumentación SOMI XVI*, Querétaro, México, 2001.

[26] M. A. Escobar-Reina, "Realización electrónica digital de un multímetro acústico," Master's thesis, Universidad Nacional Autónoma de México, 2004. [Online]. Available: https://ru.dgb.unam.mx/handle/DGB_UNAM/TES01000329183

[27] J. I. Cervantes-Cruz and F. Orduña-Bustamante, "Realización electrónica analógica de un multímetro acústico," in *Memorias del Congreso de Instrumentación SOMI XVI*, Querétaro, México, 2001.

[28] J. I. Cervantes-Cruz, "Instrumentación electrónica analógica de un sensor acústico de dos micrófonos," Bachelor's thesis, Facultad de Ingeniería, Universidad Nacional Autónoma de México, 2005. [Online]. Available: https://ru.dgb.unam.mx/handle/DGB_UNAM/TES01000339970

[29] L. E. Kinsler, A. R. Frey, A. B. Coppens, and J. V. Sanders, *Fundamentals of Acoustics*, 4th ed. New York, NY: John Wiley & Sons, Inc., 2000.

[30] H. Cohen, *Numerical approximation methods*. New York, NY, USA: Springer, 2011.

[31] L. N. Trefethen, *Approximation theory and approximation practice*. Philadelphia, PA, USA: SIAM, 2013.

[32] A. S. Sedra and P. O. Brackett, *Filter theory and design: active and passive*. Beaverton, OR, USA: Matrix, 1978.

[33] L. Xu, "A proportional differential control method for a time-delay system using the Taylor expansion approximation," *Applied Mathematics and Computation*, vol. 236, pp. 391–399, 2014.

[34] V. Hanta and A. Procházka, "Rational approximation of time delay," *Institute of Chemical Technology in Prague. Department of computing and control engineering. Technická*, vol. 5, no. 166, p. 28, 2009.

[35] R. Piche, "Low-order rational all-pass approximations to e^{-s}," in *IFAC Proceedings Volumes*, vol. 23, no. 8. Elsevier, 1990, pp. 183–186.

[36] L. D. Paarmann, *Design and analysis of analog filters: A signal processing perspective*. Boston, MA, USA: Kluwer, 2001.

[37] J. Lam, "Analysis on the Laguerre formula for approximating delay systems," *IEEE transactions on automatic control*, vol. 39, no. 7, pp. 1517–1521, 1994.

[38] K. Perev, "Approximation of pure time delay elements by using Hankel norm and balanced realizations," *Problems of Engineering Cybernetics and Robotics*, vol. 64, pp. 24–37, 2011.

[39] P. M. Makila and J. R. Partington, "Laguerre and Kautz shift approximations of delay systems," *International Journal of Control*, vol. 72, no. 10, pp. 932–946, 1999.

[40] P. Mäkilä and J. Partington, "Shift operator induced approximations of delay systems," *SIAM Journal on Control and Optimization*, vol. 37, no. 6, pp. 1897–1912, 1999.

[41] G. S. Stubbs and C. H. Single, "Transport delay simulation circuits," Atomic Power Division, Westinghouse Electric Corporation, Tech. Rep., 1956. [Online]. Available: https://books.google.com/books?vid=4HAnAqWKPOEC

[42] C. F. Hepner, "Improved methods of simulating time delays," *IEEE Transactions on Electronic Computers*, no. 2, pp. 239–243, 1965.

[43] J. R. Kiseda and D. J. Ford, "Ripple-type time delay networks using elliptic functions," *Transactions of the American Institute of Electrical Engineers, Part I: Communication and Electronics*, vol. 78, no. 6, pp. 996–1102, 1960.

[44] K. L.-C. Su, *Time-domain synthesis of linear networks*. Englewood Cliffs, NJ, USA: Prentice-Hall, 1971.

[45] B. Rakovich and B. Djurich, "Chebyshev approximation of a constant group delay with constraints at the origin," *IEEE Transactions on Circuit Theory*, vol. 19, no. 5, pp. 466–475, 1972.

[46] A. Hausner and C. M. Furlani, "Chebyshev all-pass approximants for time-delay simulation," *IEEE Transactions on Electronic Computers*, no. 3, pp. 314–321, 1966.

[47] S. H. Al-Amer and F. M. Al-Sunni, "Approximation of Time-Delay Systems," in *Proceedings of the 2000 American Control Conference. ACC (IEEE Cat. No. 00CH36334)*. Chicago, Illinois, USA: IEEE, 2000.

[48] W. D. T. Davies, "On the analog simulation of a pure time delay," *Simulation*, vol. 18, no. 5, pp. 161–170, 1972.

[49] V. M. Alfaro, "Nuevas aproximaciones del tiempo muerto para estudios de control," *Ingeniería: Revista de la Universidad de Costa Rica*, vol. 13, no. 1, pp. 41–52, 2003.

[50] B. Ulmann, *Analog computing*. Munich, Germany: Oldenbourg Wissenschaftsverlag, 2013.

[51] A. Hausner, *Analog and analog/hybrid computer programming*. Englewoods Cliffs, NJ, USA: Prentice-Hall, 1971.

[52] G. Tomlinson, "Synthesis of delay networks for an analogue computer," in *Proceedings of the Institution of Electrical Engineers*, vol. 112, no. 9. IET, 1965, pp. 1806–1814.

[53] A. Carlson, G. Hannauer, T. Carey, and P. J. Holsber, Eds., *Handbook of analog computation*. Princeton, NJ, USA: Electronic Associates, Inc., 1967.

[54] H. D. Huskey and G. A. Korn, Eds., *Computer handbook*. New York, NY, USA: McGraw-Hill, 1962.

[55] S. Franco, *Design with operational amplifiers and analog integrated circuits*. New York, NY, USA: McGraw-Hill, 2002.

[56] T. Deliyannis, Y. Sun, and J. K. Fidler, *Continuous-time active filter design*. Boca Raton, FL, USA: CRC press, 1999.

[57] G. S. Moschytz and P. Horn, *Active filter design handbook*. Chichester, UK: Wiley, 1981.

[58] G. S. Moschytz, "A general all-pass network based on the sallen-key circuit," *IEEE Transactions on Circuit Theory*, vol. 19, no. 4, pp. 392–394, 1972.

[59] ——, *Linear integrated networks: design*. New York, NY, USA: Van Nostrand Reinhold Company, 1975.

[60] R. Orban, "Active all-pass filters for audio," *Journal of the Audio Engineering Society*, vol. 39, no. 4, pp. 250–260, 1991.

[61] J. Friend, C. Harris, and D. Hilberman, "STAR: An active biquadratic filter section," *IEEE Transactions on Circuits and Systems*, vol. 22, no. 2, pp. 115–121, 1975.

[62] T. Deliyannis, "High-Q factor circuit with reduced sensitivity," *Electronics Letters*, vol. 26, no. 4, pp. 577–579, 1968.

[63] W.-K. Chen, *Passive and active filters: theory and implementations*. Wiley, 1986.

[64] L. P. Huelsman, *Active and passive analog filter design: an introduction*. New York, NY, USA: McGraw-Hill, 1993.

[65] P. A. Mohan, *VLSI analog filters: active RC, OTA-C, and SC*. New York, NY, USA: Springer, 2012.

[66] R. Schaumann, M. Ghausi, and K. R. Laker, *Design of analog filters: pasive, active RC, and switched capacitor*. Englewood Cliffs, NJ, USA: Prentice-Hall, 1990.

[67] K. L.-C. Su, *Analog filters*, 2nd ed. Norwell, MA, USA: Kluwer, 2002.

[68] *Dual Balanced Line Receiver ICs*, 1280, THAT Corporation, 2007, rev. 01. [Online]. Available: http://www.thatcorp.com/datashts/THAT_1280-Series_Datasheet.pdf

[69] *Operational Amplifiers, LowNoise, Dual and Quad*, MC33079, ON Semiconductor, 2011, rev. 9. [Online]. Available: https://www.onsemi.com/pdf/datasheet/mc33078-d.pdf

[70] C. D. Motchenbacher and J. A. Connelly, *Low-noise electronic system design*. New York, NY, USA: Wiley, 1993.

[71] D. Self, *Small signal audio design*, 3rd ed. New York, NY, USA: Routledge, 2020.

[72] P. Horowitz and W. Hill, *The art of electronics*, 3rd ed. New York, NY, USA: Cambridge, 2015.

[73] M. Blencowe, "Input protection for low-distortion op-amp circuits," *Electronic Design*, 2020. [Online]. Available: https://www.electronicdesign.com/technologies/analog/article/21131760/input-protection-for-lowdistortion-opamp-circuits

[74] J. Buxton, *Careful Design Tames High Speed Op Amps*, Analog Devices, Norwood, MA, USA, 1991, AN-257 Application Note. [Online]. Available: https://www.analog.com/media/en/technical-documentation/application-notes/AN-257.pdf

[75] W. Jung, *Op Amp applications handbook*. Burlington, MA, USA: Newnes, 2005.

[76] *Precision Micropower Shunt Voltage Reference*, LM4040-EP, Texas Instruments Inc., 2011. [Online]. Available: https://www.ti.com/lit/ds/symlink/lm4040c25-ep.pdf?ts=1664228620099&ref_url=https%253A%252F%252Fwww.ti.com%252Fproduct%252FLM4040C25-EP%252Fpart-details%252FLM4040C25MDBZTEP

[77] C. Bateman, "Capacitor sound 4," *Electronics World*, vol. 108, no. 1799, pp. 40–47, 2002.

[78] ——, "Capacitor sound 5," *Electronics World*, vol. 108, no. 1800, pp. 44–51, 2002.

[79] ——, "Capacitor sound 6," *Electronics World*, vol. 109, no. 1801, pp. 44–51, 2003.

Appendix A

MATLAB® Scripts

Single-Amplifier General Biquad Script for the $H_P(s)$ Circuit.

This script computes the resistor values for the first term of $H_P(s)$ with Padé coefficients using the ANSM. Full equations can be found in [63]. The DC gain value is set at unity.

José María Gómez Pérez, UNAM, México City, 2022

Contents

Enter parameters

```
tau = 3.5329e-05; %select delay time constant 'tau'
bet = 0.85;       %select value of beta
r2 = 20e3;        %select value for r2
gam = 0.1;        %select value of gamma, ratio between r2 and RC
Rb=1e3;           %select value for Rb
C2 = 1e-9;        %select capacitor C2 value.
a = 1;            %select C1 to C2 ratio
```

Computation

```
C1 = a*C2;
A = 1;
r1 = r2*gam;
K = 1;
b2 = A;
b1 = A*3/(tau);
b0 = A*3/(tau^2);
a0 = 3/(tau^2);
a1 = (3/(tau))*(1-bet)/(1+bet);
R1 = 2*gam/(C2*(-a1+sqrt(a1^2+4*a0*(1+C1/C2)*gam)));
K1 = (b2+b0*(1+C1/C2)*R1^2*C2^2-b1*R1*C2)/(1+gam);
K3 = b2;
R2 = 1/(R1*C1*C2*a0);
K2 = b2;
R3 = inf;
R4 = R1/K1;
R5 = 1/(1/R1-1/R4);
RD = (1/K2)/((1/K2-1)*(1/r1));
RC =1/(1/r1-1/RD);
Ra = (K-1)*Rb;
```

Display values

```
R1_tx = num2str(R1);
R2_tx = num2str(R2);
R4_tx = num2str(R4);
R5_tx = num2str(R5);
RC_tx = num2str(RC);
RD_tx = num2str(RD);
r1_tx = num2str(r1);
r2_tx = num2str(r2);
Ra_tx = num2str(Ra);
Rb_tx = num2str(Rb);
C1_tx = num2str(C1);
C2_tx = num2str(C2);
disp(['R2: ',R2_tx]); disp(['R4: ',R4_tx]);
disp(['R5: ',R5_tx]); disp(['RC: ',RC_tx]); disp(['r2: ',r2_tx]);
disp(['C1: ',C1_tx]); disp(['C2: ',C2_tx]);
```

Single-Amplifier General Biquad Script for the $H_U(s)$ Circuit.

This script computes the resistor values for the first transfer function in $H_U(s)$ using Padé coefficients. Full equations can be found in [63].

José María Gómez Pérez, UNAM, México City, 2022

Contents

Enter parameters

```
tau = 3.5329e-05; %select delay time constant 'tau'
bet = 0.85;       %select value of beta
r2 = 10e3;        %select value for r2
gam = 0.1;        %select ratio between r1 and r2 (r1 is an intermediate
                       %value used to compute RC)
C2 = 10e-9;       %select value for capacitor C2
a = 1/21.276595745; %select C1 to C2 ratio
A = 2.05555555555556; %select DC gain (this value should be close to 1)
Rb=3;             %select value for Rb (it should be very small), the resulting
                  %value of Ra should be as small as possible when compared to r2
```

Computation

```
r1 = r2*gam;
C1 = a*C2;
K = 1;
b2 = A;
b1 = A*3/(tau);
b0 = A*3/(tau^2);
a0 = 3/(tau^2);
a1 = (3/(tau))*(1+bet)/(1-bet);
K3 = 1e-6;
R1 = 2*gam/(C2*(-a1+sqrt(a1^2+4*(1+C1/C2)*a0*gam)));
K1 = (b2+b0*(1+C1/C2)*R1^2*C2^2-b1*R1*C2)/(1+gam);
```

```
b2 = b2/K1;
b1 = b1/K1;
b0 = b0/K1;
K = K1*K;
R3 = (1+gam)*(b2-K3)/(R1*C1*C2*(b0-a0*b2));
R2 = 1/(R1*C1*C2*a0+gam/R3);
K2 = b2;
R3 = inf;
R5 = inf;
R4 = R1;
RD = (1/K2)/((1/K2-1)*(1/r1));
RC =1/(1/r1-1/RD);
Ra = (K-1)*Rb;
```

Display values

```
R1_tx = num2str(R1);
R2_tx = num2str(R2);
R3_tx = num2str(R3);
R4_tx = num2str(R4);
RC_tx = num2str(RC);
RD_tx = num2str(RD);
r1_tx = num2str(r1);
r2_tx = num2str(r2);
Ra_tx = num2str(Ra);
Rb_tx = num2str(Rb);
C1_tx = num2str(C1);
C2_tx = num2str(C2);
disp(['R2: ',R2_tx]); disp(['R4: ',R4_tx]); disp(['RC: ',RC_tx]);
disp(['RD: ',RD_tx]); disp(['r2: ',r2_tx]); disp(['Ra: ',Ra_tx]);
disp(['Rb: ',Rb_tx]); disp(['C1: ',C1_tx]); disp(['C2: ',C2_tx]);
```